AD-A090 558 ILLINOIS UNIV AT URBANA-CHAMPAIGN DEPT OF AERONAUTICA--ETC F/G 21/5
FLUID MECHANICAL PROCESSES OF DEFLAGRATION TO DETONATION TRANSI--ETC(U)
MAR 80 S J HOFFMAN, H KRIER AFOSR-77-3336
UNCLASSIFIED AAE-80-2 AFOSR-TR-80-1064 NL

1 OF 2
AD
A090558

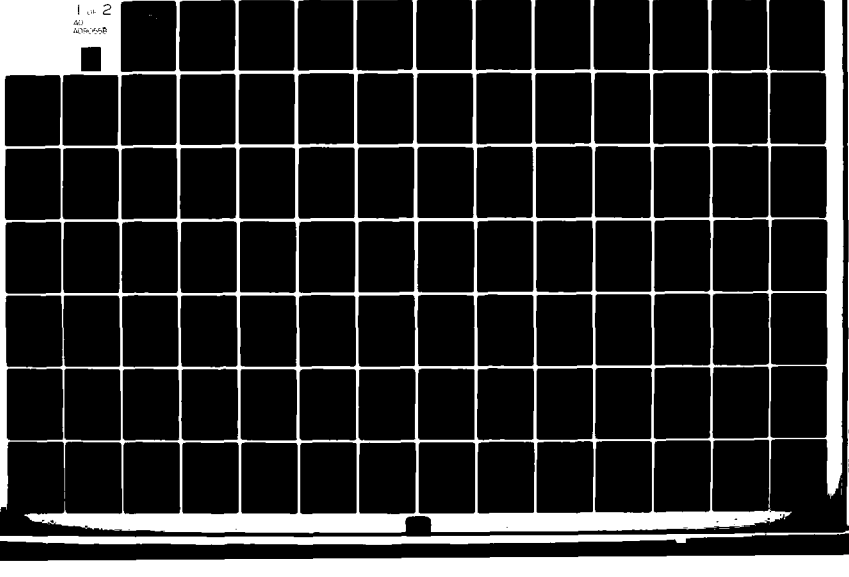

LEVEL II

12

AAE

AERONAUTICAL AND ASTRONAUTICAL ENGINEERING DEPARTMENT

ENGINEERING EXPERIMENT STATION, COLLEGE OF ENGINEERING, UNIVERSITY OF ILLINOIS, URBANA

Aeronautical and Astronautical Engineering Department
University of Illinois at Urbana-Champaign

Technical Report AAE-80-2
UILU-Eng-80-0502

Prepared for

Air Force Office of Scientific Research
Aerospace Sciences Directorate
Bolling Air Force Base, D.C.

FLUID MECHANICAL PROCESSES OF DEFLAGRATION TO DETONATION TRANSITION IN BEDS OF POROUS REACTIVE SOLIDS.

by

Stephen J. Hoffman and Herman Krier

Approved for public release; distribution unlimited
Grant No. AFOSR-77-3336 March 1980

ABSTRACT

The fluid mechanical processes which characterize a transition from deflagration to detonation in granular beds of solid propellant have not at present been sufficiently refined to allow accurate modelling of the phenomenon. In an attempt to improve this situation, this report has investigated what might be considered basic mechanisms and consequences that arise from a set of assumptions for the governing and constitutive equations which take into account the two phase nature of this problem. A qualitative description of the flow process is made, based on observations obtained from DDT experiments. From this, certain conclusions are reached as to the properties needed by propellants to exhibit a deflagration to detonation transition (DDT). The numerical integration scheme itself is examined in detail in order to further understand the consequences of its use. Also, two scenarios for DDT are presented which exhibit characteristics similar to those derived from experimental evidence. Conclusions as to the direction of future research are made based on the results obtained from the work which led to these two basic mechanisms for DDT.

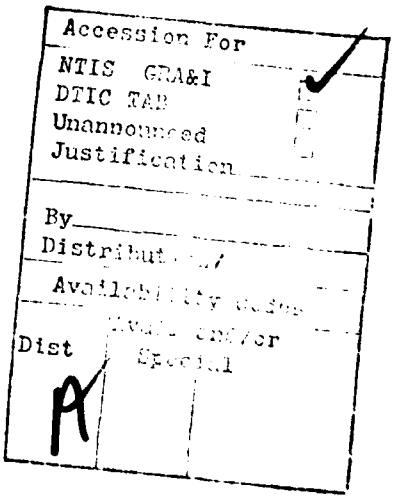

TABLE OF CONTENTS

LIST OF SYMBOLS

Symbols	Definition	Units	
		English	SI
b_1, b_3	Burning rate proportionality constant	$\frac{in/s}{(psi)^n}$	$\frac{m/s}{(N/m^2)^n}$
b_2	Burning rate constant	in/s	m/s
B	Particle stress proportionality constant	$\frac{lb_f}{in^2}$	$\frac{N}{m^2}$
B_v	Density dependent variable covolume	$\frac{in^3}{lb_m}$	$\frac{m^3}{Kg}$
c	Sound speed	in/s	m/s
C_D	Drag modification (permeability) coefficient		
c_p	Specific heat at constant pressure	$\frac{BTU}{lb_m-^oR}$	$\frac{J}{Kg-^oK}$
c_v	Specific heat at constant volume	$\frac{BTU}{lb_m-^oR}$	$\frac{J}{Kg-^oK}$
E	Total energy	$\frac{BTU}{lb_m}$	$\frac{J}{Kg}$
E^{CHEM}	Chemical energy released during combustion	$\frac{BTU}{lb_m}$	$\frac{J}{Kg}$
f_{pg}	Interphase drag coefficient		
$f(\phi)$	Particle-particle interaction function		
$\overline{F}$	Interphase drag per unit volume	$\frac{lb_f}{in^3}$	$\frac{N}{m^3}$
g_c	Gravitational unit conversion factor	$\frac{lb_m-in}{lb_f-s^2}$	
h_{pg}	Convective heat transfer coefficient	$\frac{BTU}{in^2-s-^oR}$	$\frac{J}{m^2-s-^oK}$

Symbols	Definition	Units	
		English	SI
k	Thermal conductivity of gas	$\frac{BTU}{in\text{-}s\text{-}^{\circ}R}$	$\frac{J}{m\text{-}s\text{-}^{\circ}K}$
K	Bulk modulus	$\frac{lb_f}{in^2}$	$\frac{N}{m^2}$
ℓ	Particle stress exponent		
n	Burning rate index		
N	Number of grid points in which data is stored		
Nu	Nusselt number		
P	Gas pressure	$\frac{lb_f}{in^2}$	$\frac{N}{m^2}$
Pr	Prandtl number		
Q	Interphase convective heat gransfer	$\frac{BTU}{in^3\text{-}s}$	$\frac{J}{m^3\text{-}s}$
r_p	Particle radius	in	m
$\dot{r}$	Propellant burning rate	$\frac{in}{s}$	$\frac{m}{s}$
R	Gas constant	$\frac{BTU}{lb_m\text{-}^{\circ}R}$	$\frac{J}{Kg\text{-}^{\circ}K}$
$\overline{R}$	Universal gas constant	$\frac{BTU}{lbmole^{\circ}R}$	$\frac{J}{Kg\text{-}mole^{\circ}K}$
Re	Reynolds number		
S	Surface area of particles	in^2	m^2
t	Time	sec	sec
Δt	Time step	sec	sec
T	Temperature	$^{\circ}R$	$^{\circ}K$
T_{IGN}	Ignition temperature	$^{\circ}R$	$^{\circ}K$

Symbols	Definition	Units	
		English	SI
u	Velocity	$\frac{in}{s}$	$\frac{m}{s}$
V	Volume	in^3	m^3
V_f	Flame speed	$\frac{in}{s}$	$\frac{m}{s}$
x	Linear distance	in	m
Δx	Grid size	in	m
Γ	Mass source/sink term	$\frac{lb_m}{in^3\text{-}s}$	$\frac{N}{m^3\text{-}s}$
μ	Gas viscosity	$\frac{lb_m}{in\text{-}s}$	$\frac{Kg}{m\text{-}s}$
ρ	Density	$\frac{lb_m}{in^3}$	$\frac{Kg}{m^3}$
τ	Stress	$\frac{lb_f}{in^2}$	$\frac{N}{m^2}$
ϕ	Porosity (V_g/V_m)		
ϕ_c	Critical porosity		
ϕ_{LL}	Lowest porosity attainable based on geometric constraints		
ϕ_{UL}	Porosity above which particles do not touch		

Subscripts

o	Initial condition
1	Gas phase
2	Particle phase
g	Gas phase

Symbols	Definition	Units	
		English	SI
j	j^{th} grid space		
Min	Minimum		
Mix	Mixture		
p	Particle phase		
TOT	Total		

LIST OF FIGURES

Page

LIST OF TABLES

CHAPTER ONE

DESCRIPTION OF THE FLUID DYNAMICS OF DDT

1.1 Introduction

The work outlined in this report is a continuation of the research being conducted under the direction of Dr. Herman Krier to determine a mechanism which explains deflagration to detonation transition (DDT) in porous reactive solids. The specific regime under consideration is the DDT phenomenon observed in tightly packed beds of finely granulated, highly energetic solid propellants, a description of which can be found in Krier and Gokhale [1] with further results to be found in Krier and Kezerle [2] and Krier, Gokhale, and Hoffman [3].

The method used in analyzing this problem is basically the same as that developed in Krier and Kezerle [2], namely the use of six conservation equations based on the concept of separated continuum flow in order to accurately solve the unsteady fluid dynamics in a packed bed. The exact form of the equations used will be presented later in this report. Previous to the use of this approach, a system of equations which could be used to analyze the same problem was developed by Krier and Gokhale, based on the continuum-mixture theory put forth by Soo [4]. Under this assumption, the momentum and energy equations of the mixture described a continuum fluid in terms of the mean mass weighted mixture velocity and the mixture energy. However, the assumption that these mixture equations describe a continuum (a Navier-Stokes fluid) cannot always be adequately justified. Thus, subsequent work by Krier and Kezerle modified this approach, and assumed that

each phase independently made up a continuum. The important difference that can now be seen in the two sets of equations is the appearance of inertial-coupling (diffusion-like) terms in the balanced equations of momentum and energy. (See Soo [5].)

In addition to these conservation equations, state equations for both the gas phase and the solid phase of the bed will be used to make the computer simulation as realistic as possible. In this case, the gas state equation has been formulated to provide accurate results in the nonideal, high-pressure flow which is under consideration. The use of a state equation for the solid phase, which represents an improvement over the incompressible assumption used in previous works will allow variations in the particle density to take place.

Due to the separated nature of the flow, there must be supplemental constitutive laws which account for the interaction of the two phases of the flow. These laws take into account such factors as an interphase heat transfer and a gas-particle drag. In the studies reported, Krier-Gokhale [1] and Krier-Kezerle [2], a compaction resistance law was used that later proved to be unsatisfactory when subsequent calculations were made for packed beds of increasing length [3]. This particular problem was solved by linking the compaction resistance (particle stress) to the amount of force being applied to the bed by the interphase drag. Each individual phase also has a set of constitutive relations which are necessary to completely describe the flow. These include such equations as a law describing the axial particle stress (related to the compaction resistance law), a model to describe the movement of this stress wave, a pressure-dependent burning rate

law for the particles, and a temperature-dependent gas viscosity law. Variations in any one of these constitutive laws caused its own change in the progression of the flow through the bed. Again, results from variations in some of these laws will be presented later.

1.2 Deflagration-to-Detonation Transition (DDT)

As discussed in Krier and Kezerle [2], experimental studies of the spontaneous deflagration-to-detonation transition (DDT) in a packed bed of granular or solid propellant indicates that in the steady-state detonation phase, a pressure shock wave precedes the flame (or ignition) front. In the build-up to this phase, there appears to be two scenarios which describe the pre-detonation fluid dynamics, both of which can be inferred from experimental evidence. The first mechanism results from the work by Bernecker and Price [6], which assumes that the pressure front (not yet a shock wave) is initially behind the flame front. But due to the rapid generation of gases by the burning propellant, the pressure front is simultaneously increased in magnitude, steepened in its gradient, and accelerated towards the flame front. The point at which the pressure front overtakes the flame front is then defined as the transition point, after which the flame front, now preceded by the pressure front, moves down the bed in a self-sustaining detonation wave at a speed greater than the deflagration wave. (See Fig. 1.1.)

The second DDT mechanism can be traced to work first done by Maček [7] for DDT in solid explosives which was later expanded upon by Tarver et al. [8]. In this model, the rapid build-up of gas pressure behind the flame front sends compression waves into the compacted, but as yet

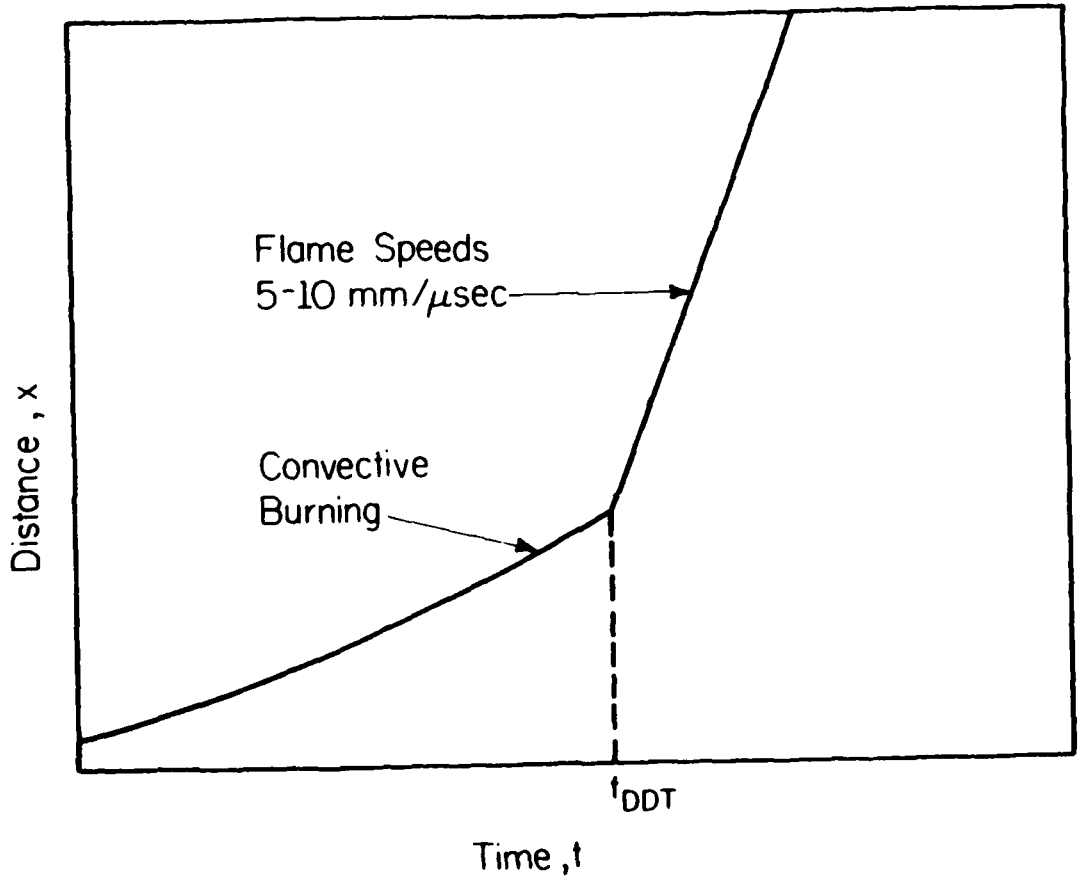

Fig. 1.1 Detonation to deflagration transition mechanism supported by experiments of Bernecker and Price [6].

unignited propellant. Due to the increase in sound speed behind successive compression waves, each wave will eventually overtake its predecessor, which will result in the formation of an insipient shock (Fig. 1.2). The shock is assumed to form some distance ahead of the flame front, resulting in a steady-state detonation wave moving forward through the unignited portion of the bed, as well as a retonation wave moving back towards, and eventually meeting, the flame front. This model has been given some experimental support for DDT in granular beds from work by Calzia and Carabin [9]. (See Fig. 1.3.) It should be noted at this point that the first mechanism could be considered a special case of the second if both the flame front and gas pressure front were to arrive at the point of formation of the insipient shock at the exact time of shock formation.

1.3 Areas of Investigation

The work presented in Krier and Kezerle [2] developed the necessary conservation equations and constitutive laws to perform the pre-detonation fluid dynamics, which is a necessary part of either of the previously mentioned DDT models. Using this set of laws, an effort to find the DDT mechanism based on the first mechanism was made by utilizing a selective variation of parameters in this set of equations. The results of this effort seemed to indicate that unless some alternative jump-like function were introduced in the equations, one does not predict the formation of a reaction front at speeds in the range of 10 mm/μsec and being supported in advance by the detonation shock. Some candidates which include the physics to allow for such jump-like function are the following concepts:

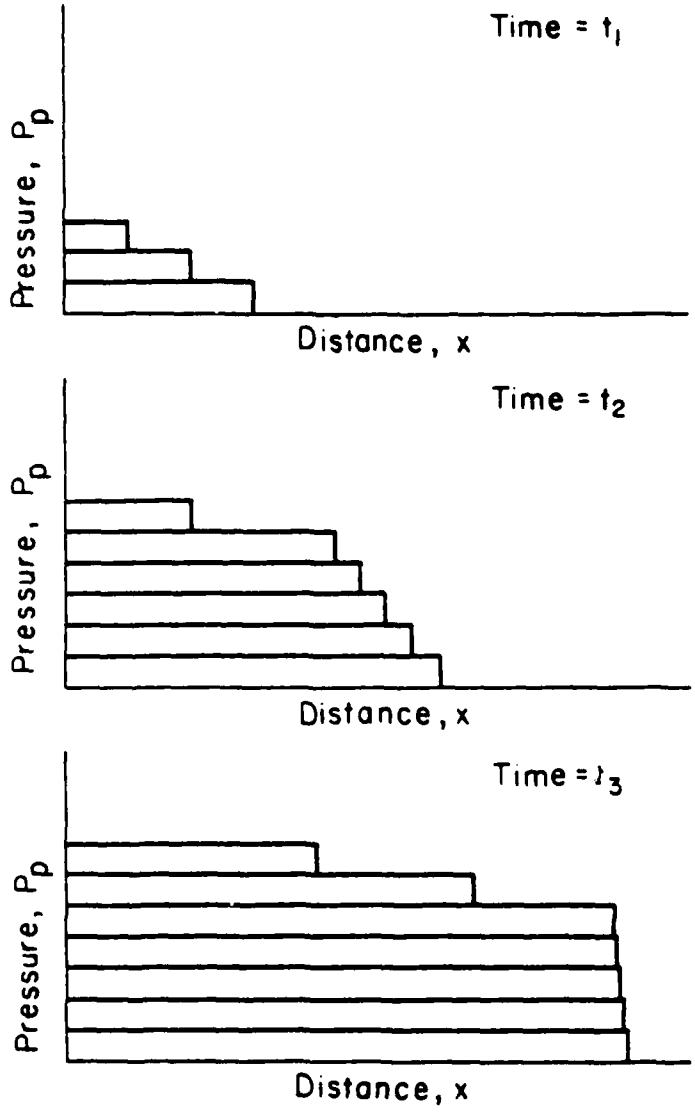

Fig. 1.2 Solid-phase compression wave buildup to a shock front.

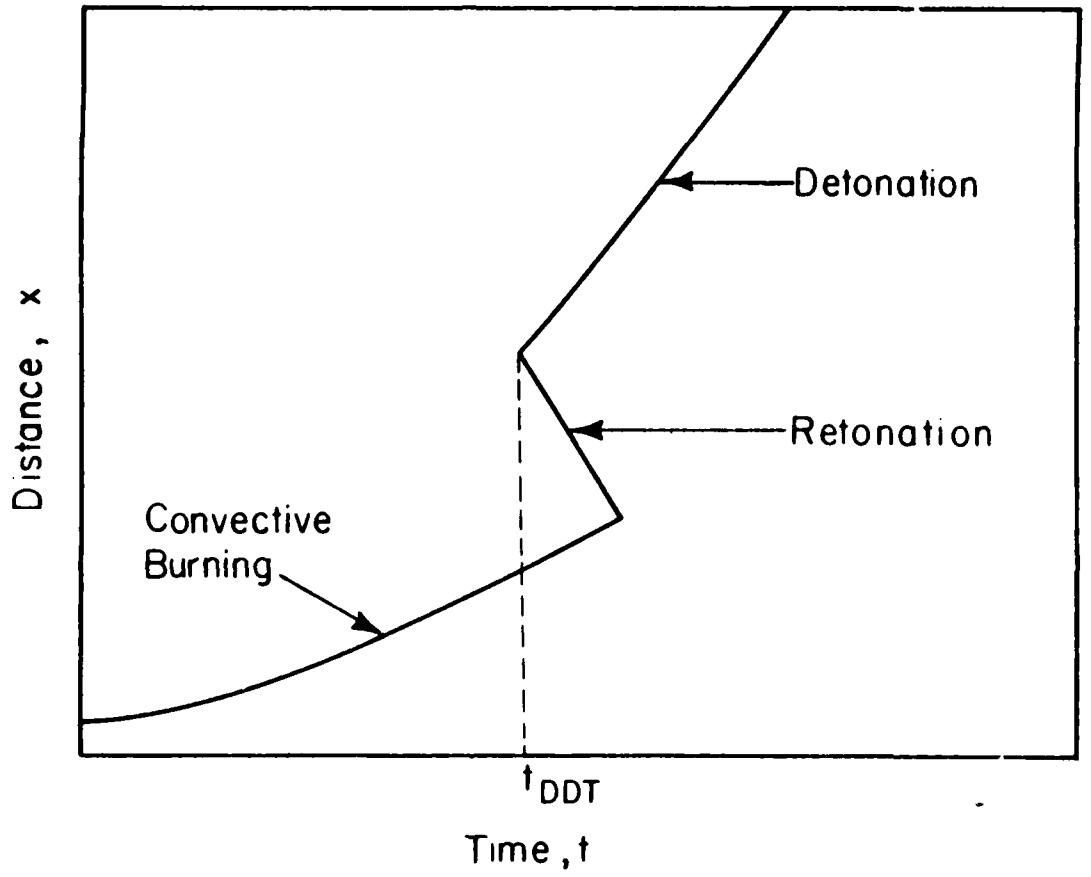

Fig. 1.3 Detonation to deflagration transition mechanism supported by experiments of Caizia and Carabin [9].

(1) At some critical high pressure, P^*, or at some critical $(dP/dt)^*$, the material burns at a "super" rate different from the rates assumed and extrapolated from the lower pressure data base.

(2) Since the burning rate, $\dot{r}$, appears only in the mass generation term, Γ, it should logically follow that one should look at other terms in Γ for use as a discontinuous type function. For example, since $\Gamma = \rho_p \dot{r}(1 - \phi)(3/r_p)$, one might wish to formulate a state equation in which either density, ρ_p, or solids loading, $(1 - \phi)$, increases discontinuously, as some high (critical) pressure.

(3) Again looking at the Γ term, one could assume that at a given instant, a critical pressure could fracture the particles thereby drastically increasing the surface to volume ratio, $(3/r_p)$.

Experimental studies to investigate these possibilities should be investigated even though verifying the results would probably prove very difficult. A limited number of these potential jump-like functions have been studied analytically and are reported herein.

With regards to the second model for DDT, the codes developed and used by Krier-Gokhale [1] and Krier-Kezerle [2] made use of a compaction resistance law that was a function of only the porosity, ϕ, which could be interpreted as the particle stress. Due to the nature of the equations, the minimum porosity always occurred in association with the gas pressure front and thus the stress wave would not propagate into the bed in a manner similar to a compression wave, but merely remain tied to the gas pressure front. In order to obtain the presumed stress wave motion, it was determined that the particle stress would need to be predicted in such a way as to correct the problem encountered earlier in the longer length

beds and to decouple the motion of the stress wave from the motion of the gas pressure front. This was accomplished by locating the point of maximum stress (presumed to be a function of both gas pressure and the drag force) and allowing that stress to propagate forward at a sound speed associated with that stress. The exact form of this sound speed relation will be detailed in Appendix A. Since there are no distinct viscosity type terms associated with the solid-phase equations which would normally account for the motion of this type of disturbance, it was felt that imposing this kind of assumption on the stress wave would simply be a shorthand way of describing the dynamic compression of a "homogeneous solid".

In general the method of investigation presented here is constructed in such a manner so as to provide conditions in which the DDT phenomenon can manifest itself. This is done by assuming that a fraction of the propellant grains are ignited at one end of a closed chamber. The mass generated in the ignition region accelerates the resulting hot gases forward, with the region behind these hot gases rapidly increasing in pressure. This pressure rise is due to the large quantities of gaseous material generated when the propellant is assumed to obey a pressure sensitive burning rate law. At this point it is presumed that one of the two transition mechanisms described above will cause the bed to exhibit a DDT. Regardless of the mechanism which causes the transition, a detonation can be said to have begun when the pressure front precedes the flame front and both move through the bed at a speed which is characteristic of a detonation wave for the type of propellant and initial porosity used. In this report, the flame front will be defined as the locus of points which mark the position in the bed

of the initial particle ignition. The definition of the pressure front will depend on the transition mechanism being considered and thus will be deferred until Chapter Three in which particular cases will be discussed in detail.

CHAPTER TWO

THE GOVERNING EQUATIONS FOR UNSTEADY, ONE-DIMENSIONAL, TWO-PHASE FLOW

2.1 Introduction

The set of conservation equations and constitutive laws that make up the governing equations for this investigation are, for the most part, the same as those found in Krier and Kezerle [2]. As mentioned earlier, the approach taken in developing the conservation equations assumes that there are two distinct continua, one for solids and one for the gas, each moving through its own control volume. Due to this approach the sum of these two volumes must represent an average mixture volume while at the same time the equations which describe the two continua must account for the effect that one flow has on the other. To obtain this, distinct equations for continuity, momentum, and energy are written for each phase which recognize that each phase occupies only part of the total volume and utilizes inertial-coupling terms which disappear when the two sets of equations are summed together. A detailed derivation of these equations is presented in Appendix A of Krier and Kezerle [2]. However, due to the two detonation mechanism theories being considered, certain modifications must be included and will be noted when made.

2.2 Assumptions

The following are the set of assumptions and limitations placed on the governing equations used in this analysis.

(1) Each phase of the flow is a continuum thus allowing for unique derivations.

(2) Although each phase is a continuum, they are considered interdispersed which is reflected in the conservation equations by the presence of inertial-coupling terms.

(3) The flow is quasi-one-dimensional, that is, the total cross-sectional area of the flow is equivalent to the sum of the cross-sectional area of each phase.

(4) During combustion, the solid phase always loses mass to the gas phase (i.e., $\Gamma \leq 0$).

(5) The equations are laminar in that the turbulence resulting from the two-phase nature of the flow has been averaged out.

(6) All gases obey a nonideal Nobel-Abel equation of state with a variable covolume.

(7) All gases are inviscid in nature with the exception of their action in the drag relation.

(8) In those relations which use the gas viscosity or conductivity, these properties are assumed to be functions of temperature.

(9) The specific heats, c_p and c_v, of both phases are considered constant.

(10) The solids obey the Tait equation of state.

(11) Conductive or radiative heat transfer is neglected.

(12) All particles are spherical.

2.3 Conservation Equations

In order to uniquely describe the properties of the two-phase flow, the following nine variables must be determined: ρ_g, ρ_p, u_g, u_p, T_g, T_p, P_g, P_p, and ϕ. Since there are nine unknowns, nine equations must be supplied in order to find a singular solution. The following conservation

equations can be used to provide six of the necessary relations.

Gas Continuity

$$\frac{\partial \rho_1}{\partial t} = - \frac{\partial (\rho_1 u_g)}{\partial x} + \Gamma \tag{2.1}$$

Solid Continuity

$$\frac{\partial \rho_2}{\partial t} = - \frac{\partial (\rho_2 u_p)}{\partial x} - \Gamma \tag{2.2}$$

Gas Momentum

$$\frac{\partial (\rho_1 u_g)}{\partial t} = - \frac{\partial (\rho_1 u_g^2)}{\partial x} - \phi \frac{\partial P_g}{\partial x} - \bar{F} + \Gamma u_p \tag{2.3}$$

Solid Momentum

$$\frac{\partial (\rho_2 u_p)}{\partial t} = - \frac{\partial (\rho_2 u_p^2)}{\partial x} - (1 - \phi) \frac{\partial P_p}{\partial x} + \bar{F} - \Gamma u_p \tag{2.4}$$

Gas Energy

$$\frac{\partial (E_{g_T} \rho_1)}{\partial t} = - \frac{\partial (u_g E_{g_T} \rho_1 + u_g \phi P_g)}{\partial x} + \Gamma \left(\frac{u_p^2}{2} + E_g^{CHEM} \right) - \bar{F} u_p - \dot{Q} \tag{2.5}$$

Particle Energy

$$\frac{\partial (E_{p_T} \rho_2)}{\partial t} = - \frac{\partial (u_p E_{p_T} \rho_2 + u_p (1-\phi) P_p)}{\partial x} + \Gamma \left(\frac{-u_p^2}{2} + E_p^{CHEM} \right) + \bar{F} u_p + \dot{Q} \tag{2.6}$$

Where, we define

Phase densities $\rho_1 = \phi \rho_g$ $\rho_2 = (1-\phi) \rho_p$ (2.7a)

Porosity $\phi = \frac{V_g}{V_{Mix}}$; solid loading: $(1-\phi) = \frac{V_p}{V_{Mix}}$ (2.7b)

Total internal energy (gas)

$$E_{g_T} = E_g + \frac{1}{2} u_g^2 \qquad \text{and} \qquad E_g = c_{v_g} T_g \tag{2.7c}$$*

Total internal energy (particles)

$$E_{p_T} = E_p + \frac{1}{2} u_p^2 \qquad \text{and} \qquad E_p = c_{v_p} T_p \tag{2.7d}$$*

In this case, the subscript "g" denotes the gas phase while the "p" indicates the particle phase. Here, E^{CHEM} refers to the chemical energy released in burning. The seventh and eighth equations needed are the equations of state associated with each phase. For the gas, the Nobel-Able equation is used

$$P_g = \frac{\rho_g R_g T_g}{1-\rho_g B_v} \tag{2.8}$$

where B_v is the covolume, a term that is a function of gas density. The use of B_v results in a useful nonideal equation at high gas pressures. In this study it is assumed that

$$\frac{1}{1-\rho_g B_v} = a + b\rho_g + c\rho_g^2 + d\rho_g^3 \tag{2.9}$$

where a = 1.0, b = 1.0, c = 0.5, d = 0.3, and ρ_g is in grams/cm^3. This equation results from an assumption that the gas particles behave as hard spheres during any interaction. Appendix D will show that one can use Eq. (2.7c) for the gas internal energy given the form of Eqs. (2.8) and (2.9).

---

*Here c_{v_g} = 0.30316 BTU/Lbm°R and c_{v_p} = 0.42442 BTU/Lbm°R. Both are assumed average constants, independent of temperature.

2.4 Constitutive Relation for P_p

As described by Wallis [10], a packed bed placed under a compressive load can be further compacted. However, there is a force which resists this compaction that depends on the stress-strain relationship of the particle lattice which is not necessarily the same as that of a homogeneous solid made from the same material. The compressive load on the bed will be split between the two phases in proportion to the porosity. So the resultant force on the particles will be a function of the porosity, the porosity gradient, and possibly other factors. There can be a variety of formulations that could be used to relate this particle-particle interaction through a stress, which is termed here as P_p. That is,

$$P_p = P_p\ (\phi, \frac{d\phi}{dx}, (\Delta V_{Mix})\ldots \text{ etc.})$$

One formulation would be to assume that P_p is a function of porosity only. This approach, taken by Kuo and Summerfield [11], resulted in an equation of the form

$$P_p = \begin{cases} \dfrac{B[(1-\phi_c)^{-1} - (1-\phi)^{-1}]}{(1-\phi)} & \text{if } \phi \leq \phi_c \\ 0 & \text{if } \phi > \phi_c \end{cases} \tag{2.10}$$

where ϕ_c is the porosity above which the particles do not touch. (See Appendix B.) In order to get some idea of the validity of this equation, the relation for P_p can be used to derive a bulk modulus for the particle lattice which one would expect to increase as the solids loading increases. One defines the bulk modulus, K, as

$$K = \left(-\frac{\partial P_p}{\partial V_{Mix}}\right)\left(V_{Mix}\right) \tag{2.11}$$

which for Eq. (2.10) becomes

$$K = \left\{-B\left[(1-\phi_c)^{-1}(1-\phi)^{-2} - 2(1-\phi)^{-3}\right]\frac{1-\phi}{V_{Mix}}\right\} V_{Mix} \qquad (2.12)$$

In the above relation it can be shown, that for a negligible change in the volume of the solids, that $d\phi/dV_{Mix} = (1-\phi)/V_{Mix}$

As indicated in Fig. 2.1 the bulk modulus does not increase as porosity decreases and is therefore suspect. In addition, this formulation does not take into account certain constraints which are present if one considers only spherical particles. In this case the particle-particle interaction term must prevent compaction below a porosity of $\phi = 0.2595$. This limitation results from the fact that the greatest possible compaction of spherical particles results from a face centered cubic lattice, where

$$\phi_{MIN} = 1 - \left(\frac{16\pi}{3}\right)\left(\frac{\sqrt{2}}{4}\right)^3 = 0.2595 \qquad (2.13)$$

(Details of this calculation and other limits on the porosity of sphere can be found in Appendix B.) Given this type of constraint, there is no guarantee that Eq. (2.10) would under all conditions provide such a proper lower packing limit.

One approach toward satisfying this limit is to modify the particle momentum equation so that the particles cannot be accelerated forward once critical lower porosity level is reached. A modification of this type would cause Eq. (2.4) to look like

$$\frac{\partial(\rho_2 u_p)}{\partial t} = -\frac{\partial(\rho_2 u_p^2)}{\partial x} - \Gamma u_p + \left[1 - f(\phi)\right]\left[\overline{F} - (1-\phi)\frac{\partial P_p}{\partial x}\right] \qquad (2.14)$$

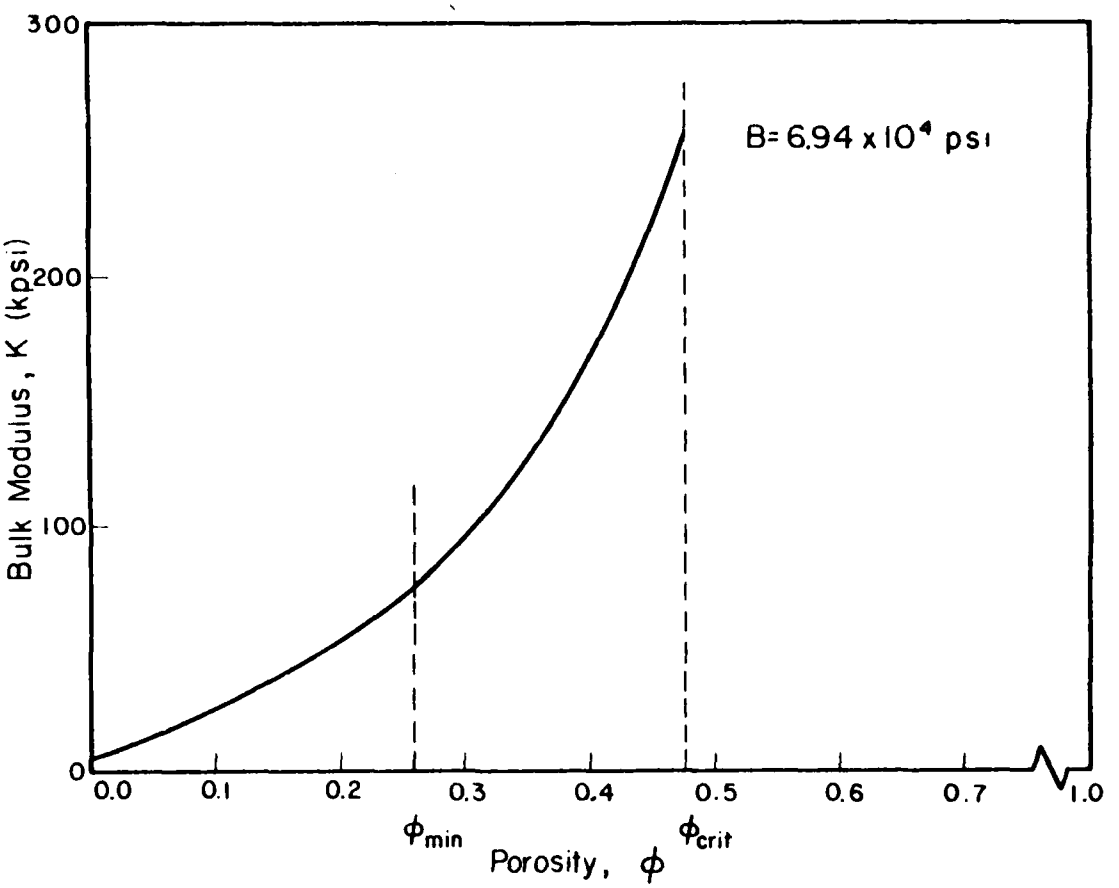

Fig. 2.1 Bulk modulus versus porosity for particle-particle interaction law of Kuo and Summerfield [11].

where $f(\phi)$ is defined as

$$f(\phi) = \begin{cases} 0 & \phi > \phi_{UL} \\ \left(\dfrac{\phi_{UL}-\phi}{\phi_{UL}-\phi_{LL}}\right)^{\ell} & \phi_{UL} \geq \phi \geq \phi_{LL} \\ 1.0 & \phi < \phi_{LL} \end{cases} \tag{2.15}$$

Here ϕ_{UL} is the upper limit on the porosity for a packed bed, ϕ_{LL} lower limit on the porosity, and ℓ is an exponent chosen to reflect the properties of the particle lattice. Figure 2.2 shows the variation of $f(\phi)$ with porosity for various values of the constant, ℓ.

Equation (2.14) indicates that the drag force has a decreasing effect on the particle acceleration as some lower limit to the porosity is reached. However, the gas phase will still feel the full effect of the drag on its deceleration. (Recall that most experiments used to determine the drag relation for a porous media are made through a bed of essentially non-moving particles.) The apparent discrepancy in these two statements is the origin of the constitutive relation for P_p. This relation comes about through the assumption that the drag force not involved in accelerating the particles is instead stressing the particle bed, which is the definition for P_p. Thus, P_p is now related to the drag, $\overline{F}$, in the following manner, namely

$$P_p = (\overline{F}) \left(\frac{\phi_{UL}-\phi}{\phi_{UL}-\phi_{LL}}\right)^{\ell} \tag{2.16}$$

An important observation about this type of formulation, i.e., either Eq. (2.10) or (2.16), is that the stress on the particles is

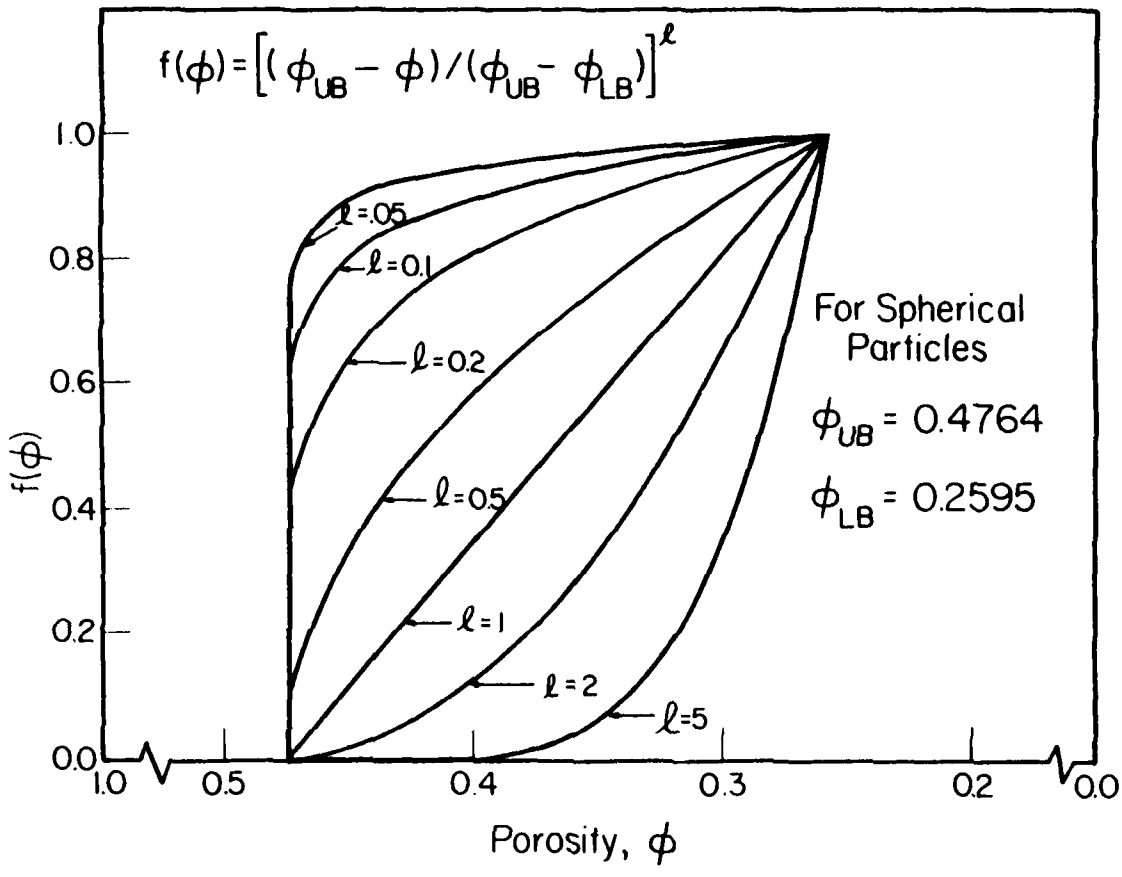

Fig. 2.2 Variation of particle-particle resistance function, $f(\phi)$, with porosity.

localized. The particles are not dynamically loaded as would happen if the solid were cemented into a pseudo-homogeneous material. In this latter case, fundamental continuum mechanics predicts that a stress at one point in the material would propagate into an unstressed region at a rate which is proportional to both the average sound speed and the particle velocity (i.e., a right running or left running characteristic). Since the particles are now considered compressible, the sound speed will vary proportionately with the solid phase density, the details of which are presented in Appendix A.

Therefore, an alternate constitutive relation (if one wishes to include dynamic compressibility) is to model the particles as a contacting, but obviously very porous, solid and to assume that while the particles are in contact with each other a stress wave whose magnitude is defined in Eq. (2.16) moves through the bed at a speed equal to the sum of the sound speed behind the wave and the local particle velocity.

2.5 Additional Constitutive Relations

In order to complete the analysis of Eqs. (2.1) through (2.6) it is necessary to define certain criteria and interaction laws with the use of known physical relationships or through the use of experimentally established laws. These include

(1) An ignition criterion based on the bulk temperature of the particles.

(2) The propellant burning rate, $\dot{r}_p$.

(3) The gas generation rate, Γ, which for spherical particles is

$$\Gamma = \left(\frac{3}{r_p}\right)(1-\phi)\rho_p \dot{r}_p \tag{2.17}$$

(4) The interphase heat transfer rate, $\dot{Q}$, which is defined as

$$\dot{Q} = h_{pg}(T_g - T_p)(\phi)(S/V)_p \tag{2.18}$$

where $(S/V)_p$ is the surface to volume ratio for the particles and h_{pg} is the interphase heat transfer coefficient, which is discussed in Appendix C.

(5) The interphase drag, $\bar{F}$, which is defined as

$$\bar{F} = \left[\frac{\mu(U_g - U_p)(1-\phi)^2}{4r_p^2\,\phi^2}\right] f_{pg} \tag{2.19}$$

where μ is the gas phase viscosity and f_{pg} is the interphase drag coefficient which is presented in Appendix C.

(6) The temperature dependent gas viscosity.

The constitutive relations presented here differ very little from those presented in Krier and Kezerle [2], where additional background has been given.

2.6 Numerical Integration Technique

In order to solve this set of hyperbolic nonlinear partial differential equations, the two step predictor-corrector numerical integration scheme developed by MacCormack was used. This is the same type of scheme as detailed in Ref. 2 with a few exceptions which will be outlined below.

Throughout this investigation the total bed length was usually set at 3 inches with the Δx set at 0.05 inches. This value of Δx was determined to provide the largest mesh size for repeatable calculations. The value of L = 3 inches gave moderate computing charges. The Δt

(for this Δx) is calculated using the Courant, Friedrichs, Levy stability criteria [12], namely

$$\frac{\Delta t[C + |u|]}{\Delta x} \leq 1 \tag{2.20}$$

Here, C and $|u|$ are the maximum gas phase or solid phase sound speed and phase velocity, respectively, and not the mixture average values as utilized by Krier and Kezerle [2]. This was done to provide more stable solutions for all classes of problems studied here. To satisfy the inequality in Eq. (2.20) the value of unity was set equal to 0.7.

Even with the use of a guaranteed stability criterion for the linear form of the hyberbolic equations, there were conditions under which the computer code would become unstable for our nonlinear set of equations. Although it was found that these instabilities, caused by severe gradients in one or more of the partial differential equations, could be removed in some cases by utilizing a smaller Δx (and its associated reduced Δt), an artificial smoothing routine was adopted to insure stability. A detailed discussion of this smoothing technique can be found in the Ph.D. dissertation of S. S. Gokhale [13]. The addition of this smoothing technique did not take place until later in this investigation. Thus, most of the results presented here did not employ artificial smoothing and hence the range of input parameters was often limited.

The boundary conditions chosen for this investigation are the same as those used by Krier and Kezerle with the exception of the choice of gradient at the wall. In this work the code was programmed to insure that all gradient terms at both end walls are zero at all times.

Two sets of initial conditions were utilized in this investigation, the choice of which one to use being somewhat arbitrary. The first set of conditions were similar in form to those used by Krier and Kezerle, namely,

(1) T_g and T_p were set by a lineal decay over the first five grid points.

(2) P_g was subject to an exponential decay throughout the bed.

(3) Velocities of both phases were set to zero over the entire length of the bed.

(4) The porosity was set at some selected value which was uniform across the total bed length.

The second set of initial conditions came about from the feeling that it was inappropriate to model a situation in which there is no gas motion in the presence of a gas pressure gradient. Thus, the second set of conditions assumes that additionally at $t = 0$, the pressure is a uniformly low constant value.

CHAPTER THREE

COMPUTED RESULTS

3.1 Introduction

As discussed in Chapter One, the investigations described in this report consist of a more detailed analysis of the fluid mechanical properties leading up to the detonation transition of a porous reactive bed as opposed to those studies carried out by Krier-Gokhale [1] and Krier-Kezerle [2]. Specifically, changes in the solid phase equations used by Krier and Kezerle were made in an attempt to gain a better understanding of the properties of a bed of closely packed particles and to determine what conditions are required for this bed to exhibit a DDT. These changes included the addition of a solid phase state equation, the definition and use of a particle pressure, and modifications to some of the various constitutive laws which are necessary to completely describe the flow. (See Appendix C.) A discussion of the effects of each of these changes on the unsteady fluid dynamics in the bed will be presented below.

However, to provide a comparison with the calculations presented in the earlier works of Krier-Gokhale and Krier-Kezerle, a baseline case was constructed to closely reflect typical results found in those studies. Table 3.1 lists the most important inputs for both the baseline calculation and for the subsequent parameter variation calculations. The results of these calculations will be presented using one or more of the following graphical formats: pressure, temperature and porosity versus distance, and the ignition front position (flame front) versus time.

TABLE 3.1

TYPICAL INPUT DATA

Parameter	Value	
	English	SIU
Initial bed temperature, T_g, T_p	530°R	294°K
Ignition energy, ΔE_{IGN}	165 BTU/LB_m	383 KJ/Kg
Ignition temperature, T_{IGN}	545°R	303°K
Initial bed porosity	0.4	0.4
Propellant burning rate constant, b_1	9.0×10^{-4} in/sec-psi^n	3.32×10^{-7} cm/sec-Pa^n
Propellant burning rate index, n	0.90	0.90
Initial propellant density, ρ_p	0.0571 LB_m/in^3	1.581 gm/cm^3
Initial bulk modulus, K_o	2.00×10^5 LB_f/in	1.38 GPa
Constant volume specific heat of the propellant, c_{v_p}	0.30316 BTU/LB_m°R	1.2665 J/gm°K
Initial grain radius, r_p	4.0×10^{-3} in	0.1016 mm
Chemical energy released, $E_{CHEM} = (E_g - E_p)^{CHEM}$	2360.9 BTU/LB_m	5479.6 KJ/Kg
Molecular weight of the gas, MW	22.6 LB_m/LB_{mole}	
Covolume of propellant gas, B_v	29.85 in^3/LB_m	1.078 cm^3/gm
Specific heat ratio of gas, γ	1.252	1.252
Constant volume specific heat of gas, c_{v_g}	0.42442 BTU/LB_m°R	1.7731 Joule/gm-°K
Gas viscosity, μ_g	2.49×10^{-6} LB_m/in-sec	4.45×10^{-4} gm/cm-sec
Universal gas constant, $\bar{R}$	1.9869 BTU/LB_{mole}°R	8.3005 Joule/gm-°K
Total bed length, L_B	3.0 in	76.2 mm
Percent heat transfer to particle after ignition	10%	10%

3.2 Baseline Case

An initial baseline case was constructed that closely resembles the conditions studied by Krier and Kezerle [2]. This calculation assumes that the solid phase is incompressible and that the packed bed obeys the particle-particle interaction law develed by Kuo-Summerfield [11]. As in Krier-Kezerle an initial uniform porosity of 0.40 (solids loading of 60%) was used.

Upon comparison of the two baseline cases, it was found that after a certain percentage of the bed had been ignited, the flow properties of each were roughly the same in magnitude. However, the time necessary to reach that percentage of ignition was now approximately 30 percent larger when compared to those results reported in Ref. 2. This was due mainly to differences in the value specified for the specific heat for the propellant and the coefficient in the interphase drag relation currently being used.

The development of the gas pressure distribution (Fig. 3.1) obviously is similar to that presented by Krier and Kezerle in that the pressure front shows a distinct tendency to build into a continental divide. A continental divide is defined here as a gas pressure spike which usually appears in the region of the deflagration front. This spike is significant in that the pressure gradients which have now been formed will cause the gas to move both towards and away from the burning zone. The reason that such a divide forms is due to the continuing availability of gas volume in the section initially ignited as the propellant burns away in an ever accelerating manner as the pressure rises. A typical value for this gradient

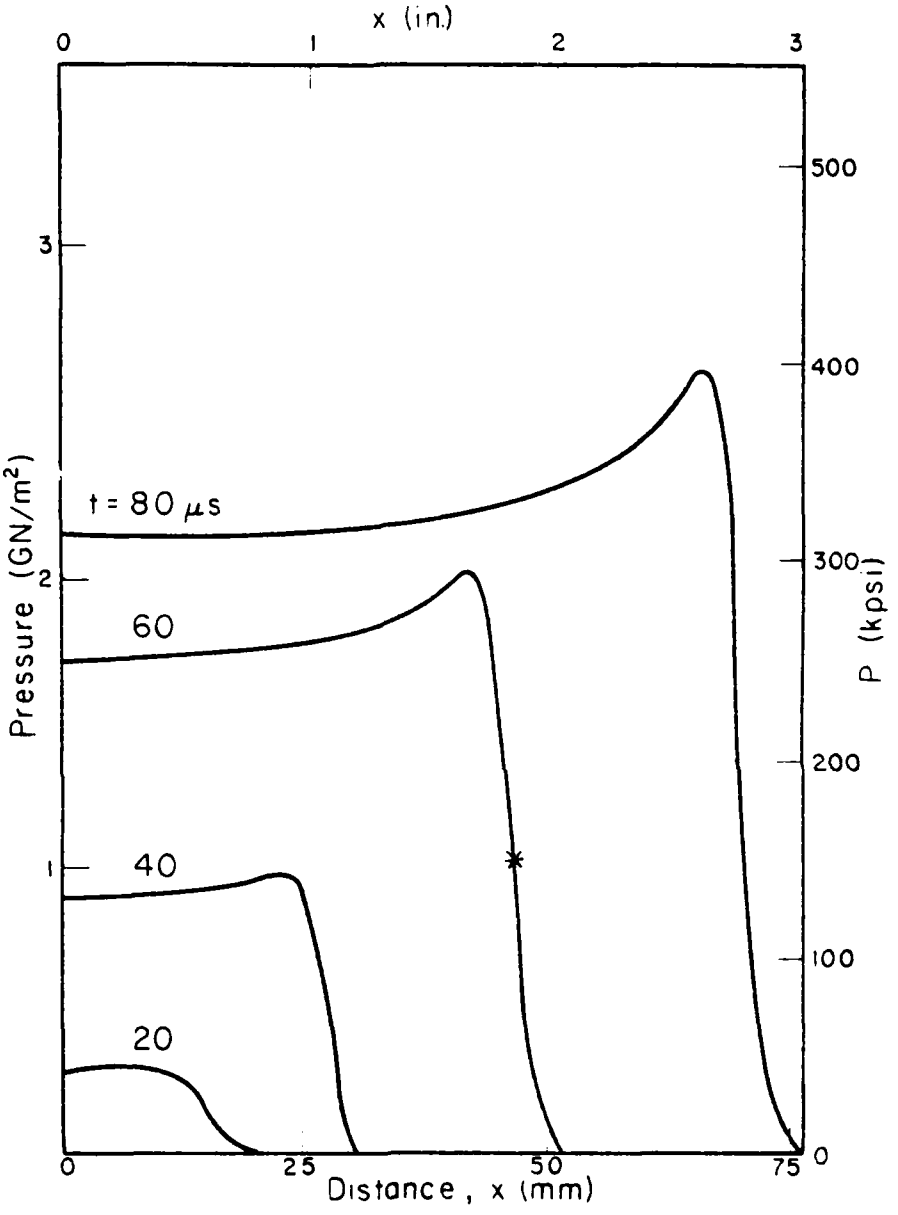

Fig. 3.1 Pressure distribution during flame spreading in an initially packed bed of small particles of solid propellant. (Figs. 3.2-3.4 show variation in other flow parameters for the same case as calculated for Fig. 3.1.)

at t = 60 μsec and x = 44.5 mm (1.75 in) is of the order of -0.3136 GPa/mm (-1.16×10^6 psi/in)

Figure 3.2 shows the progression of the ignition point through the bed; this locus is defined as the flame front. As mentioned earlier the total burn time is somewhat longer than seen in the Krier-Kezerle baseline, but the velocities at various x locations are approximately the same. The pressure front as shown in this figure was defined as being the locus of points midway between the peak of the continental divide and the ambient pressure level in front of the buildup. Using this definition, the location of the pressure front at 60 μsec has been indicated on Fig. 3.1 with an *.

A comparison of the particle and gas temperature development is shown in Fig. 3.3. Again the continental divide structure seen in the gas temperature presented in Krier-Kezerle is seen here. The severe gas temperature spike seen at 80 μsec is due more to the encounter of pressure reflection with the end wall than to some drastic change in the progression of the deflagration wave. It should be noted that no disassociation of the gases is assumed in these calculations. If real gas properties were being assumed, temperatures of this magnitude (i.e., 7500°R or greater) would certainly cause the gases to disassociate, reducing the high values predicted. The particle temperature profiles exhibit a structure similar to those presented in Ref. 2, i.e., no continental divide, but the magnitude of the temperature at later times during the convective flow sequence was brought about by the extremely small volume taken up by the solid phase (porosities of 0.96 or greater) and the high temperature of the surrounding gas. Under such conditions, even the restricted heat transfer

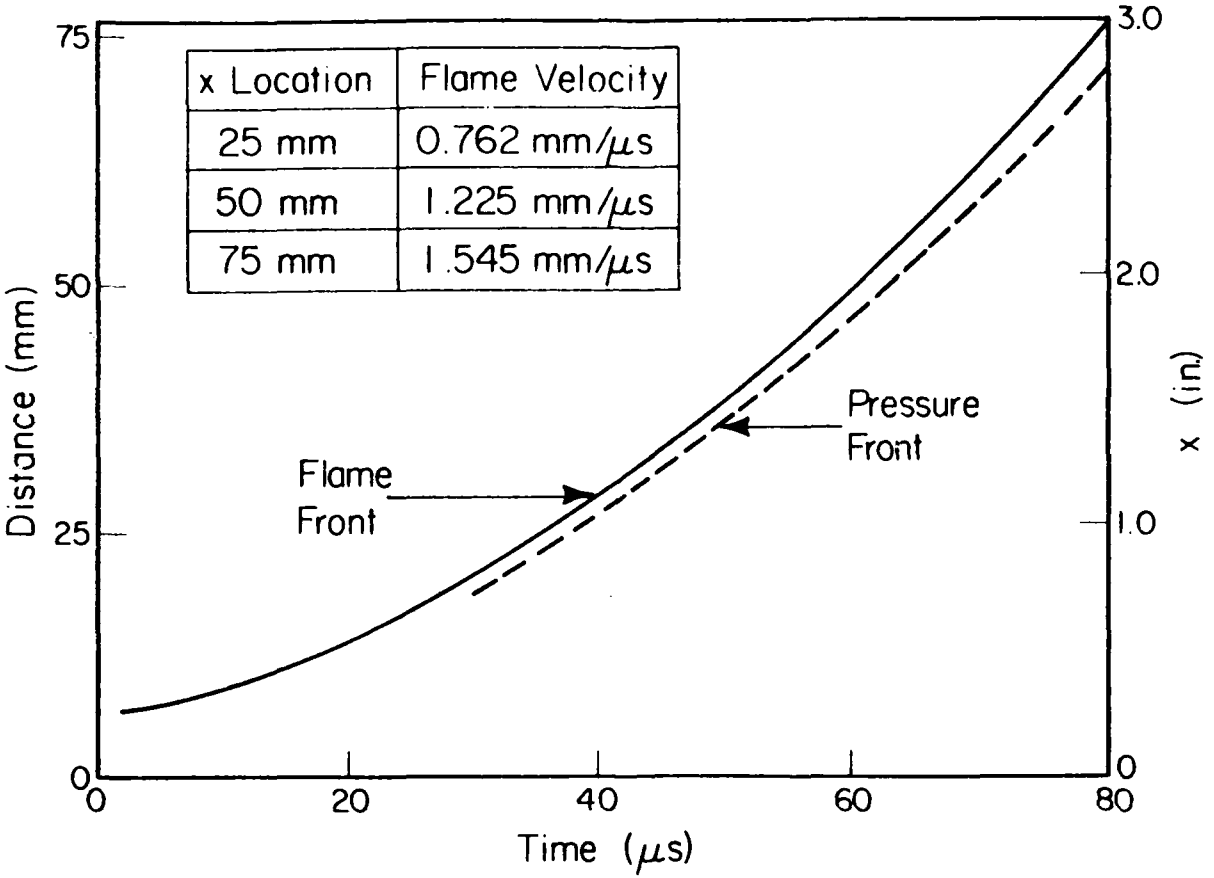

Fig. 3.2 Locus of ignition (flame) front and pressure front, the latter derived from pressure versus distance distribution.

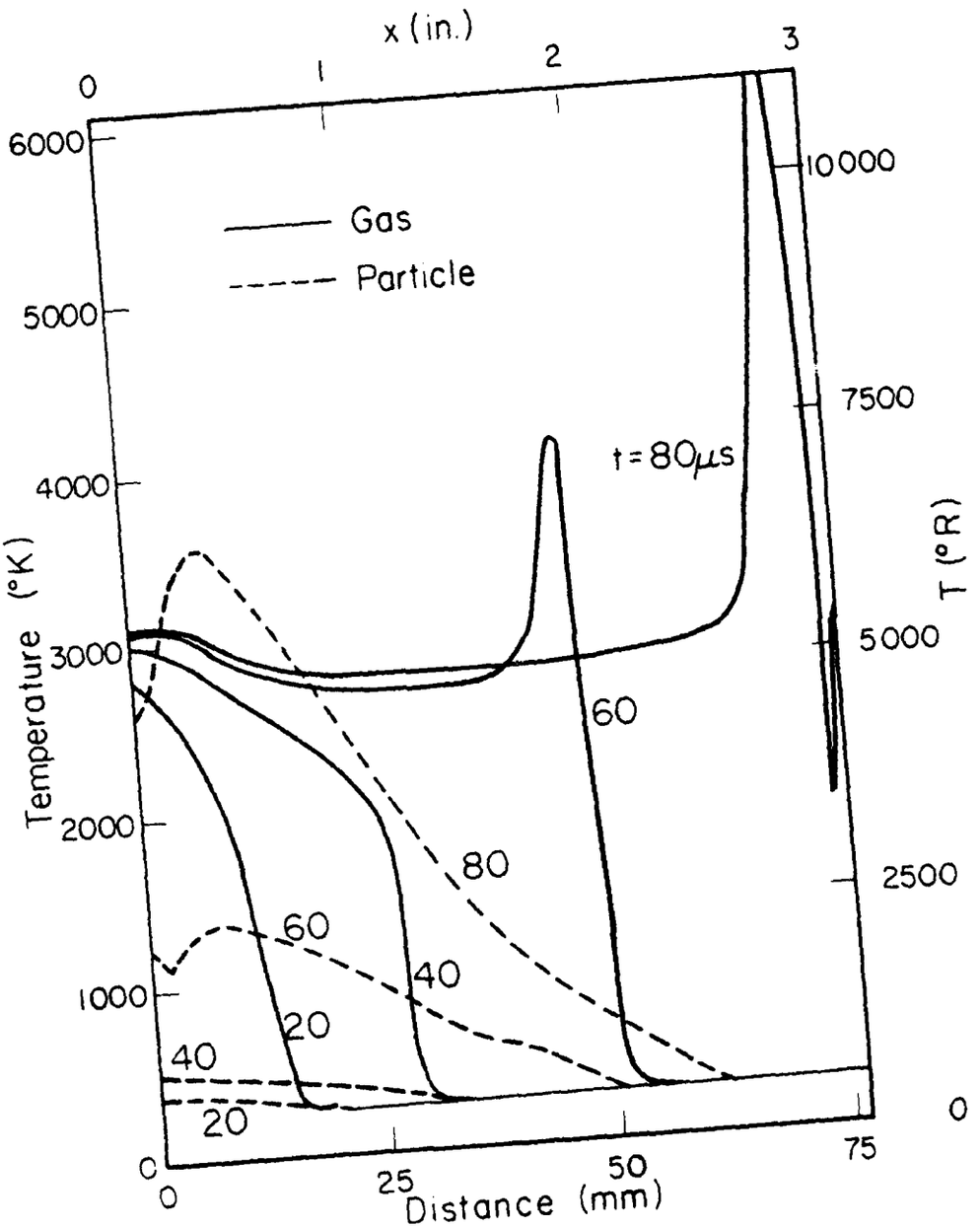

Fig. 3.3 Gas and particle temperature distribution history.

from the gas (10 percent after ignition) causes a tremendous increase in the temperature of the particles. Since it was felt that this type of phenomenon was a product of the calculation procedure and not in fact real, subsequent cases remove all heat transfer at the higher levels of porosity ($\phi \geq 0.96$). Even with the extremely high particle temperature exhibited in this case, the progress of the convective process has not been affected since the particle phase at this point is an insignificant fraction of the flow.

The porosity distribution (Fig. 3.4) exhibits a contour which is characterized by a zone in which the material is compressed to a porosity lower than the original value. The point of lowest porosity is always located ahead of the peak pressure point, but it should be noted that the compressed zone does not prevent the point of first ignition from moving through this zone. This ignition point was always found to occur at relatively low gas temperature, typically less than 1000°R. It would seem that the bed would need to be much more severely compacted to prevent any hot gases from "seeping through" before a significant pressure can be built up behind the ignition front. This seems to be a prerequisite for transition to detonation.

3.3 Variation in the Boundary Conditions and Grid Spacing

The effects of the choice of initial conditions and boundary conditions on a fluid mechanical problem are known to be significant and this situation is no exception. In previous analyses by Krier-Gokhale [1] and Krier-Kezerle [2] the boundary conditions were chosen in such a way that gradients at the wall were not constant with time.

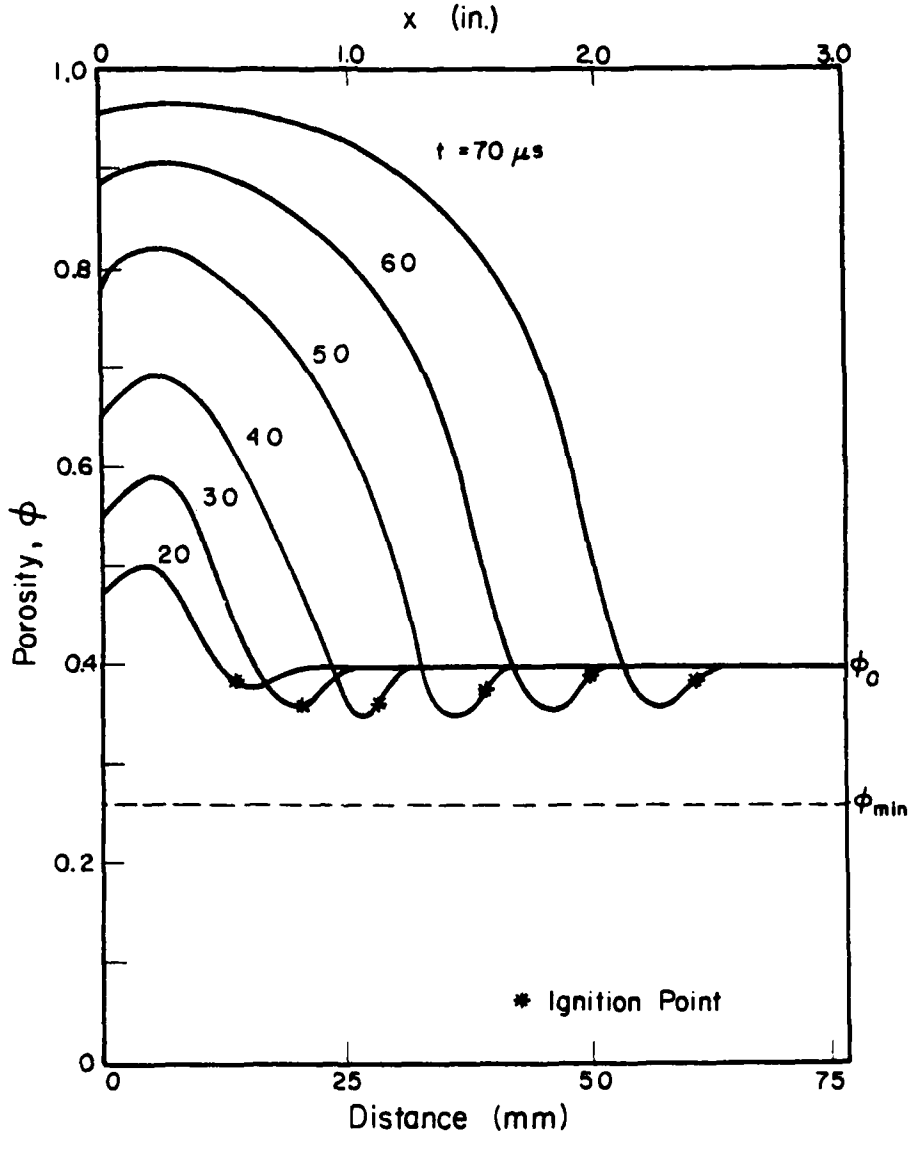

Fig. 3.4 Porosity distribution history. The (*) indicates the location of the ignition front.

It was decided here that the problem would be specified to assure that at every instant the flow gradients would be zero at least at one "wall". Such zero-gradient boundary conditions are obviously valid from an ignition and flame spreading sequence which begins in the middle of a packed bed. One can then analyze the problem in one direction only specifying the "middle" as $x = 0$. Using this approach effectively removes at the wall the $\partial/\partial x$ terms that appear in the six conservation equations. By symmetry arguments the gas and particle velocities are zero at the ignition-end wall and are zero at the far wall because of the imposed impenetrable boundary. Due to the imposed boundary conditions, care must be taken that the initial conditions ($t = 0$) satisfy all boundary conditions.

Having established the conditions for which zero-gradient boundary conditions could be used, a comparison between the use of these boundary conditions with the non-zero boundary conditions used in the baseline is presented in Fig. 3.5. The sensitivity of the flow to this change appears to be due to the fact that the zero gradient assumption effectively removes all influence of any gradient terms from the first and last grid space. This is especially significant during the early development of the deflagration since it is these gradient terms in the conservation equations which give the gases the initial impetus to move forward.

Since the initial conditions are the same in both cases, the mass generation rate will at first be approximately the same. But as the deflagration process continues, a slight change does develop as shown in the results given in Table 3.2. This information indicates that when the ignition point reaches a certain location, the zero-gradient case allows burning for a longer period of time due to the slower progression of the flame

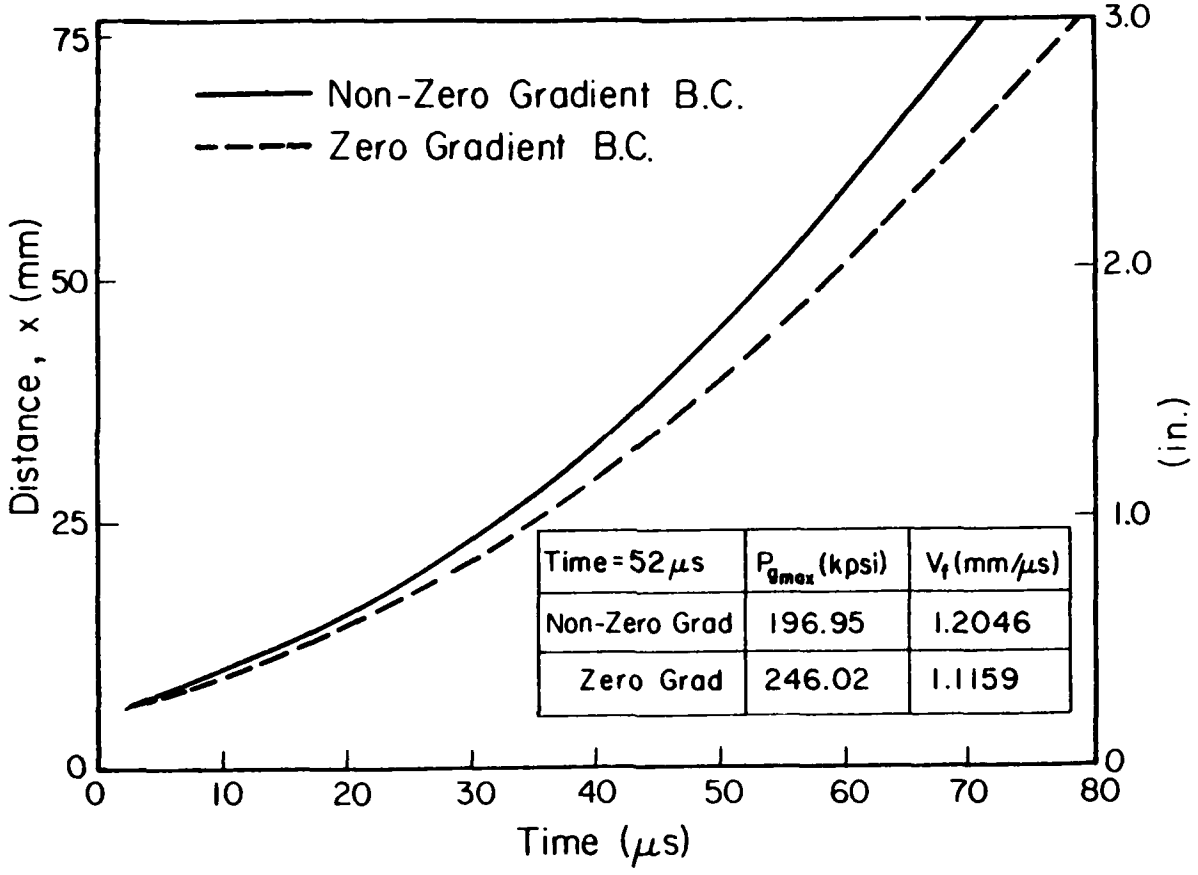

Fig. 3.5 Flame front comparison for cases with zero gradient and non-zero gradient wall boundary condition.

through bed. Thus the propellant has had time to generate more gas in a fixed amount of space which accounts for the higher gas pressure.

TABLE 3.2

Ignition Point at 50 mm (1.95 in)			
	Time (μsec)	Pg_{max} (Kpsi)	V_t (mm/μsec)
Zero gradient	58.9	291.5	1.26
Non-zero gradient	53.9	213.6	1.55

The choice of the grid spacing in any numerical integration scheme is as of much concern as the choice of boundary conditions. Once a bed length, L, is specified one would wish to determine the minimum number of grid spaces which will adequately handle all representations of spacial derivatives, in order to reduce computation costs and the number of integrations required. Table 3.3 shows that for the range of Δx used (which was found to be large enough to observe the overall trends), there is not much difference in the final gas pressure and, to a certain extent, in the total time needed to ignite the entire bed. However, the total number of integrations needed to complete the calculations is almost inversely proportional to Δx, as indicated in the table. Figure 3.6 was then constructed in an attempt to determine at what point a diminishing return was being obtained from decreases in Δx. As can be seen, there is not much

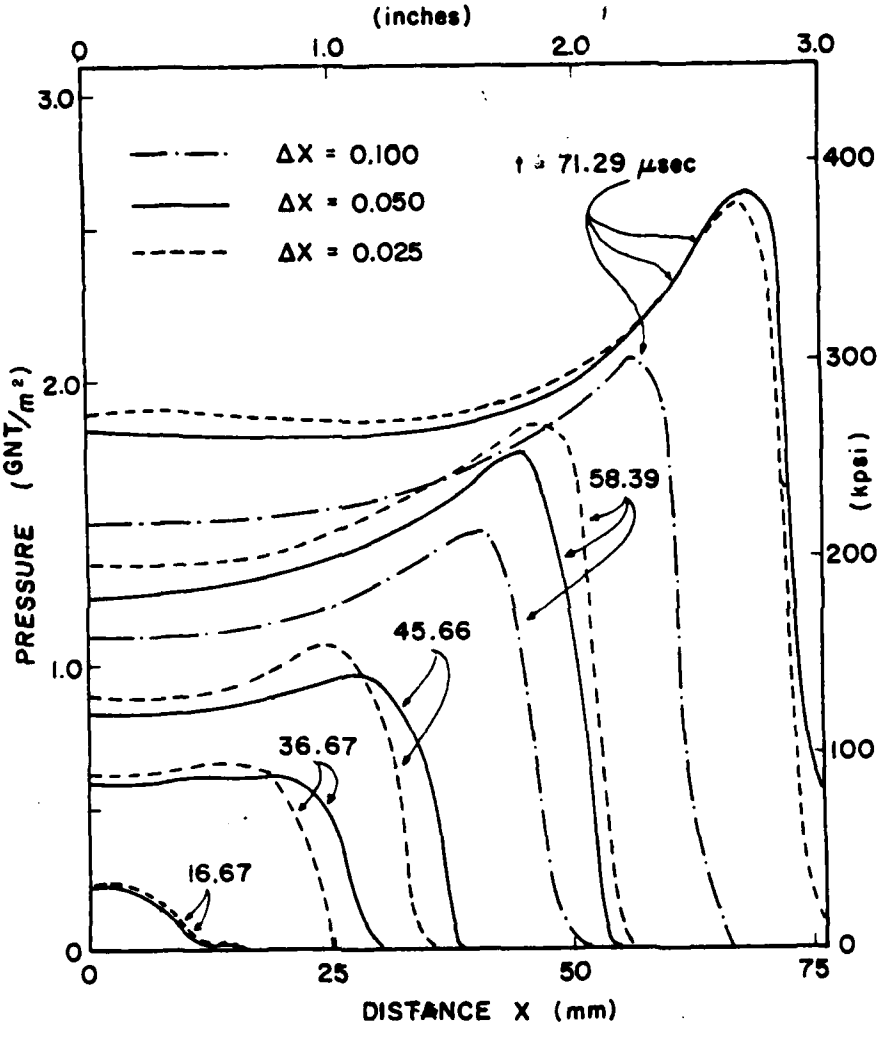

Fig. 3.6 Effects of grid spacing on the gas pressure distribution history.

TABLE 3.3

Ignition Point at 76.2 mm (3.0 in)			
Δx	t (μsec)	Pg_{max} (Kpsi)	Integrations
0.100	76.76	383.0	84
0.050	72.57	385.2	145
0.025	71.29	379.8	280

variation between a Δx of 0.050 and 0.025. This led to a decision to us a Δx of 0.050 in all subsequent calculations since the results were close to those obtained using smaller values of Δx. From to to time this comparison was repeated for other flow situations to insure that the results were essentially insensitive to the chosen Δx value.

3.4 Variation in Propellant Properties

Experimental investigations of the DDT phenomenon in porous beds carried thus far are in basic agreement concerning the necessity for a rapid pressure buildup during the deflagration phase. Figures 3.7 and 3.8 provide a comparison of the pressure buildup and flame spreading rate for two different propellants (both assumed incompressible). The propellant labeled "energetic composite" has properties of a HMX modified propellant and reflects the type of input data throughout this investigation. On the other hand, the data used for the propellant labeled "single base" is more typical of the nitrocellulose propellants. As can be seen, the energetic

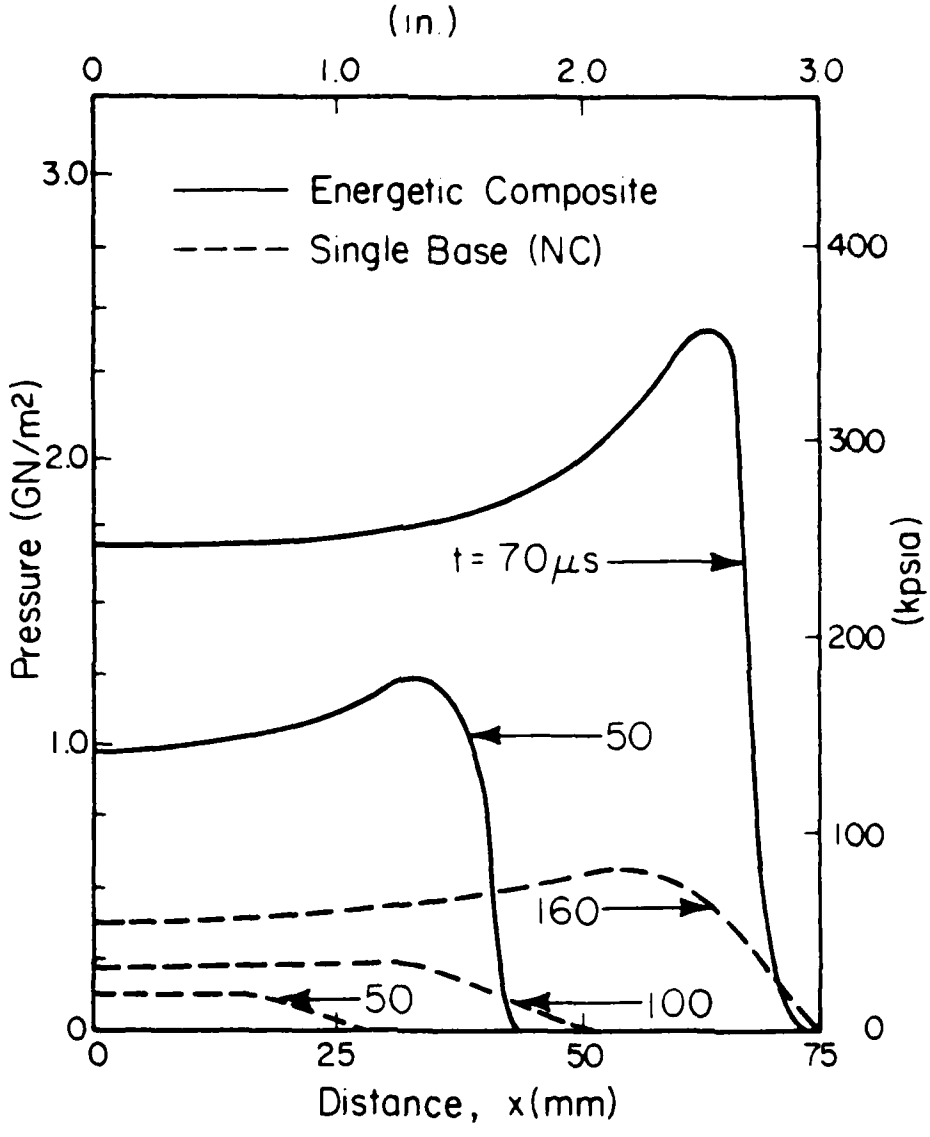

Fig. 3.7 Effects of propellant energy content on the gas pressure distribution history.

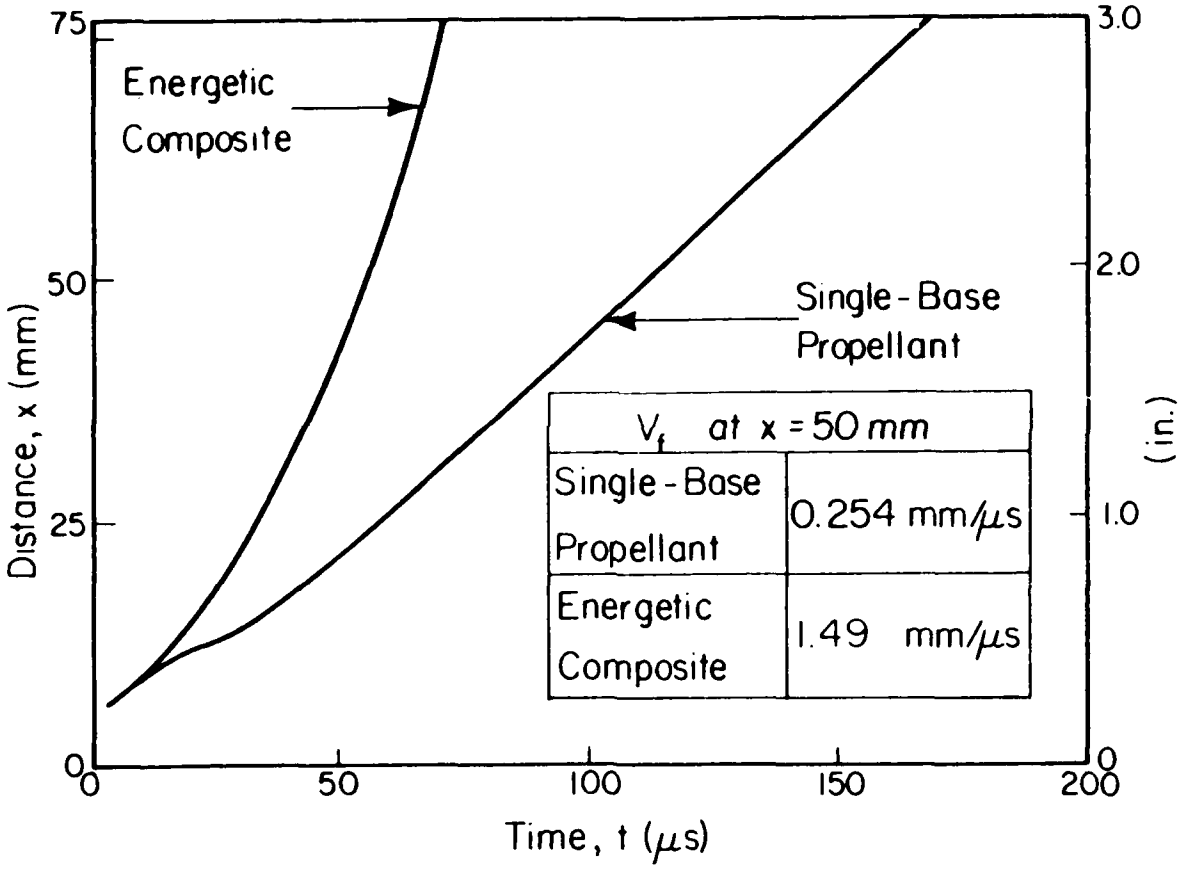

Fig. 3.8 Flame front comparison based on propellant energy content.

propellant has nearly burned through the entire bed after 70 μsec having generated a peak pressure of approximately 350 Kpsi. At this same instant, the single base propellant has ignited only half of its bed, generating a peak gas pressure of only 25 Kpsi. This indicates the expected result that conditions which might lead to shock formation and eventual detonation require high energy and relatively rapid burning rate propellant for a given bed solids loading and granulation.

However, it should be noted that the pressures predicted for the energetic compositie in Fig. 3.7 are much greater than those reported in certain experiments with porous explosives, in which a DDT occurred. (See the comment by R. D. Bernecker to the results reported by Krier and Kezerle in the Seventeenth Combustion Symposium.) The assumption of an incompressible solid is one reason for such relatively high pressures. A possible remedy for this situation is a reduction in the volume taken up by the solids thus leaving a larger volume into which the gas can expand. This can be accomplished by assuming that the particles are compressible. As mentioned earlier, a modified Tait equation gives

$$\rho_p = \rho_{o_p}\left[\frac{3p}{K_o} + 1\right]^{1/3} \tag{3.1}$$

The effect of this type of state equation on the particle density, and thus on its radius, is shown in Table 3.4 for $K_o = 2.00 \times 10^5$ psi (a soft plastic). In order to conserve the particle mass as the density increases the particle size must decrease according to the ratio, $(r/r_o) = (\rho/\rho_o)^{1/3}$.

TABLE 3.4

P (psi)	ρ/ρ_o	r/r_o
50,000	1.205	0.5714
100,000	1.357	0.4000
150,000	1.481	0.3077

Figure 3.9 shows the drastic reduction in the gas pressure that is predicted with the inclusion of this particle state equation. At any particular time, the magnitude of that pressure is nearly cut in half. Surprisingly, Fig. 3.10 shows that there is no significant reduction in the time needed to completely ignite the bed. This is caused by the fact that the decrease in particle radius allows an increase in bed porosity which allows more hot gases to move farther into the bed in a shorter period of time. However, the lower gas pressures and pressure gradients caused by this increase in porosity have exactly the opposite effect in that the acceleration terms in the gas momentum equation are reduced yielding lower forward gas velocities. The net effect of these two phenomena is to effectively cancel each other out, thus causing little change in the flame front curve.

The significant lowering of the gas pressure also has its effect on the temperatures within the bed. Figure 3.11 shows the reduction of the gas temperature to much more reasonable levels when compared to results obtained from a comparable incompressible case. Again, the high temperatures

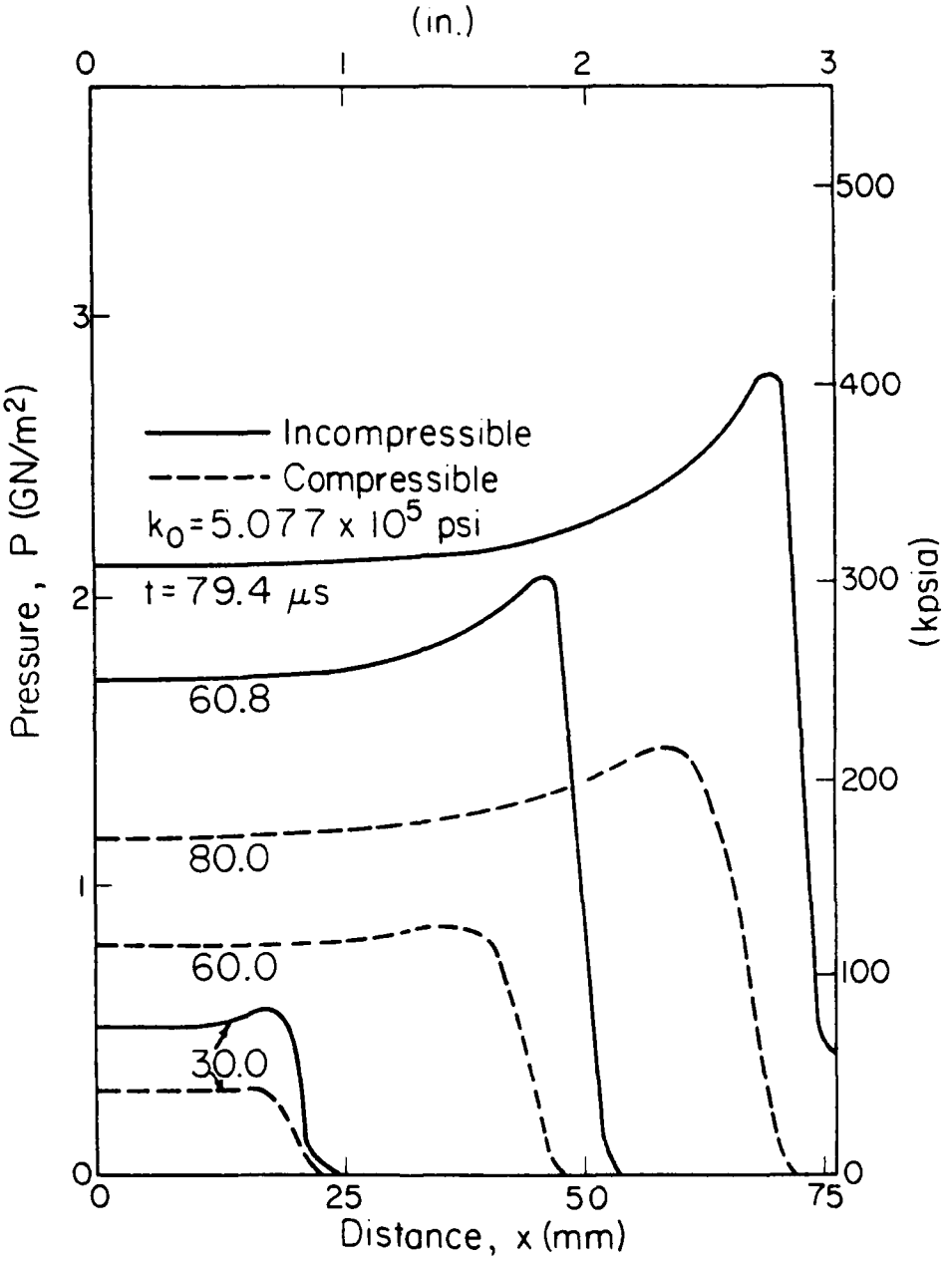

Fig. 3.9 Pressure distribution history comparing the incompressible solid to a compressible material.

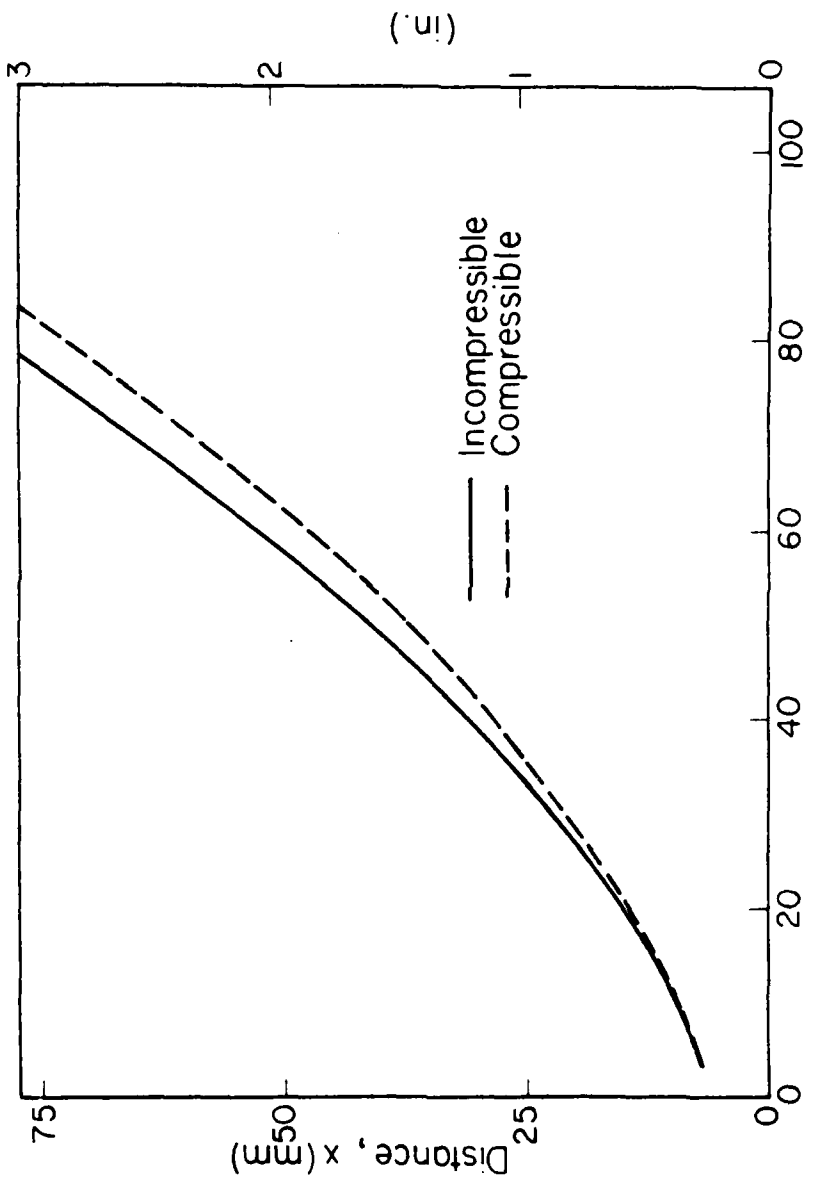

Fig. 3.10 Flame front locus as a function of the solid phase compressibility.

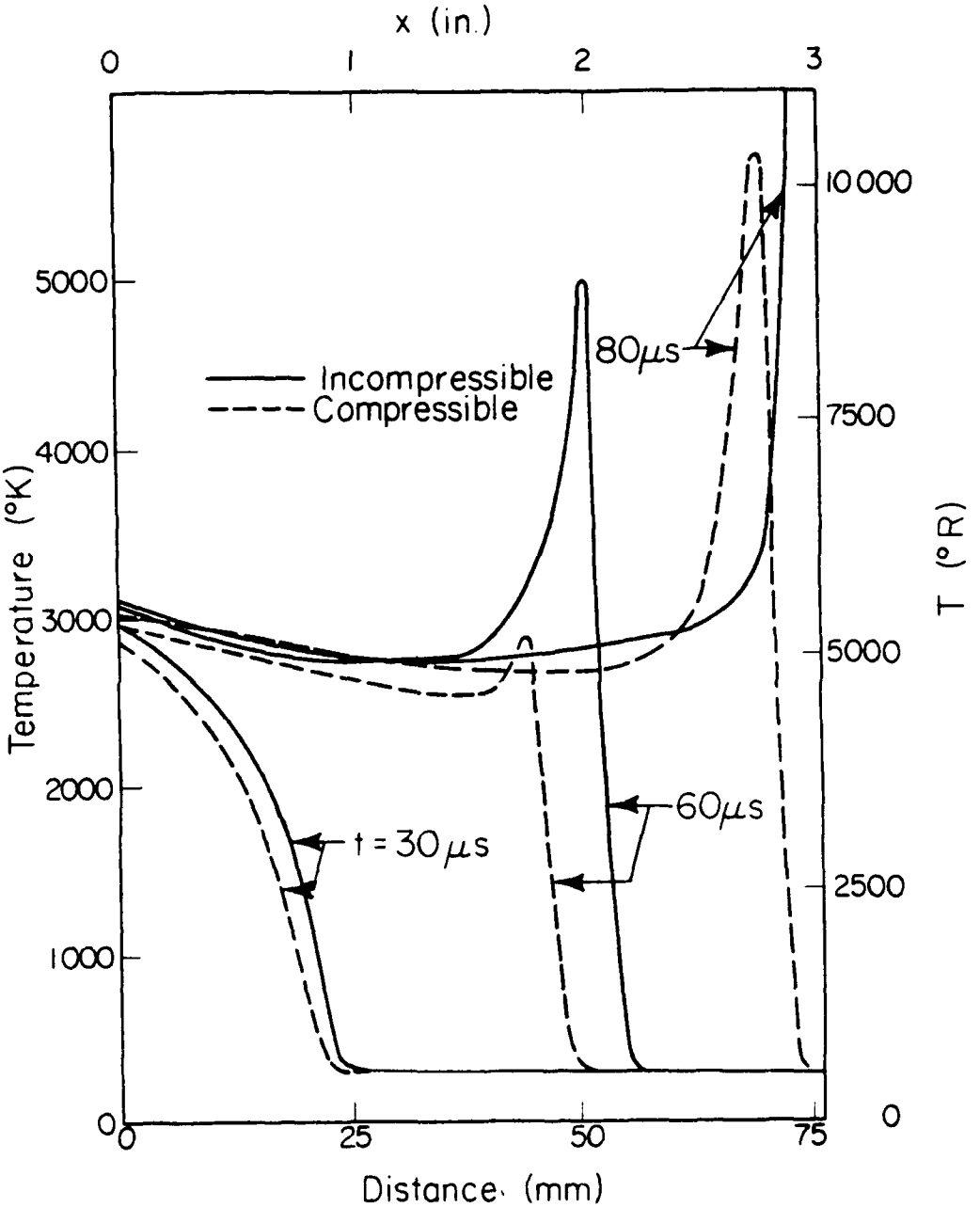

Fig. 3.11 Gas temperature comparison as a function of the solid phase compressibility.

at the far end wall are due to a reflection from that wall rather than from some significant change in the burning process. The particle temperatures exhibited in the compressible case were also much lower due to the reduction in the heat transfer from the gas.

Figures 3.12 and 3.13 allow for a comparison of the effects that two different values of the initial bulk modulus have on the properties of the system. The value of $K_o = 5.077 \times 10^5$ psi was obtained from Traver et al. [8] who were investigating the DDT phenomenon in homogeneous solid materials. The second value of the bulk modulus used ($K_o = 2.00 \times 10^5$ psi) was obtained from the sound speed calculation for the solids which was used by Krier and Kezerle as part of their stability criterion. This value was found to be typical of a soft plastic type material.

It should be noted in Fig. 3.13 that for the $K_o = \infty$ (incompressible) case, the entire bed did not ignite. This failure was due to the presence of numerical instabilities within the integration scheme. This type of problem was found to occur in regions of very steep gradients which for this case was brought about by a slight increase in the magnitude of the interphase drag. This sort of problem, and measures which can be used to correct it, are the subject of the next section.

3.5 Numerical Smoothing Techniques

The onset of severe gradients within the bed often caused a situation in which the numerical integration scheme exceeded its capacity to provide reasonable answers. The result was usually an overshoot of the absolute temperature or pressure into the negative (and thus physically impossible) region. Despite the extensive use of artificial damping

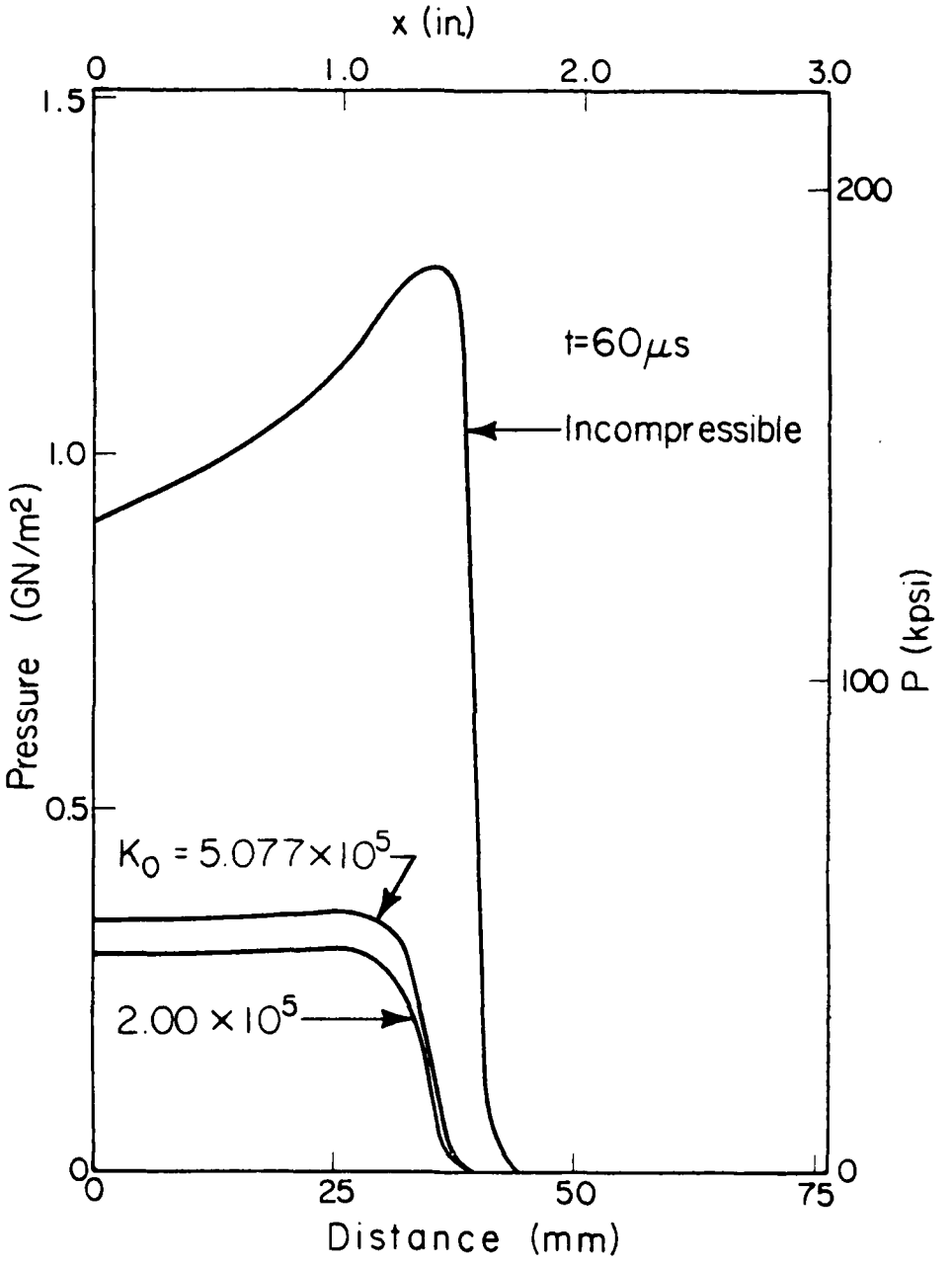

Fig. 3.12 Pressure distribution as a function of the propellant bulk modulus (at time, t = 60 μsec).

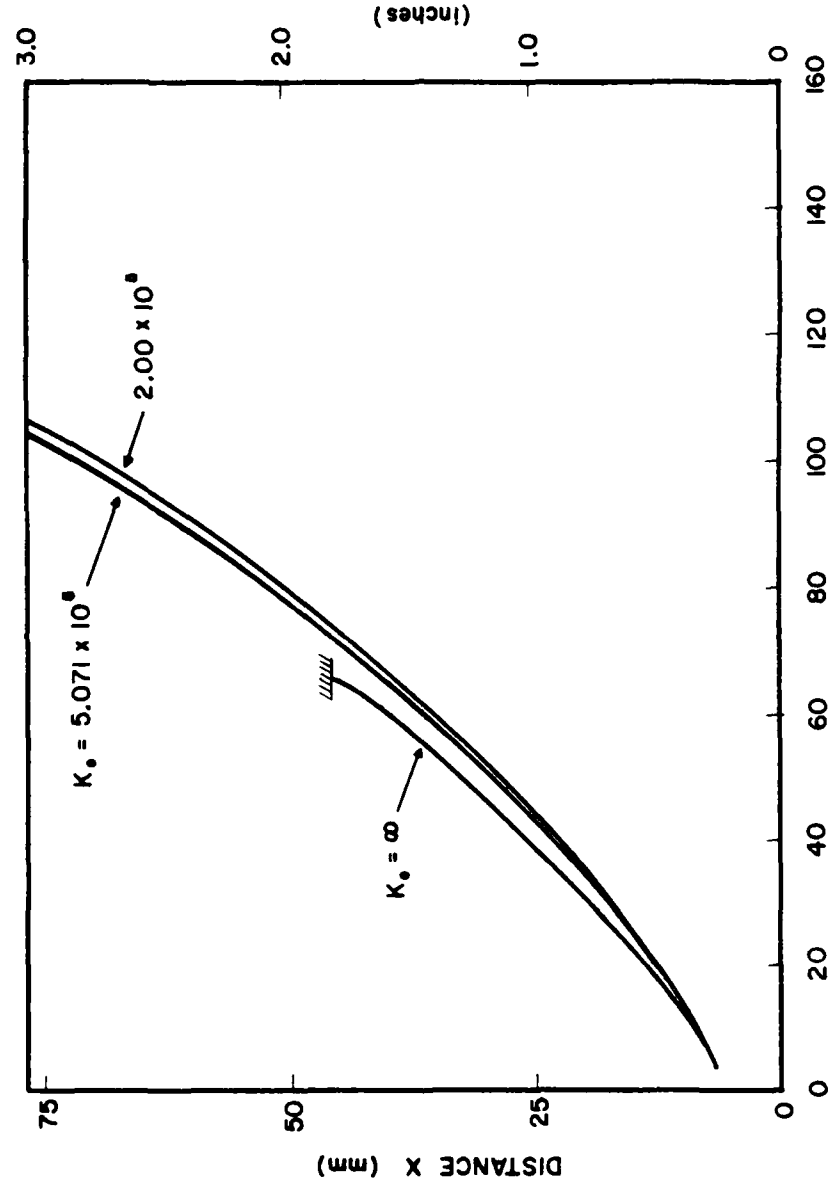

Fig. 3.13 Flame front locus as a function of the propellant bulk modulus. (Note the incompressible case, K = ∞, did not compute for the entire event.)

techniques in the literature for similar problems, it was felt that the inclusion of this type of damping would mask important information concerning the onset of a transition to detonation. For this reason, no specific damping terms were included in the integration scheme.

However, it was found that a reduction in the magnitude of the interphase drag term would allow progress to occur for cases that would otherwise be halted due to the overshoot described above. This was due to the fact that less drag allowed a higher gas velocity to occur at a certain level of porosity which, in turn, allowed gases hot enough to cause ignition to penetrate much more deeply into the bed. Once the particles had been compacted to a porosity somewhat below that which caused the numerical oscillations at the higher drag level, the hot gases would again be unable to move into the bed resulting in ever-steepening gradients and eventual numerical integration failure.

This situation is illstrated quite clearly in Figs. 3.14 and 3.15. Figure 3.14 shows the ability of the hot gases to move farther and faster into the bed as the interphase drag is multiplied by a constant factor, C_D. The pressure curves (Fig. 3.15) also indicate the relaxation of the bed as the drag is reduced. The results presented in these two graphs would seem to indicate that this C_D factor is acting as a pseudo-damping coefficient. The constant was originally used to allow for variations in the gas-particle interaction due to the uncertainty in the drag relation, which, at the high Reynold's numbers encountered in this type of flow, was being extended outside its evaluated range. Until further experiments can extend the range of validity of the interphase drag equation, the use of a C_D type coefficient must remain a legitimate option.

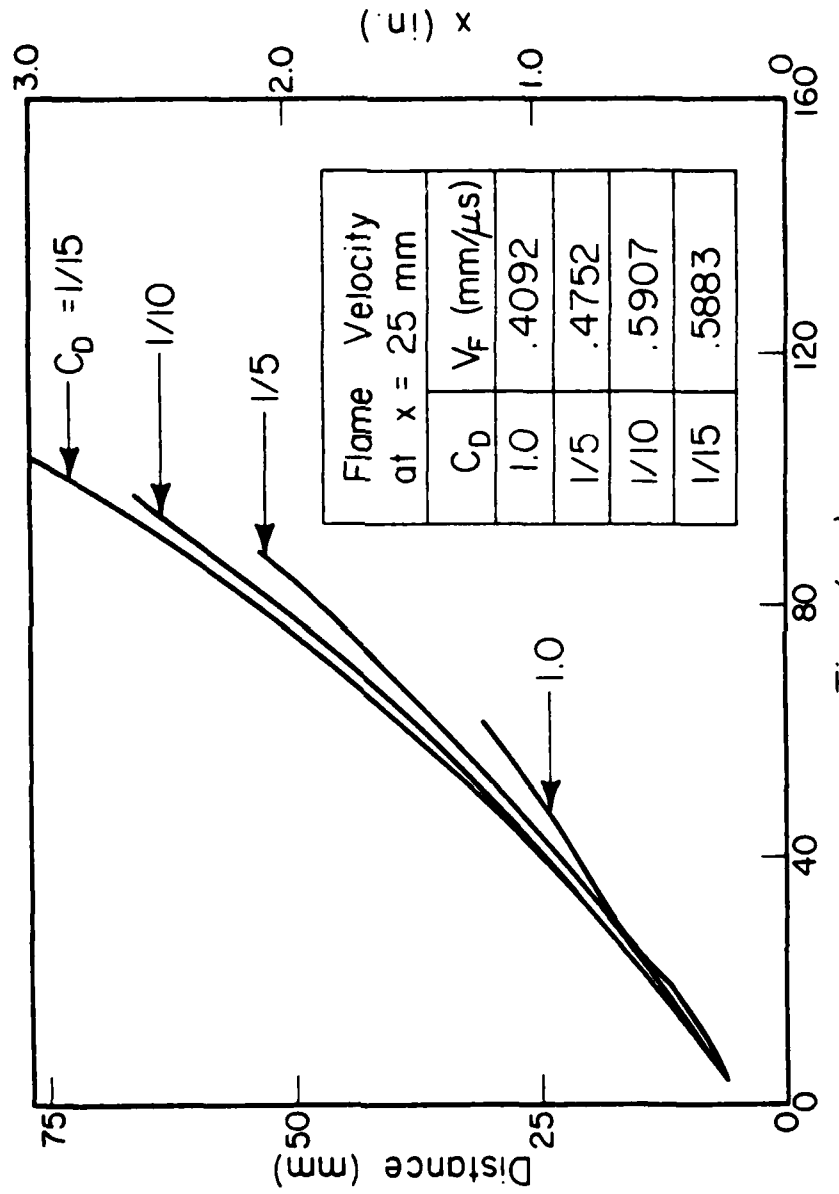

Fig. 3.14 Flame front locus as a function of bed permeability coefficient, C_D.

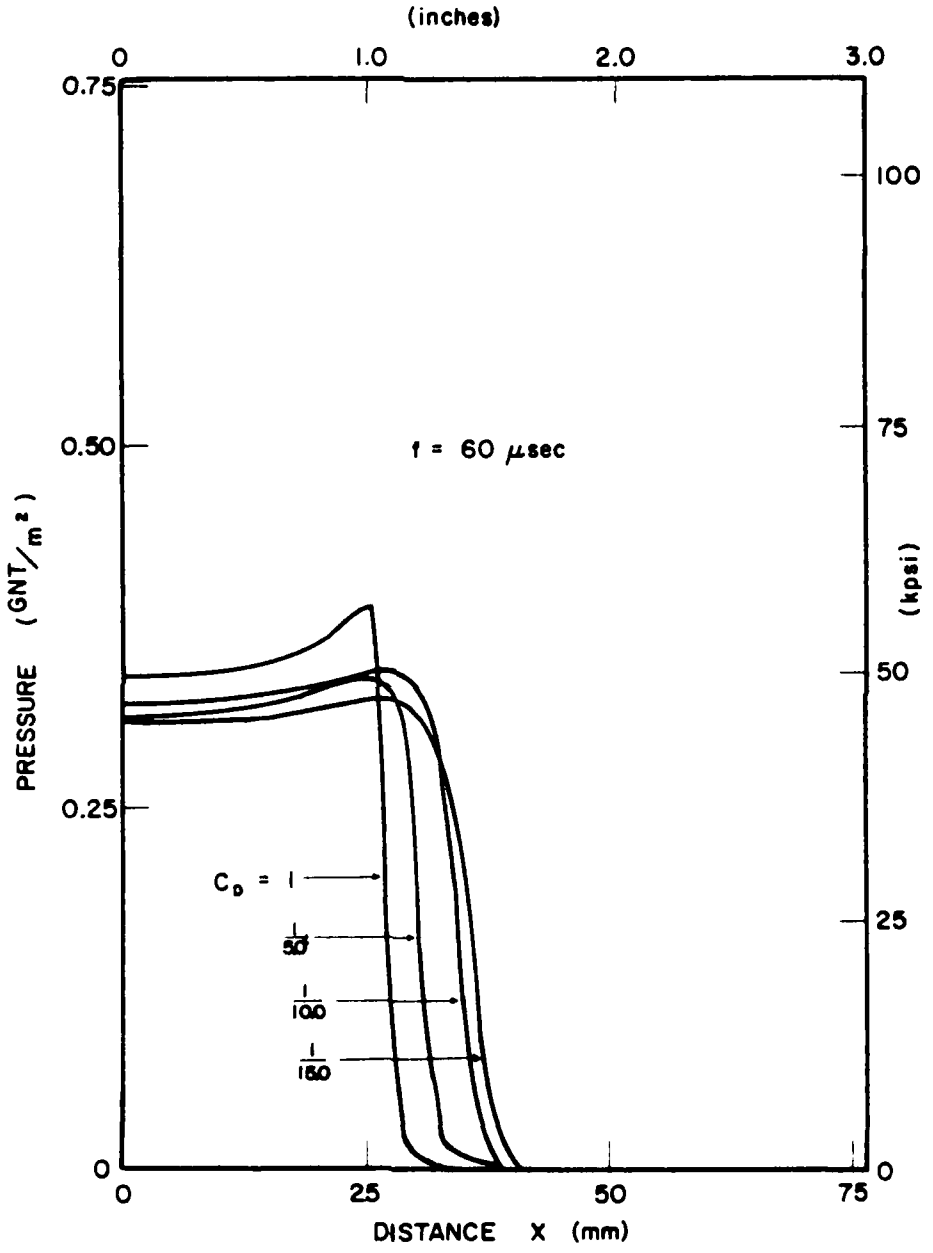

Fig. 3.15 Pressure distribution as a function of bed permeability at t = 60 μsec.

Use of this C_D factor did point to the increased range of problems which could be investigated if some sort of artificial smoothing was implemented. The fear of loosing important data subsided as it became more and more apparent that the instabilities seemed to be resulting from the integration scheme itself and not from some quality of the flow. To this end, a damping equation of the form

$$\left(\frac{\partial}{\partial t}\right)_j^{new} = (AVG)\left[\left(\frac{\partial}{\partial t}\right)_{j-1}^{old} + \left(\frac{\partial}{\partial t}\right)_{j+1}^{old}\right] + (1-AVG)\left(\frac{\partial}{\partial t}\right)_j^{old} \tag{3.2}$$

was utilized, where, the smoothing percent, AVG, must lie within the range

$$0.0 \geq AVG \geq 0.50 \tag{3.3}$$

This allows up to 50 percent of the time derivatives on either side of the term being worked on to be used in obtaining a smoother result. Figure 3.16 shows the effects of increasing the amount of smoothing on the progression of the flame front through the bed. For five percent smoothing, the gradients remained too steep to be handled by the routine. However, for smoothing of roughly 10 percent or more, the integration scheme was able to successfully predict results through the entire bed.

This increased success is not without its penalties. Figure 3.17 shows the resulting pressure profiles for various amounts of smoothing. As can be seen, an increase in the amount of smoothing has the effect of smearing out any sharp gradients to the point where useful information cannot always be obtained. Recognizing this fact, the amount of smoothing was kept as low as possible, typically less than 10 percent.

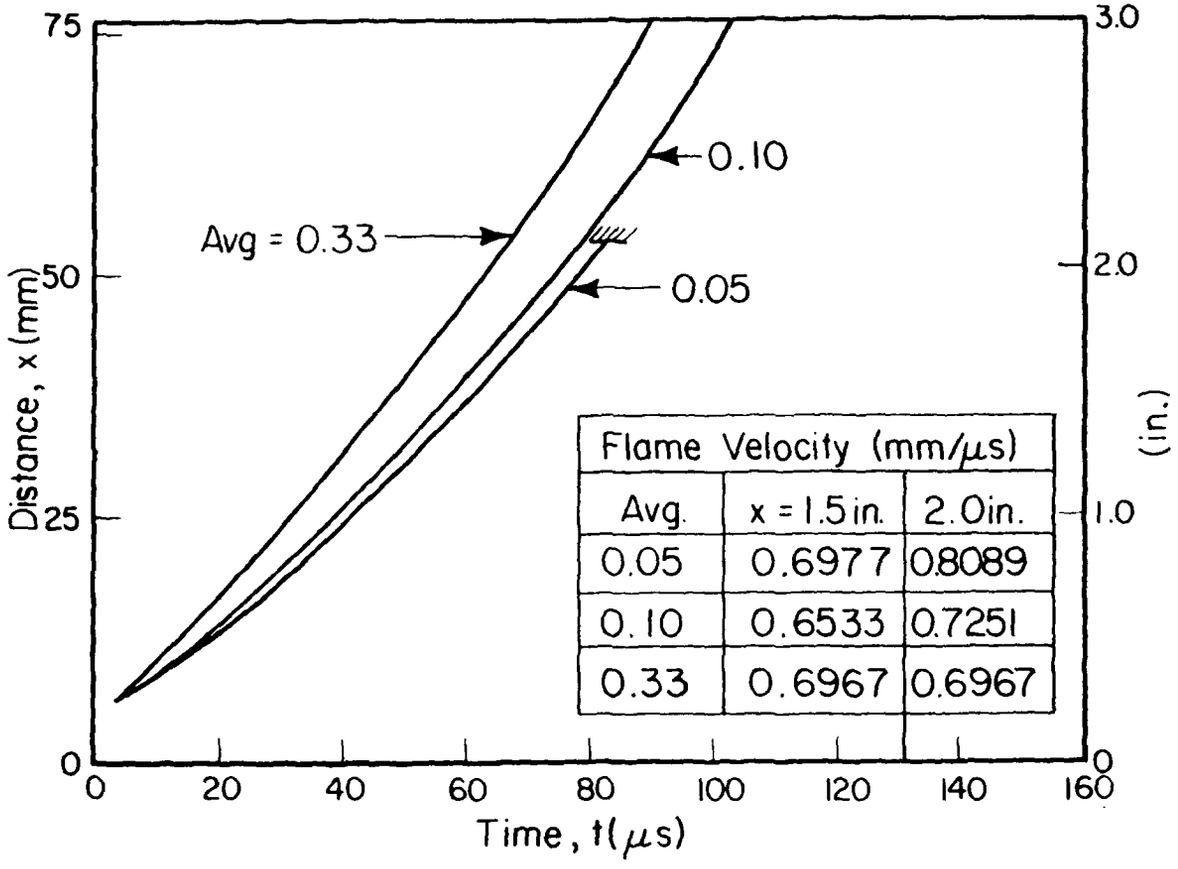

Fig. 3.16 Flame front locus variation due to numerical smoothing.

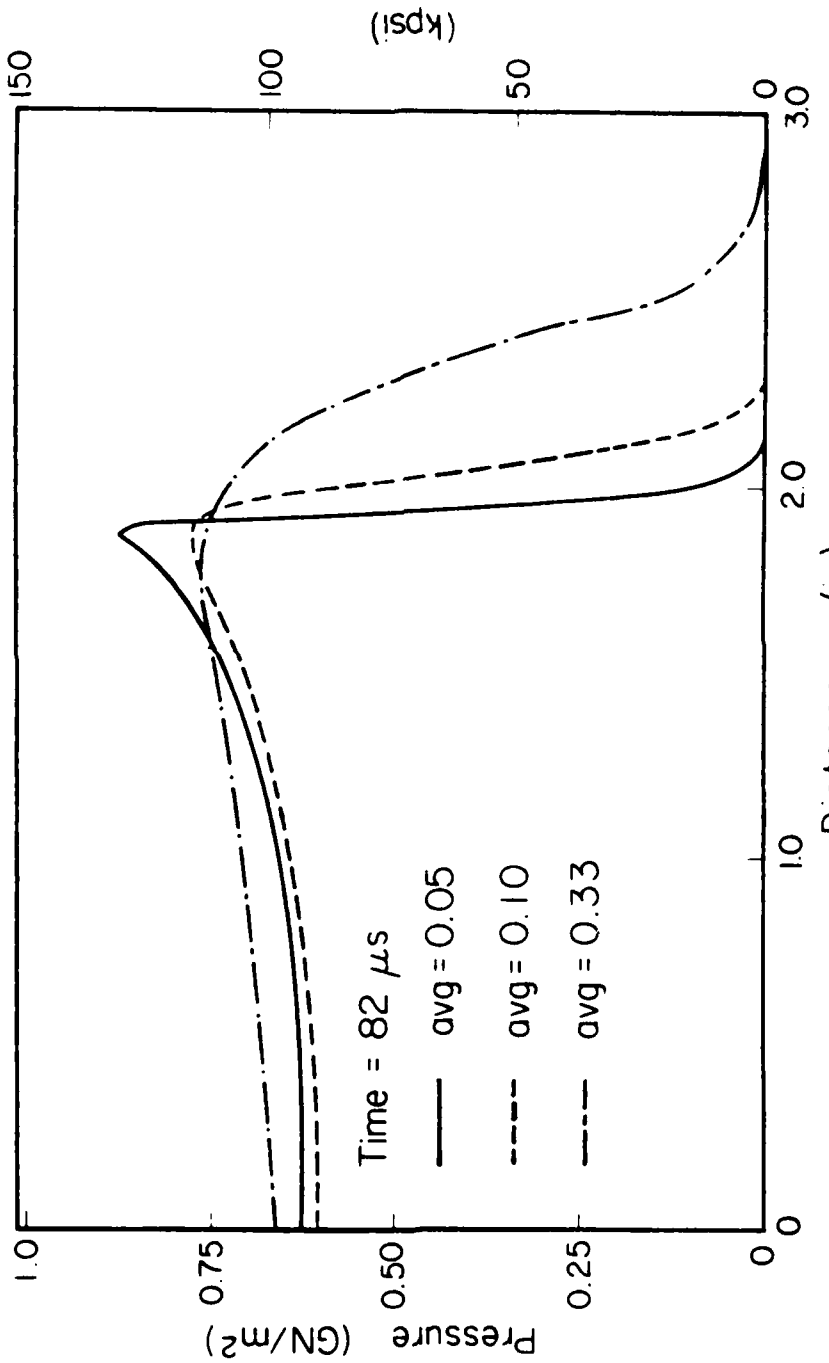

Fig. 3.17 Pressure distribution due to variation in numerical smoothing at t = 82 μsec.

3.6 Discontinuous Jump Conditions in the Gas Generation Function

As discussed in Chapter One, in order to develop a strong pressure shock and an expected abrupt change in the flame velocity, one must model a rapid increase in one of the components of the mass generation term, Γ, at some assumed critically high pressure or in some region of excess solids compaction. The term Γ (mass/volume-time) for spherical particles burning on their outer surfaces only, is

$$\Gamma = \left(\frac{3}{r_p}\right)(1 - \phi)\rho_p \dot{r}_p \tag{3.4}$$

with

$\frac{3}{r_p}$ = surface to volume ratio for spheres

ρ_p = propellant density

$\dot{r}_p$ = propellant burning rate = $\left(\frac{T_p}{T_{p_o}}\right)^m [bP^n]$

This expression allows for a number of possible changes in individual components or combinations of components at some preselected critical condition.

Figure 3.18 shows the results from two of these possibilities. Case (a) represents the unperturbed prediction of the flame front locus. Case (b) illustrates the enhancement of the flame moving through the bed by simply increasing Γ throughout the run. In this case the enhancement was the result of allowing the propellant burning rate to be augmented by the magnitude of the propellant temperature increase. The third case (case (c)) made use of an increase in the pressure exponent at some imposed critical condition, in this case where the gas pressure exceeds

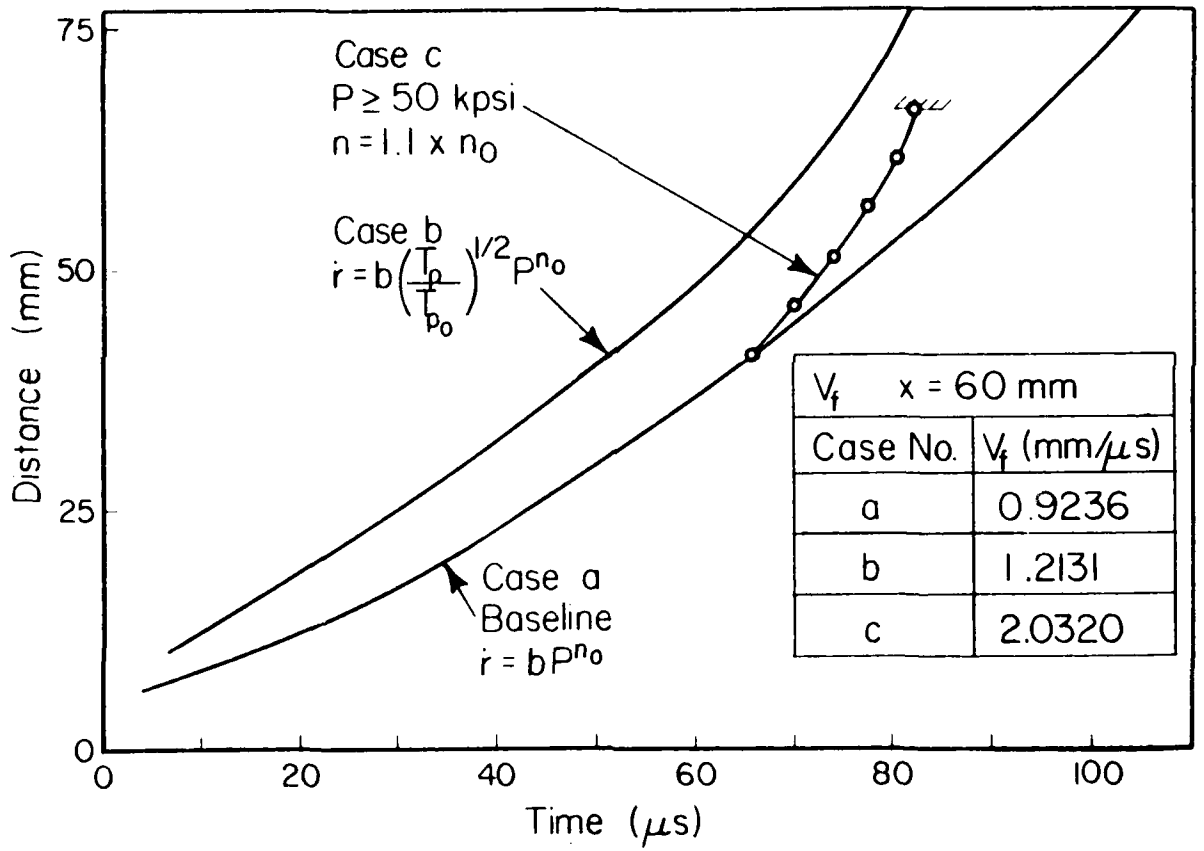

Fig. 3.18 Flame front locus as a function of burning rate equations.

50 Kpsi. The shape of the flame front is now beginning to resemble the data of Bernecker and Price [6] (discussed in Chapter One), although the ignition front velocity is still less than those reported in Ref. 6 This case did not proceed to completion due to the same type of numerical instabilities described in the previous section.

In order to limit the effect of the nonlinear source-term increase, which causes the numerical integration breakdown, case (c) was repeated by assuming only a five percent increase in the exponent n. As expected, the integration proceeded normally. As the pressure history profiles shown in Fig. 3.19 indicate, there is a significant increase in the level of the gas pressure shortly after the propellant burning rate is increased. The effect of this pressure wave increase on the motion of the flame front is shown in Fig. 3.20. It should be noted here that while the gas pressure exceeds the critical level at 40 μsec, the break in the slope of the flame front does not occur for another 10 μsec. However, when the location of the pressure front is defined as the point of maximum rate of change of slope on the pressure time plot (Fig. 3.21), as was done by Bernecker and Price [6], it can be seen that the pressure wave moves ahead of the flame at about the time of the change in the burning rate exponent. Despite the lack of high flame velocities after the transition, which may be due to the relatively low initial solids loading treated here, this flame front/ pressure front exhibits a remarkable similarity to the experimental results of Bernecker and Price.

Figures 3.22 and 3.23 (flame front loci plots) show similar behavior when changes are made to the other components of the gas generation term. Changes in the burning rate proportionality constant, b, do not show

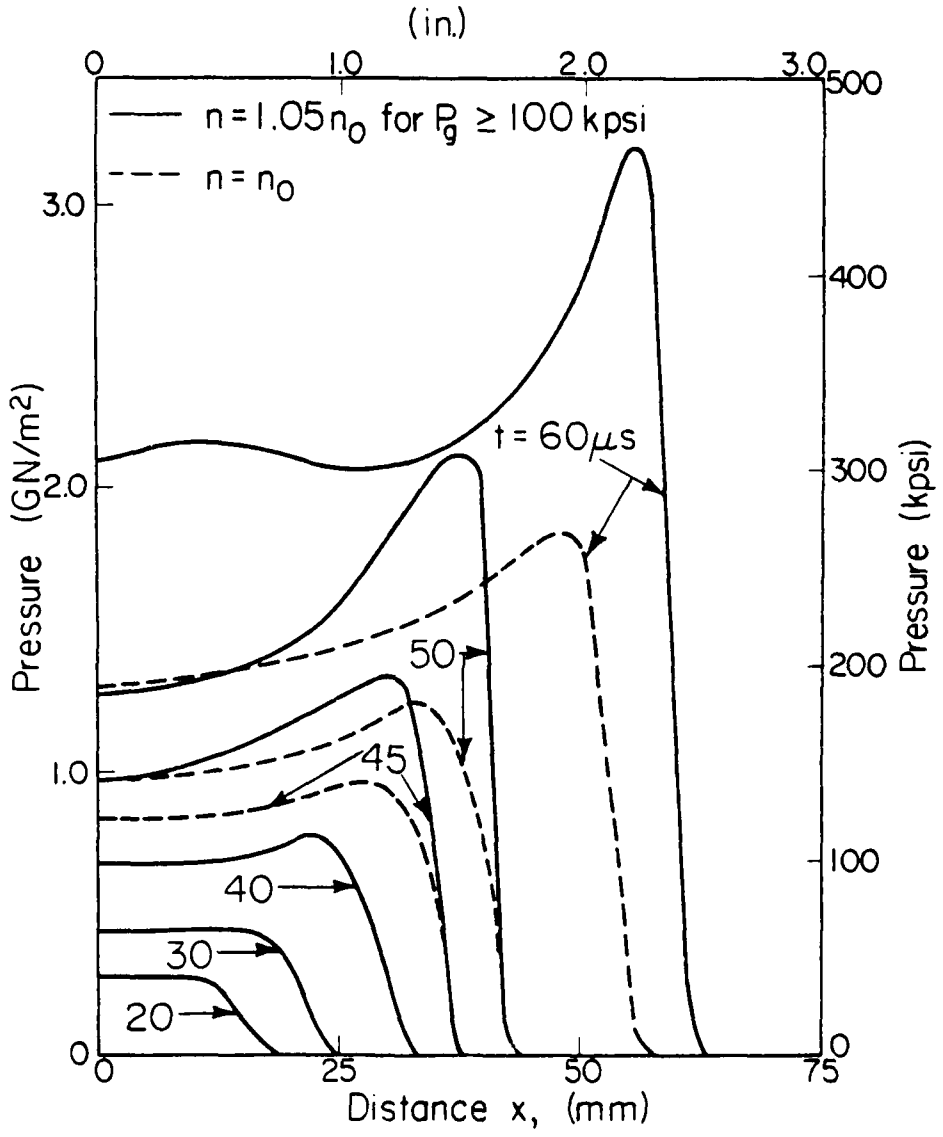

Fig. 3.19 Pressure distribution history as a function of burning rate exponent change.

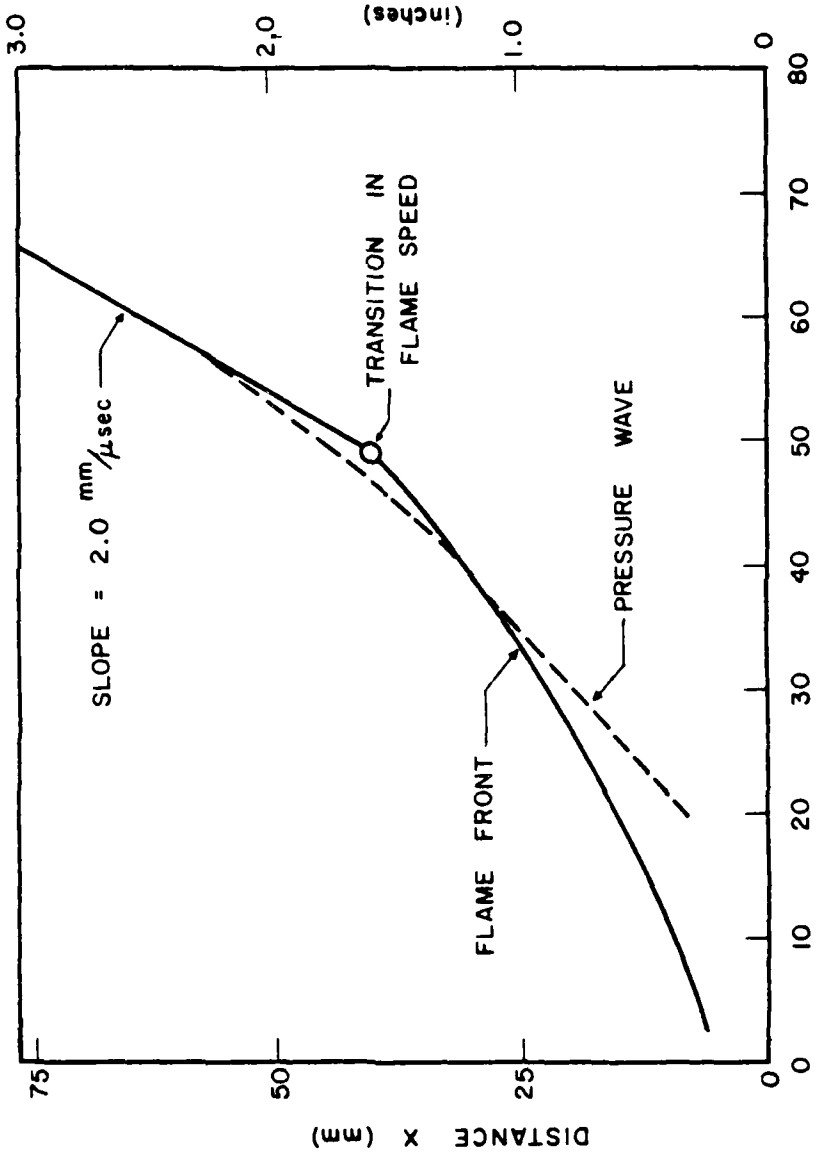

Fig. 3.20 Flame front and pressure front locus resulting from an abrupt change in burning rate at a critical pressure.

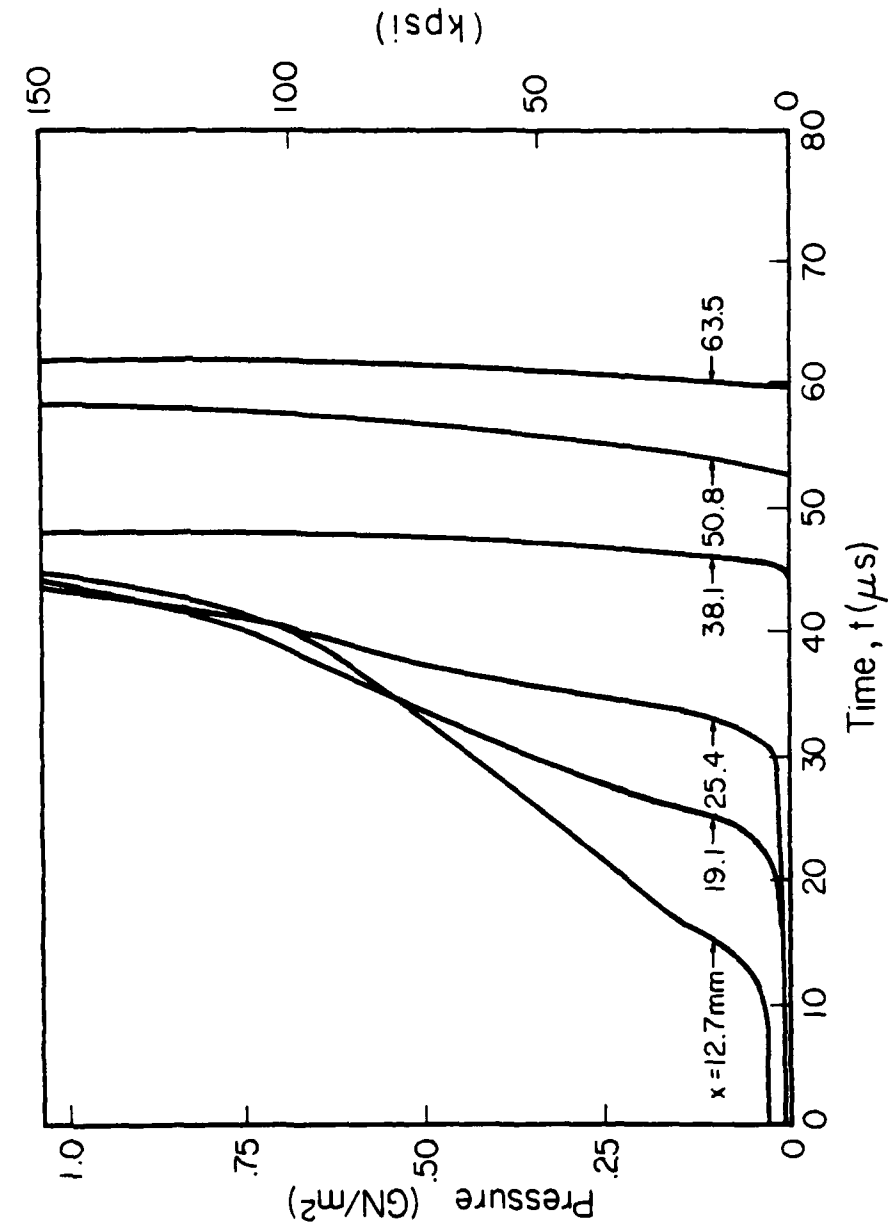

Fig. 3.21 Pressure-time variation at various locations in bed used to obtain pressure front shown in Fig. 3.20.

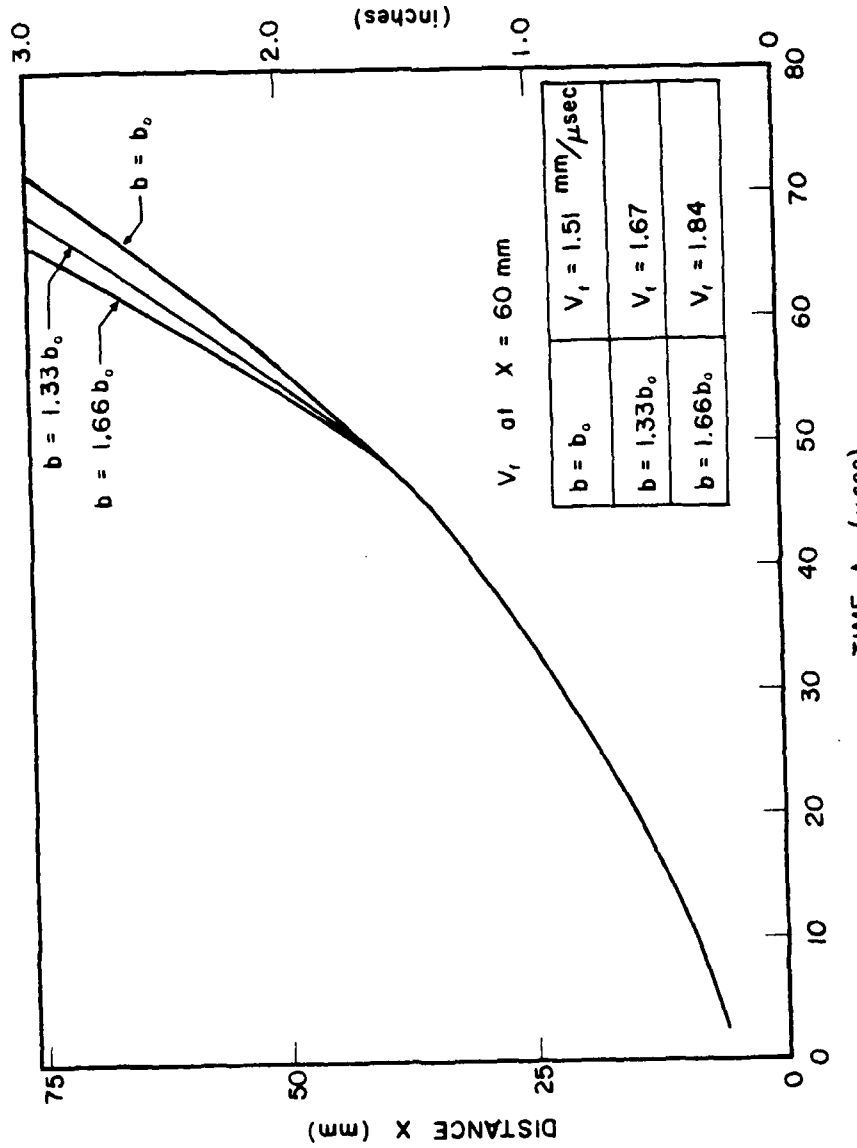

Fig. 3.22 Flame front locus resulting from an abrupt change at the critical pressure in the burning rate proportionality constant, b.

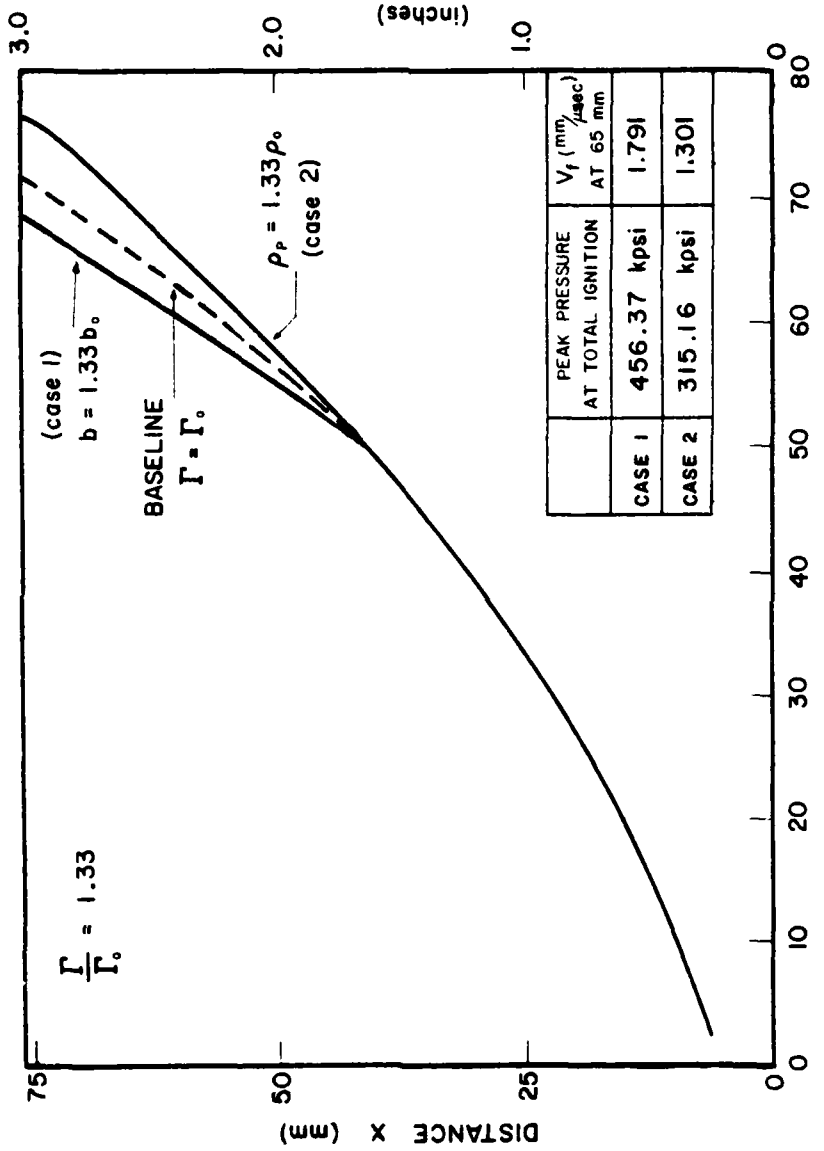

Fig. 3.23 Flame front locus resulting from an abrupt change (at the critical pressure) in the solid phase density.

as dramatic a change in the slope of the flame front simply because the assumed increased values of b were not as large as the increase due to the pressure-power law function. An assumed abrupt change in the solid density at some prescribed high pressure produces results similar to those found when the addition of a state equation was made, namely, a reduction in the slope of the flame front instead of an increase.

3.7 Modification of the Solid Phase Momentum Equation and the Introduction of Stress Wave Motion

The previous section introduced a possible mechanism which yields results supportive of the first DDT scenario described in Section 1.2. But in all cases described to this point there was no evidence of a compression wave moving through the unignited portion of the bed. This meant that conditions for the second DDT scenario were not being modeled. Modifications necessary to obtain this type of physical effect included the introduction of a new compaction resistance law, a modification of the solid phase momentum equation and the assumption that a solid phase stress wave will move through the unignited part of the bed at the solid phase sound speed behind the wave. The details of each of these new assumptions are presented below.

In Chapter Two, problems encountered with the particle-particle interaction law developed by Kuo and Summerfield [11] were discussed and a substitute relation based on the minimum allowable compaction was outlined. This new compaction resistance law was to be used in association with a new solid phase momentum equation which took the final form

$$\frac{\partial}{\partial t}(\rho_2 u_p) = -\frac{\partial}{\partial x}(\rho_2 u_p^2) - \Gamma u_p$$

$$+ [1-f(\phi)](\overline{F} - (1-\phi)\frac{\partial}{\partial x}(f(\phi)\overline{F})] \qquad (3.5)$$

where, as defined previously,

$$\rho_2 = (1-\phi)\rho_p \qquad (3.6)$$

$$f(\phi) = \left[\frac{\phi_{UL} - \phi}{\phi_{UL} - \phi_{LL}}\right]^{\ell} \qquad (3.7)$$

$\phi_{UL} \equiv$ porosity above which the particles do not touch (3.8)

$\phi_{LL} \equiv$ minimum allowable porosity based on the geometry of individual particles (3.9)

$$f(\phi)\overline{F} = P_p \qquad (3.10)$$

Figures 3.24 and 3.25 show the the effects on the flame front locus and the pressure profiles of the addition of these two modifications for various values of the exponent ℓ. For ℓ set equal to zero, $f(\phi)$ is equal to unity for all values of porosity less than ϕ_{UL}. This means that once the particles are touching, they cannot be compacted further since they cannot be accelerated forward and all the force exerted by the drag is taken up by a localized stress on the particles. As the value of ℓ is increased, more and more of the drag force is used to accelerate the particles forward. This results in the flame front moving into the bed at a faster rate since the particles are being moved forward at a faster rate. This also means

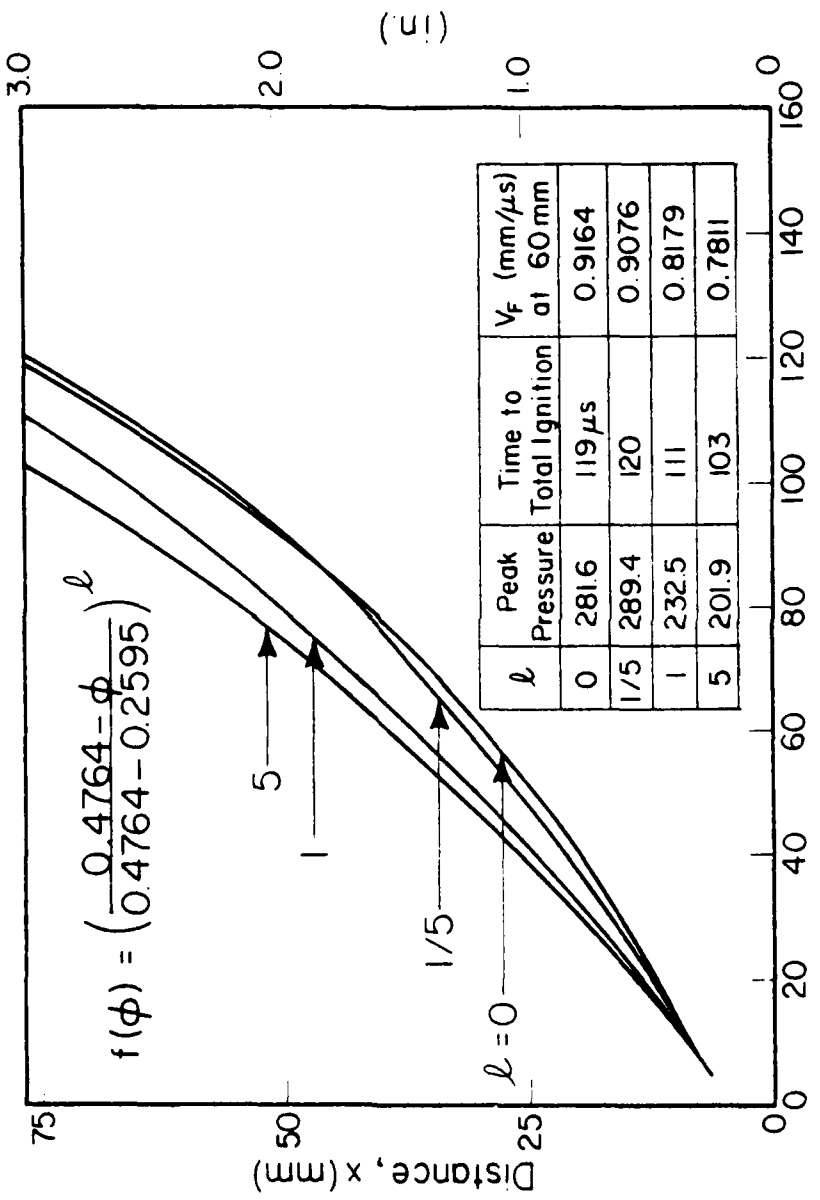

Fig. 3.24 Flame front locus as a function of the particle-particle resistance function.

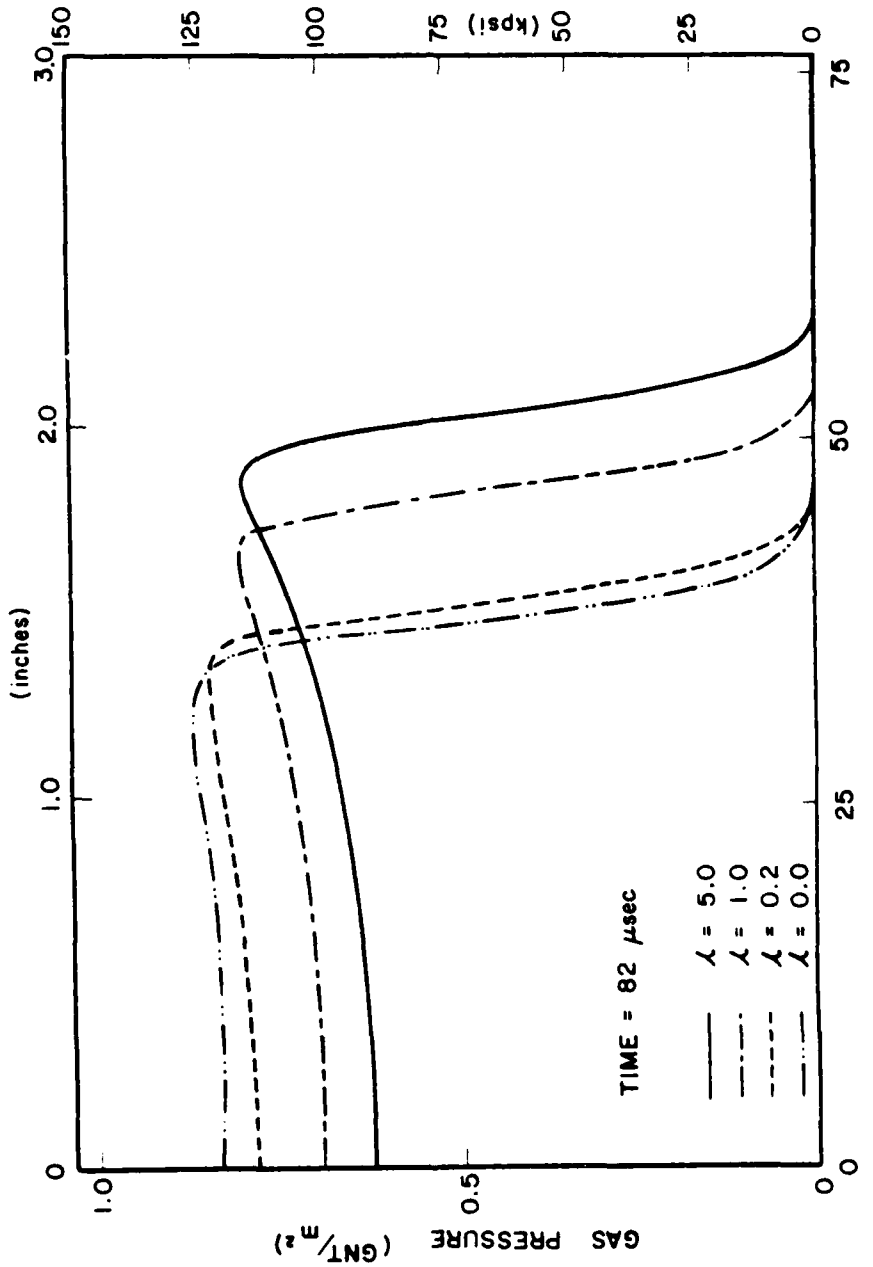

Fig. 3.25 Pressure distribution as a function of particle-particle resistance function (at time of 82 μsec).

that there is additional volume available for the gases behind the flame front which results in a lower gas pressure. Both of these events are illustrated in Figs. 3.24 and 3.25.

A comparison of a case using the Kuo-Summerfield formulation for the compaction resistance with a case using the equation described above is shown in Figs. 3.26 and 3.27. For this comparison a value of unity for the exponent ℓ was chosen since it represents a simple linear decrease in the acceleration caused by the drag and P_p forces. As can be seen, for this case the Kuo-Summerfield law allows a bit more compaction to take place which in turn yields a slightly higher flame spreading rate and a lower gas pressure. Thus, if a value of ℓ somewhat greater than one were assumed, a set of results similar to those produced by the Kuo-Summerfield equation would be obtained without the questions raised in Chapter Two. Even with the ability to produce similar results at these relatively high porosities, the results would become different as ϕ_{LL} is reached since the Kuo-Summerfield law allows the further compaction of the particles below $\phi = \phi_{LL}$.

Having now defined a particle pressure in Eq. (3.10) as

$$P_p = f(\phi)\overline{F} \tag{3.10}$$

it is possible to define a sound speed through the solid phase based on the logic developed in Appendix A. This information can now be used in conjunction with an application of basic continuum mechanics to define the velocity with which a stress wave will move through the unignited bed. Figure 3.28 shows clearly the progression of this stress wave through the bed far in advance of the gas pressure front. Since it was assumed that

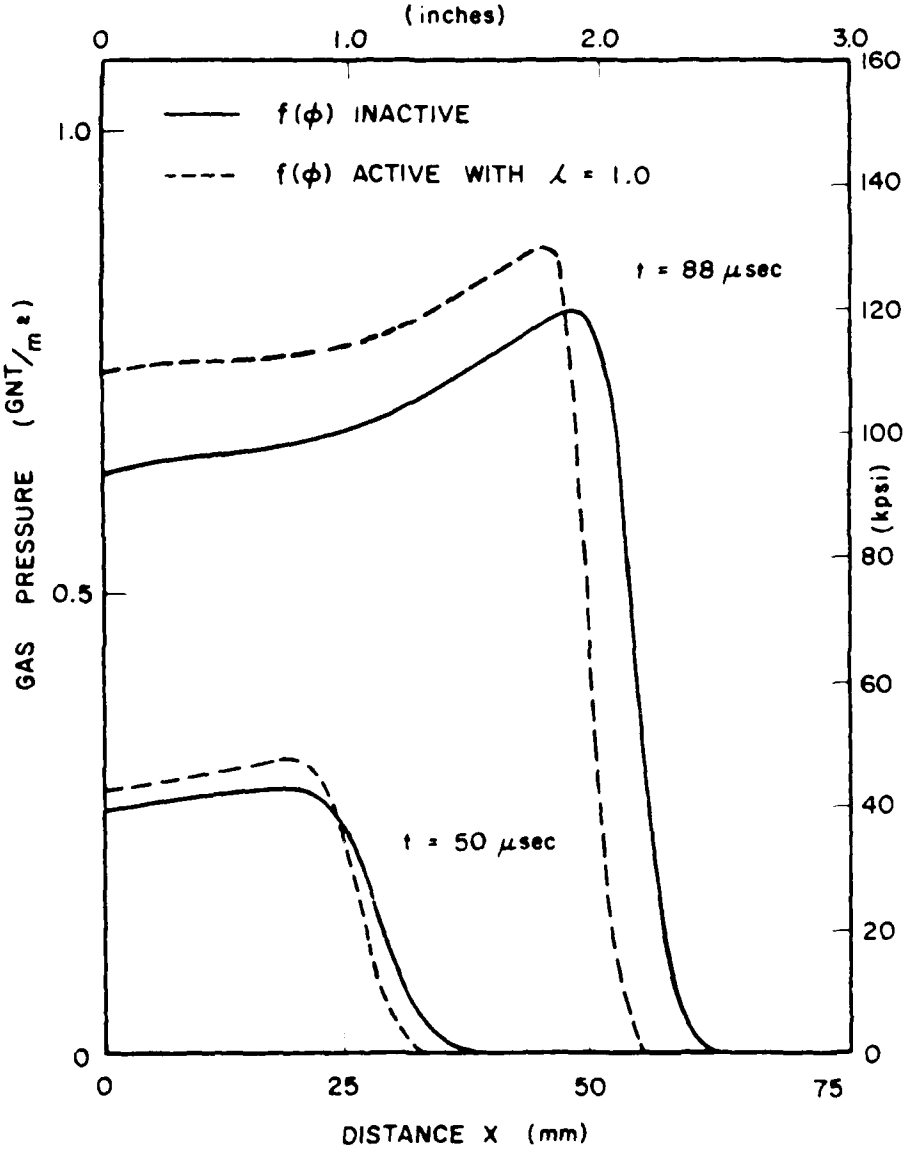

Fig. 3.26 Gas pressure distribution comparison for two different particle-particle resistance functions.

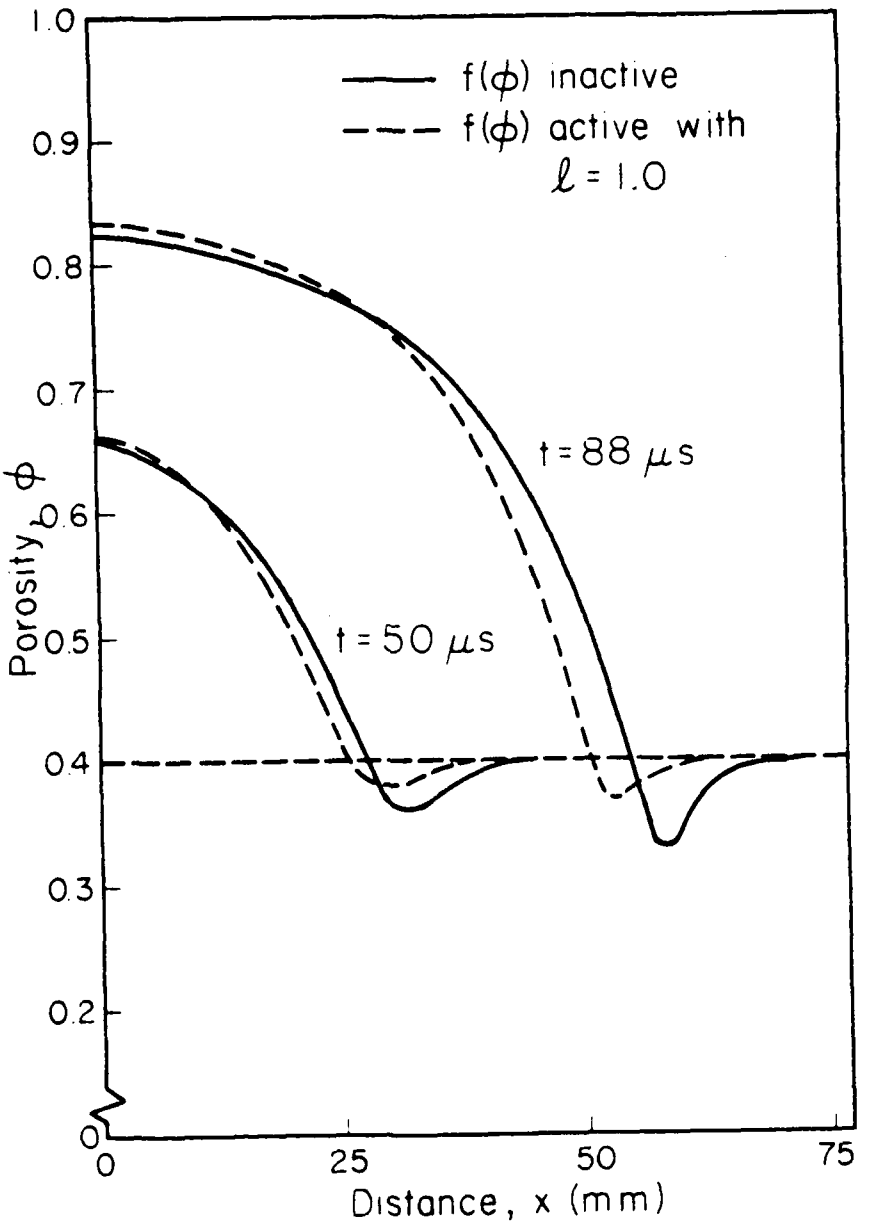

Fig. 5.27 Porosity distribution comparison for two different particle-particle resistance functions.

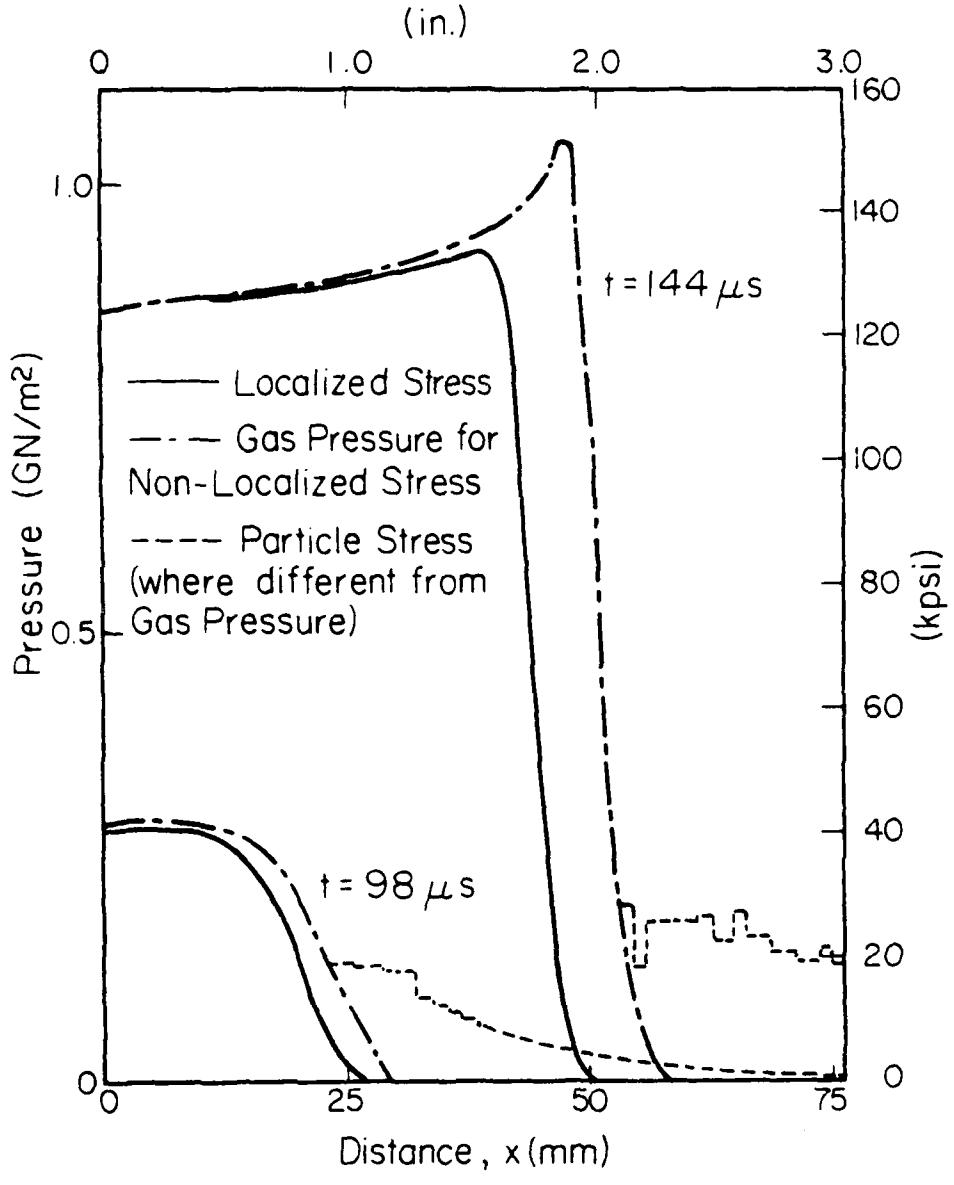

Fig. 3.28 Pressure distribution comparison (at two different times) for localized and non-localized solid phase stress.

this stress wave could affect the particle density in the same manner as the gas pressure, the particles are compressed and moved slightly forward by this P_p force. The net effect is to increase the porosity in front of the gas pressure wave allowing hot gases to penetrate forward much more quickly and ignite a greater portion of the bed in the same amount of time. This increase in the porosity and the associated increase in the flame speed are shown in Figs. 3.29 and 3.30.

However, it is also well known from fundamental continuum mechanics that the formation of an insipient shock, which was the goal behind this particular investigation, will only result if the source of the compression waves is accelerating forward. The case which is represented in Figs. 3.28 through 3.30 does not exhibit this necessary behavior until the final stages of the burn with the result that the particle stress is increased in a gradual manner until the bed is completely ignited with no sign of shock formation.

A possible remedy to this situation is to increase the bulk modulus of solid phase which would have the dual effect of increasing the forward velocity of the compression waves and decrease the amount of compression in the solid phase. Increasing the sound speed, i.e., the compression wave speed, would increase the potential for shock formation in a bed of this short length. A decrease in the amount of compression will under these circumstances have the effect of slowing down the progression of the flame front. This is so since the porosity will not be increased as much. Calculations with an assumed increased bulk modulus showed that indeed the above events do occur, but again the forward acceleration of the compression

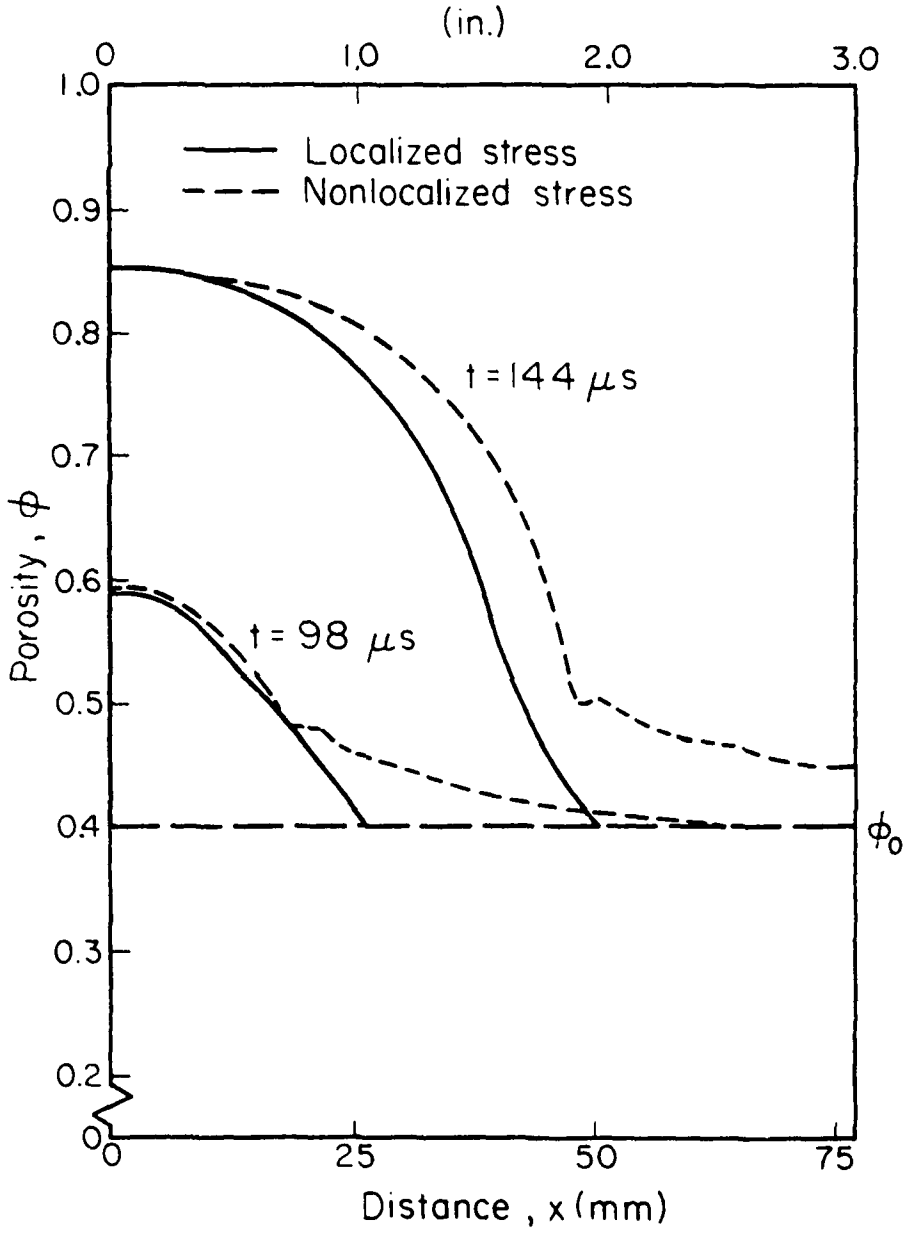

Fig. 3.29 Porosity distribution comparison for localized and non-localized solid phase stress.

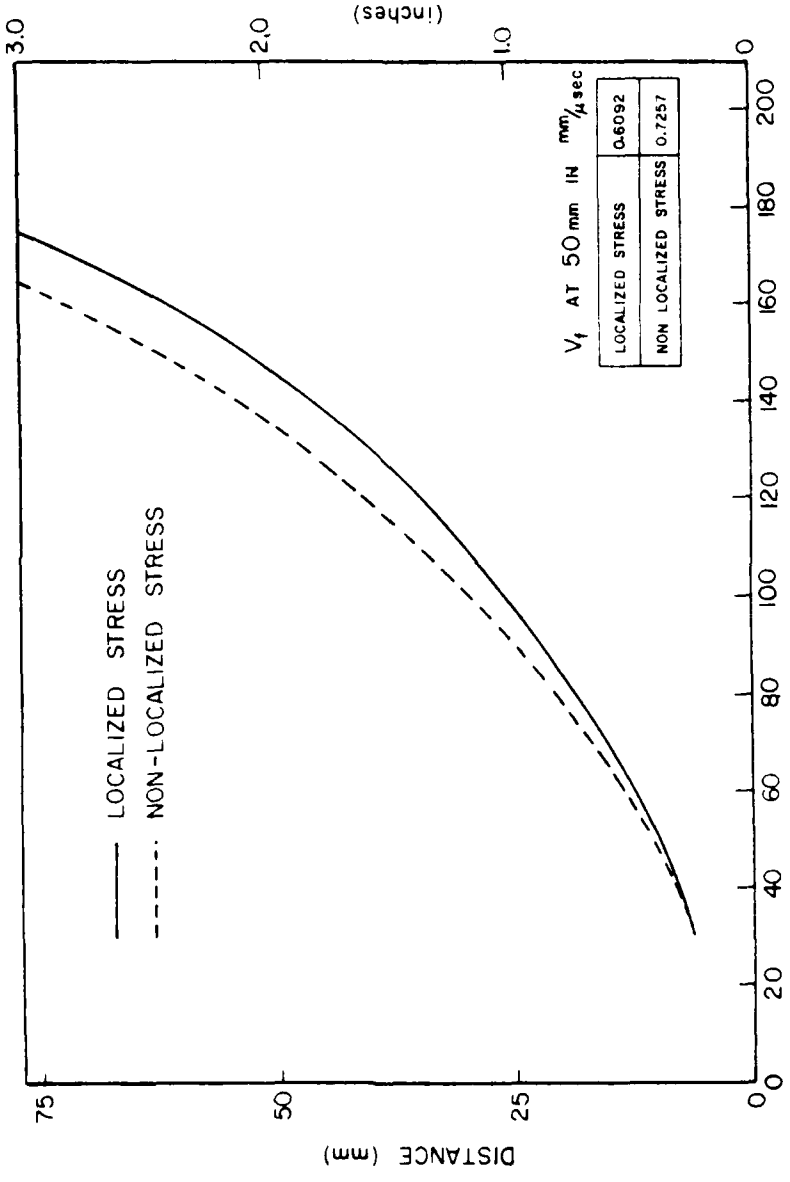

Fig. 3.30 Flame front locus comparison for localized and non-localized solid phase stress.

wave source was not proper to develop an insipient shock. The increase in the solid phase bulk modulus does have the effect of compressing a sufficient number of particles against the back wall to cause the gas to be compressively heated due to the decrease in the volume available for it. This eventually resulted in the gas obtaining a high enough temperature to ignite the particles before the arrival of the deflagration front. However, this was a result of the fact that the wall allowed no further motion of the particles and not from the desired shock initiation.

Based on the investigations presented in this section, it appears that there is a great deal of potential in exploring this latter scenario. It also shows that a great deal more must be known about the mechanics of a bed of closely packed, individual solid particles. A large number of assumptions had to be made here that were not entirely satisfactory due to this lack of information.

CHAPTER FOUR

CONCLUSIONS

4.1 Summary of Investigations

The work presented in this report represents a continuation of the efforts begun by Krier-Gokhale [1] and Krier-Kezerle [2] to correctly model the deflagration to detonation transition phenomenon. In these previous studies, the investigation was focused on determining a set of governing equations which properly described the peculiar nature of the flow and with properly incorporating these equations into a numerical integration scheme. This study essentially began with these developed codes and to determine the sensitivity of the various assumptions made previously in an attempt to better understand the properties of the flow which are necessary to correctly model a smooth transition to detonation.

To this end, the boundary conditions and grid spacing were examined and, in the case of the boundary condition, were modified to reflect the assumption that the gradients at the boundaries should be zero. The dimensions of the grid spacing was varied until a size was found which gave proper accuracy and minimum computing costs.

Concerning basic properties of the propellant itself, it was shown that the energetic composite class of materials was much more sensitive to the rapid increases in pressure and in flame velocity than were the single base propellants, as expected. It was also shown that introducing a solid phase state equation to allow the particles to compress dramatically improves the characteristics of the flow properties when compared with the results obtained in experiments. The introduction of compressibility

allowed for a significant decrease in the gas pressure and temperature to levels more in line with the values found in these experiments, while retaining approximately the same flame front velocity found using the incompressible assumption.

In an attempt to increase the range of problem that could be accommodated by this code, a smoothing function was introduced to suppress numerical oscillations which occurred with certain input conditions. These oscillations were also found to be suppressed by a reduction in the grid which, through the Courant-Friedrichs-Levy stability criterion [12], also reduced the time step. But a reduction of this type of course increased the computing time, costs, and even accuracy. It was found that numerical stability could be improved by gradually reducing the time step below the Courant-Friedrichs-Levy criterion as the gradients became more severe without changing the grid size. While this also increased the computer time needed, the increase was not significant. This was due to the fact that although the number of integration cycles was increased, the number of steps per cycle remained the same.

At this point, an investigation of two different theories concerning the DDT mechanism was carried out to determine what type of modifications would be necessary to model these two theories. In order to reproduce the first mechanism, which has its origins in experimental work by Burnecker and Price [6], a modification which yielded positive results was to abruptly increase the magnitude of the gas generation term. The most dramatic effects of such a change were produced by changing the exponent in the pressure sensitive burning rate law at some imposed critical pressure level.

The second mechanism, which had its origin in the work of Maček [7],

was modeled here by modifying the solid phase momentum equation which in turn allowed a particle stress to be defined. This stress term, coupled with an expression for the solid phase sound speed, created a situation in which compression waves could move forward into the bed with the potential for the formation of an insipient shock. While no such strong shock formation has been calculated as yet, work is continuing to expand and refine this approach.

4.2 Future Areas of Investigation

The work presented in this report has, among other things, served the purpose of focusing attention on various aspects of the DDT phenomenon which will require a much more thorough understanding before any significant confidence in the results can be obtained.

For example, it is unknown at this time if the fundamental relationships for the drag and heat transfer are valid at the high Reynolds numbers encountered in this type of flow. Results presented in Section 3.5 show what kind of effect a reduction in the drag relation can have on the progress of the flow. It is also uncertain what effect the large gas pressures have on the burning rate of these types of propellants. That is, dynamic burning rate phenomena may negate the use of the rate equation used in Chapter Three.

The large pressure buildups in the short time periods which occur in this type of problem would be expected to create some sort of dynamic compaction in the porous bed. But again, the nature of this compaction is not fully understood and therefore cannot be properly modeled in this code. Further experimentation will need to be conducted if questions of this type are to be answered.

Further improvements in the code itself can be obtained with the introduction of concepts commonly used in detonation physics. This would include the use of a revised gas generation term which reflects the increased mass transformation rates which occur in a detonation [14]. Use would also need to be made of detonation chemistry which allows for the shock initiation of the types of materials being considered here. An example of the possible use of this concept is to allow an abrupt change in the burning rate exponent as was done in Section 3.6. However, this increased burning rate probably should be limited to what could be called the shock front, that is, the exponent increase should be confined to that region where the gas pressure is increasing at some critical rate with respect to time. As has been shown throughout Chapter Three, this type of zone is always found to be closely coupled to the ignition front.

An indication of the results of this type of localized burning rate increase are presented in Figs. 4.1 and 4.2. Specifically, the exponent n is increased from n_o to $n_o + \Delta n$, only when $dP/dt > 1.5 \times 10^3$ psi/ sec and only if the pressure gradient, dP/dx is negative. Although these results resemble those shown in Section 3.6, the logic used here models a sequence of events which is much closer to the circumstances known to occur in a detonation. The flame front velocities which occur after the break in its slope were found to be constant, which is another important characteristic of a detonation. And finally, the crossing of the flame front by the pressure front before the break in the flame front slope was found to occur in all the cases presented in Fig. 4.1. But due to the means by which the reaction zone was defined (in this case, the restriction that $dP/dx < 0$), the pressure front eventually dropped below the flame front for the higher

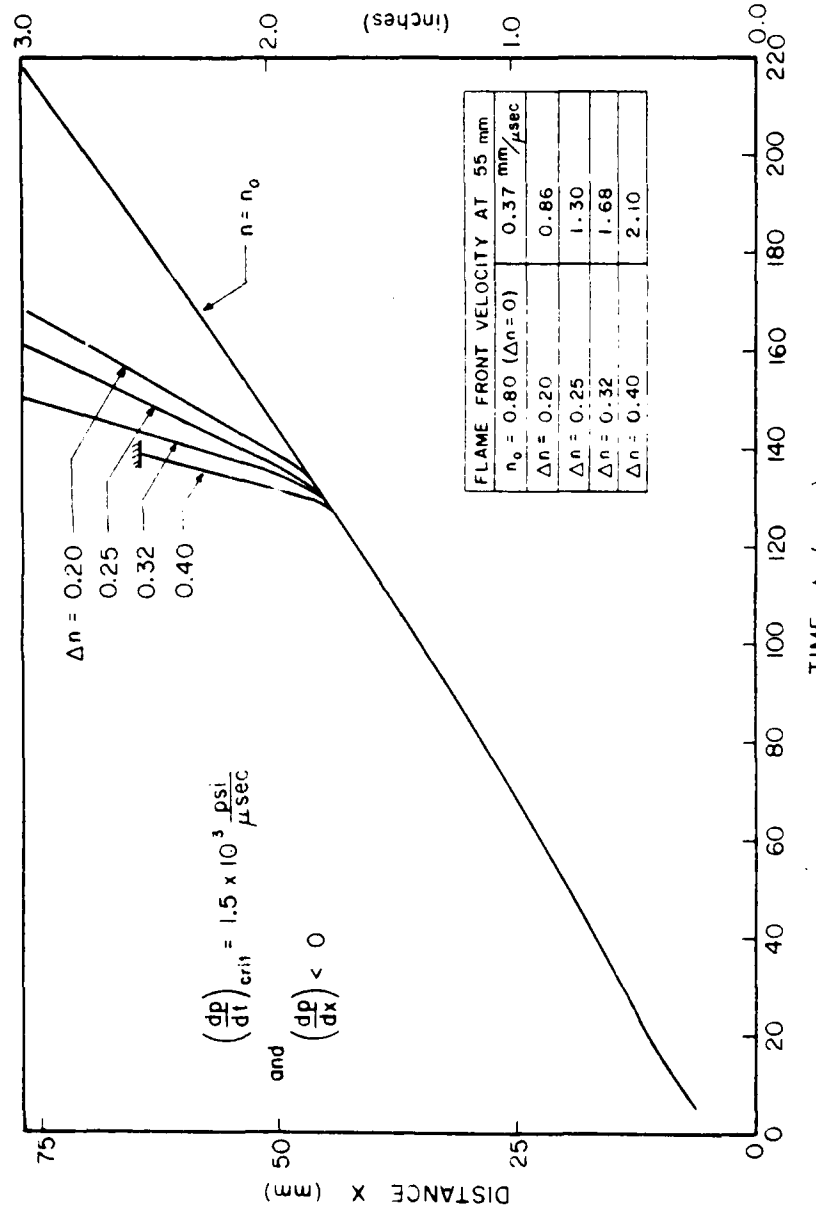

Fig. 4.1 Flame front locus resulting from an abrupt change (at the critical pressure gradient) in the burning rate exponent. (Limited to the localized region of the pressure front.)

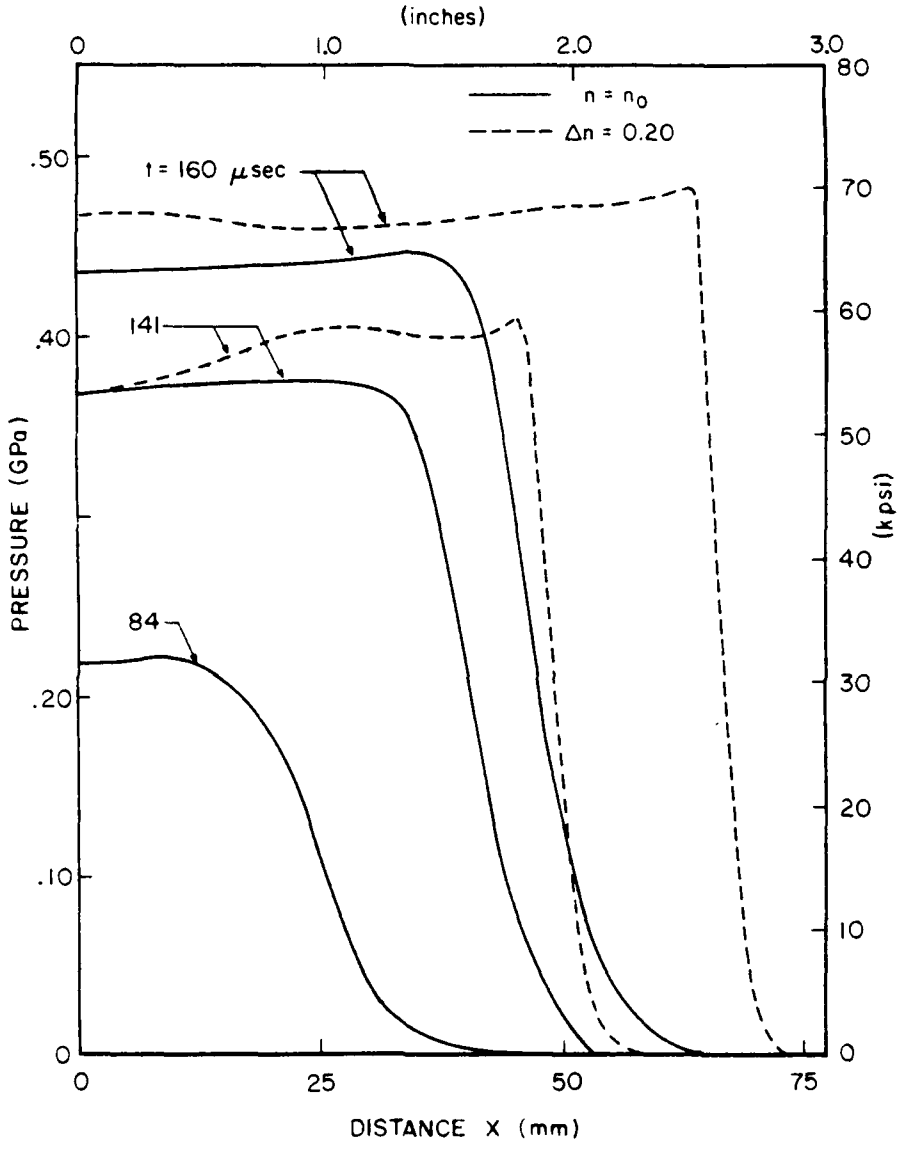

Fig. 4.2 Pressure distribution history as a function of burning rate exponent change. (Limited to the localized region of the pressure front.)

values of Δn as the burn progressed. This was caused by the fact that increases in Δn resulted in a steepening of the pressure-distance curve which in turn caused the reaction zone to become narrower in extent and thus less powerful in its motion through the bed. This problem can be rectified by using a somewhat more complicated means of defining the reaction zone which will allow the thickness of the zone to be maintained at a desired level independent of the pressure-distance curve.

It should be noted that in all the cases presented in this report, the initial solids loading is only 60 percent (porosity, ϕ, = 0.40) while the experiments of Burnecker and Price [6] as well as those of Calzia and Carabin [9] had initial solids loading ranging approximately from 80 to 90 percent. Appendix B shows that an initial solids loading of 74 percent is the maximum attainable with uniform spheres, which is a basic assumption in this code. To treat higher values of solids loading one must assume that a bed of multisized particles is being used. This leads to a number of difficulties concerning the proper method of partitioning flow properties such as the interphase drag and heat transfer. (For a discussion of these difficulties and their potential solution see the Ph.D. thesis of S. S. Gokhale [13].)

Another aspect which should be looked into both as a means of improving this code in particular and for solving this DDT problem in general is to review again the numerical scheme itself. The full effects of the numerical smoothing function introduced in Section 3.5 have not been exhustively studied and refinements are certainly not out of the question. The use of a "rezoning" technique in which either the grid spacing or the time step or both are decreased in regions of severe gradients may prove

to be very valuable in obtaining better accuracy for the same or even lower computing time and costs. Reasonable solutions may not be acquired from any of these suggestions until larger computers become available since many of the calculations encountered thus far entailed calculating small differences of large numbers.

Finally, it should again be pointed out that, although a number of difficulties and constraints have been discussed in this section, many of the problems would not be recognized as such without the progress that has been made in this work. Further research into these problems will certainly make progress towards a solution to the overall prediction of deflagration to detonation transition.

REFERENCES

(1) Krier, H. and Gokhale, S. S., "Modeling of Convective Mode Combustion to predict detonation transition", AIAA J. 16, 177-183 (February 1978).

(2) Krier H. and Kezerle, J. "A Study of Unsteady One-Dimensional Two-Phase Reactive Particle Flow", Dept. of Aero. and Astro. Eng., Univ. of Illinois, Urbana, IL., Report UILU-Eng 77-0517 (1977).

(3) Krier, K., Gokhale, S., and Hoffman, S., "Unsteady Two-Phase Flow Analysis Applied to Deflagration-To-Detonation Transition", AIAA Paper No. 78-1013, presented at the 14th AIAA/SAE Propulsion Conference (July 1978).

(4) Soo, S. L., Fluid Dynamics of Multiphase Systems, Blaisdell Publishing Co., Waltham, Mass. (1967).

(5) Soo, S. L., "On One-Dimensional Motion of a Single Component in Two-Phases", Int. J. of Multiphase Flow 3, 79-82 (1976).

(6) Bernecker, R. R. and Price, D., "Studies in the Transition to Detonation in Granular Explosives", Combust. and Flame 22, Parts I-II, pp. 111-129, Part II, pp. 161-170 (1974).

(7) Maček, A., "Transition from Deflagration to Detonation in Cast Explosives", J. Chem. Phys. 31, 162 (1959).

(8) Traver, C. M., Goodale, T. C., Shaw, R., and Cowperthwaite, M., "Deflagration-to-Detonation Transition Studies for Two Potential Isomeric Cast Primary Explosives", Sixth Symposium on Detonation, Office of Naval Research Report ACR-221, pp. 231-249, US Government Printing Office, Washington, D.C. (August 1976).

(9) Calzia, J. and Carabin, H., "Experimental Study of the Transition from Burning to Detonation", Fifth Symposium on Detonation, Office of Naval Research Report 184, pp. 230-241, US Government Printing Office, Washington, D.C. (August 1972).

(10) Wallis, G. B., One-Dimensional Two-Phase Flow, New York: McGraw-Hill Book Company (1969).

(11) Kuo, K. K. and Summerfield, H., "High Speed Combustion of Mobile Granular Solid Propellants", Fifteenth Symposium on Combustion, The Combustion Institute, Pittsburgh, PA, pp. 515-525 (August 1974).

(12) Ames, W. F., Nonlinear Partial Differential Equations in Engineering, New York: Academic Press (1965).

(13) Gokhale, S. S., Theoretical Studies in the Transition to Detonation of Granular Solid Propellants, Ph.D. Dissertation, University of Illinois at Urbana-Champaign, Dept. Aero. & Astro Eng. (January 1980).

(14) Fickett, W. and Davis, W. C., "Detonation", University of California Press, Berkeley, CA (Los Alamos Series in Basic and Applied Sciences) (1979).

(15) Kuo, K. K., Vichnevetsky, R., and Summerfield, M., "Theory of Flame Front Propagation in Porous Propellant Changes", AIAA J. 2, 443-451 (April 1973).

(16) Krier, H., Rajan, S., and VanTassell, W. F., "Flame Spreading and Combustion in Packed Beds of Propellant Grains", AIAA J. 14, 301-309 (March 1976).

(17) Denton, W. H., "General Discussion of Heat Transfer", Institute of Mechanical Engineers and American Society of Mechanical Engineers, London, p. 370 (1951).

(18) Kuo, K. K. and Nydegger, C. C., "Flow Resistance Measurements and Correlation in a Packed Bed of Ball Propellants", J. of Ballistics 2(1), 1-26 (1978).

(19) Lee, J. F. and Sears, F. W., Thermodynamics. Reading, MA: Addison-Wesley Publishing Company (1955).

AD-A090 558 ILLINOIS UNIV AT URBANA-CHAMPAIGN DEPT OF AERONAUTICA--ETC F/G 21/5
FLUID MECHANICAL PROCESSES OF DEFLAGRATION TO DETONATION TRANSI--ETC(U)
MAR 80 S J HOFFMAN, H KRIER AFOSR-77-3336
UNCLASSIFIED AAE-80-2 AFOSR-TR-80-1064 NL

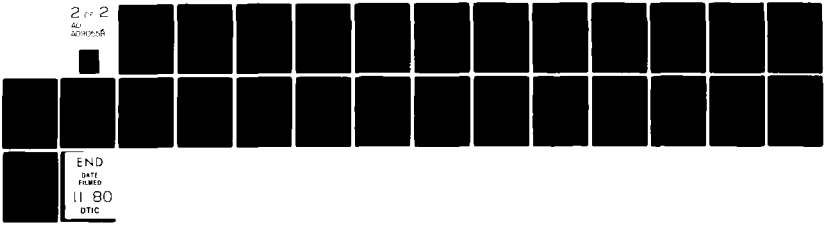

END
DATE FILMED
11 80
DTIC

APPENDIX A

PARTICLE BULK MODULUS AND SOUND SPEED

The general equation for the sound speed, c, in a solid is usually defined as

$$c = \sqrt{\frac{K}{\rho_p}} \tag{A.1}$$

where K is the bulk modulus. But, assuming nothing is known about the variation of K, this equation would appear to force the sound speed to decrease as the particle density increases which seems inconsistent with the normal occurrence of sound speed varying in the same manner as the density.

This indicates that the bulk modulus also varies with density which can be determined from the definition of the bulk modulus once a state equation has been specified. It has been assumed in this work that the particles obey a modified form of the Tait equation

$$p_p = \frac{\rho_{p_o} c_o^2}{3} \left[\left(\frac{\rho_p}{\rho_{p_o}} \right)^3 - 1 \right] = \frac{K_o}{3} \left[\left(\frac{\rho_p}{\rho_{p_o}} \right)^3 - 1 \right] \tag{A.2}$$

Since the bulk modulus is defined as

$$K = \frac{P - P_o}{\left[\frac{V_o - \bar{V}}{V_o} \right]} = - V_o \frac{dP}{dV} \tag{A.3a}$$

the Tait equation is the only expression necessary to determine its variation with pressure or density. First, it should be noted that for a

fixed mass

$$\frac{P-P_o}{\left[\frac{V_o-V}{V_o}\right]} = \frac{P-P_o}{\left[\frac{\frac{1}{\rho_o}-\frac{1}{\rho}}{\frac{1}{\rho}}\right]}$$

Using this, the bulk modulus can be written as

$$K = -\frac{1}{\rho_{p_o}} \frac{dP}{d\left(\frac{1}{\rho_p}\right)} \tag{A.3b}$$

From equation (A.2)

$$P = \frac{K_o}{3}\left[\left(\frac{1}{\rho_{p_o}}\right)^3\left(\frac{1}{\rho_p}\right)^{-3} - 1\right]$$

$$\frac{dP}{d\left(\frac{1}{\rho_p}\right)} = \left[\left(\frac{1}{\rho_{p_o}}\right)^3 \frac{K_o}{3}\right](-3)\left(\frac{1}{\rho_p}\right)^{-4} \tag{A.4}$$

Substituting this into (A.3b)

$$K = \left(-\frac{1}{\rho_{p_o}}\right)\left[\left(\frac{1}{\rho_{p_o}}\right)^3 \frac{K_o}{3}\right](-3)\left(\frac{1}{\rho_p}\right)^{-4} \tag{A.5a}$$

$$= K_o\left(\frac{\rho_p}{\rho_{p_o}}\right)^4 \tag{A.5b}$$

$$= \left(\rho_{p_o} c_o^2\right)\left(\frac{\rho_p}{\rho_{p_o}}\right)^4 \tag{A.5c}$$

This can now be put back into (A.1) to find the actual variation in sound speed with respect to particle density:

$$c = \left[\frac{c_o^2 \rho^3 p}{\rho p_o^3} \right]^{1/2} \qquad \text{(A.6)}$$

This equation now shows sound speed increasing as density increases, as would be expected.

APPENDIX B

POROSITY LIMITS FOR SPHERICAL PARTICLES

The following calculations are provided so that a geometrical association can be made with certain values of the porosity, ϕ. It should be noted that for uniform spherical particles, case (A) represents the lower bound for ϕ while case (C) is the upper bound.

Case (A) Face Centered Cubic (See Fig. B.1.a)

$$\phi = \frac{V_T - V_P}{V_T} = \frac{b^3 - 4[(4/3)\pi r^3]}{b^3}$$

For this configuration $r = \frac{\sqrt{2}}{4} b$. Thus

$$\phi = \frac{b^3 - (16/3)(\pi)(\sqrt{2}/4)^3 b^3}{b^3}$$

$$= 0.2595$$

Case (B) Body Centered Cubic (See Fig. B.1.b)

$$\phi = \frac{V_T - V_P}{V_T} = \frac{b^3 - 2(4/3)(\pi) r^3}{b^3}$$

For this configuration, $r = \frac{\sqrt{3}}{4} b$. Thus

$$\phi = \frac{b^3 - 2(4/3)(\pi)(\sqrt{3}/4)^3 (b^3)}{b^3}$$

$$= 0.3198$$

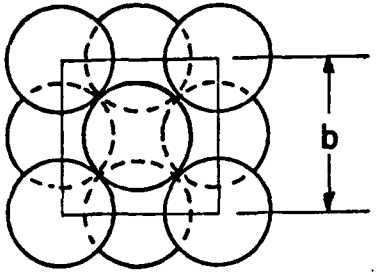

Fig. B.1.a

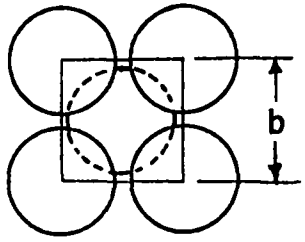

Fig. B.1.b

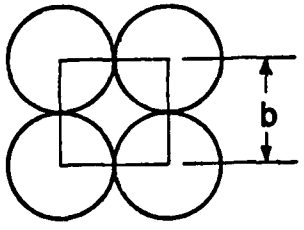

Fig. B.1.c

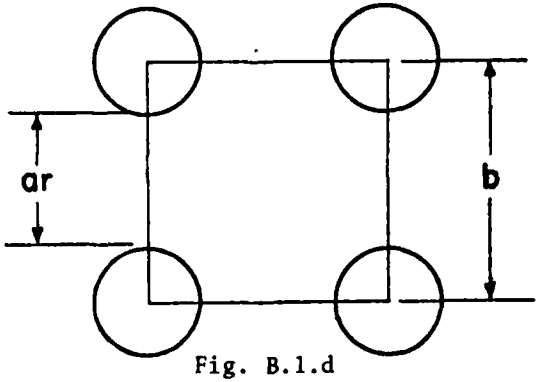

Fig. B.1.d

Fig. B.1 Relative geometry of spherical particles at various porosity levels.

Case (C) Simple Monoclinic (See Fig. B.1.c)

$$\phi = \frac{V_T - V_P}{V_T} = \frac{b^3 - (4/3)(\pi)r^3}{b^3}$$

For this configuration, $r = \frac{b}{2}$

$$\phi = \frac{b^3 - (4/3)\pi b^3/8}{b^3}$$

$$= 0.4764$$

Case (D) No Particle Contact (See Fig. B.1.d)

$$\phi = \frac{V_T - V_P}{V_T} = \frac{b^3 - (4/3)\pi r^3}{b^3}$$

In this configuration, $r = \frac{b}{a+2}$

$$\phi = \frac{b^3 - (4/3)(\pi)(1/[a+2])^3 b^3}{b^3}$$

$$= 1 - (4\pi/3)(1/[a+2])^3$$

A plot of ϕ vs a is provided in Fig. B.2. As can be seen, as a approaches zero ϕ approaches the value found in Case (C) as would be expected.

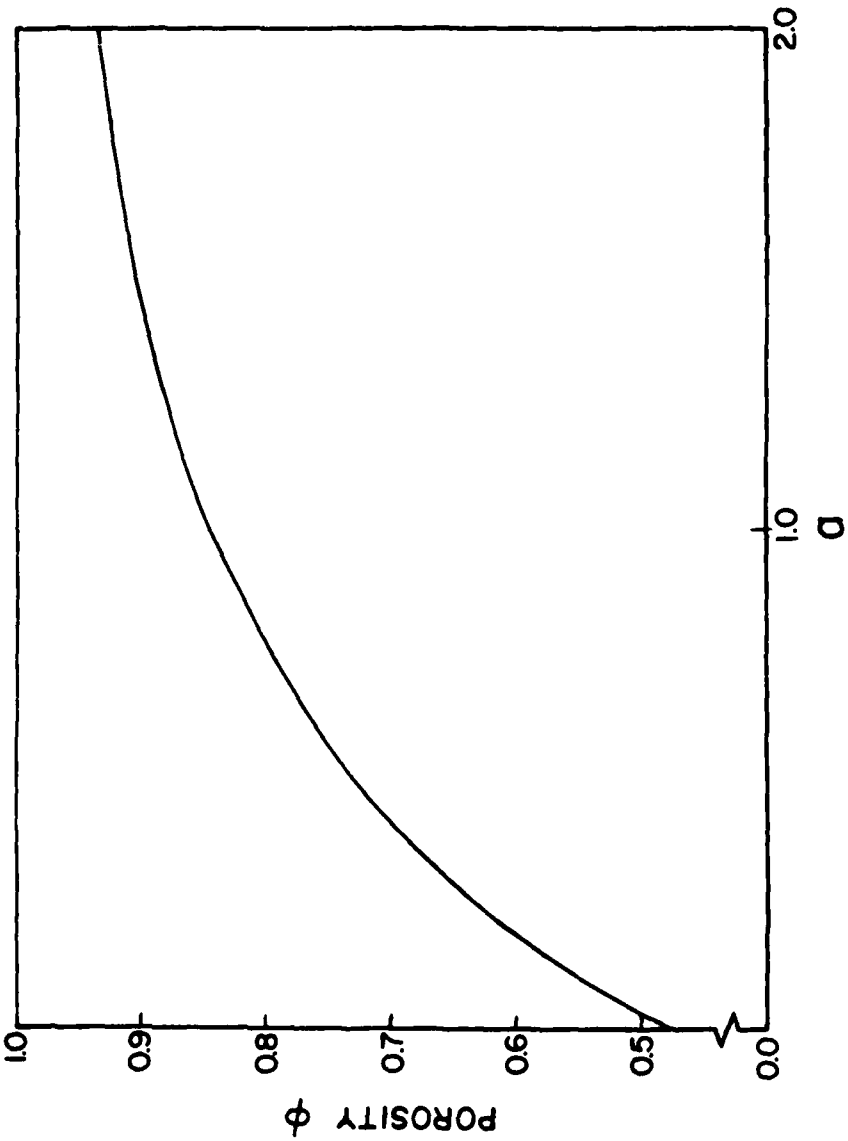

Fig. B.2 Relative particle distances for a fluidized bed.

APPENDIX C

CONSTITUTIVE RELATIONS

This section describes in more complete detail the constitutive relations and criteria outlined in Chapter Two.

Due to the selection of separate energy equations for each phase of the flow it becomes impractical to use the method of Kuo *et al.* [15] to define an ignition temperature based on the solution of the heat conduction equation for the particles. Instead, the method proposed by Krier *et al.* [16] in which a "bulk particle temperature", defined as the average temperature of the solids, was used as the critical variable for determining ignition. Under this approach, ignition occurs once the bulk temperature reaches some critical T_{IGN} which is less than the critical surface temperature used by Kuo *et al.* [15].

Convective heat transfer between the hot gases and the particles made use of Denton's [17] heat transfer coefficient

$$h_{pg} = 0.65\left[\frac{K_g}{2r_p}\right]\left[\frac{\rho_g|U_g-U_p|(\phi)(2r_p)}{\mu_g}\right]^{0.7}[Pr]^{0.33} \qquad (C.1)$$

where K_g is the thermal conductivity of the gas, μ_g is the viscosity of the gas, and Pr is the Prandtl number of the gas phase.

Due to questions concerning the alteration of the boundary layer around a burning particle which in turn alters the convective heat transfer, it has been assumed that the above value for the heat transfer coefficient is reduced, once the particle is ignited, to one-tenth of the value used if the particle were not burning.

The drag relation used in this investigation is that devised by

Kuo and Nydegger [18], namely: $\bar{F} = [\mu_g(\Delta U)/4r_p^2]\, f_{pg}$

$$\bar{F} = \frac{\mu_g(U_g - U_p)}{(2r_p)^2}\left[\frac{1-\phi}{\phi}\right]^2 \underbrace{\left[276.23 + 5.05\left(\frac{Re_p}{1-\phi}\right)^{0.87}\right]}_{f_{pg}} \tag{C.2}$$

where Re_p is the Reynold's number based on the particle radius

$$Re_p = \frac{2r_p\rho_g\phi|U_g - U_p|}{\mu_g} \tag{C.3}$$

The value for the gas viscosity, μ_g, used in the last three equations was assumed to vary with temperature only. Ideally, the variation should be with respect to both temperature and pressure due to the extremely high values for both of these parameters. However, no such relation could be found so the following relation was settled on as being the most applicable.

$$\mu_g = \mu_{g_o}\left[\frac{T_g}{T_{g_o}}\right]^{0.65} \tag{C.4}$$

where μ_{g_o} and T_{g_o} are initial conditions for each variable.

The burning rate law used throughout this work is the simple pressure dependent relation

$$\dot{r} = b_2 + b_1(P_g)^n \tag{C.5}$$

where b_1, b_2, and n are constants. Occassional use was made of a variation of this law

$$\dot{r} = b_2 + b_3\left(\frac{T_g}{T_{g_o}}\right)^m (P_g)^n \tag{C.6}$$

which will be noted when used.

APPENDIX D

ANALYSIS OF THE INTERNAL ENERGY RELATION WHEN UTILIZING A NONIDEAL STATE EQUATION

From simple thermodynamics one can write the internal energy as

$$de = \left(\frac{\partial e}{\partial T}\right)_v dT + \left(\frac{\partial e}{\partial v}\right)_T dv \tag{D.1}$$

where

e = the internal energy

T = temperature

v = the specific volume ($= 1/\rho$)

It can also be shown that

$$\left(\frac{\partial e}{\partial T}\right)_v = c_v \tag{D.2}$$

and

$$\left(\frac{\partial e}{\partial v}\right)_T = \frac{\beta T}{\kappa} - p_g \tag{D.3}$$

These last two equations are derived in detail in Lee and Sears [19]. However, by definition

$$\beta = \text{coefficient of volume expansion} = \left(\frac{1}{v}\right)\left(\frac{\partial v}{\partial T}\right)_p \tag{D.4}$$

$$\kappa = \text{isothermal compressibility} = -\left(\frac{1}{v}\right)\left(\frac{\partial v}{\partial P}\right)_T \tag{D.5}$$

These two partial derivatives can now be evaluated using the equation of state since they contain only state variables.

This analysis will proceed without regard for the exact form of B_v

in order to keep the results as general as possible. In order to analyze Eq. (D.4), the state equation

$$P_g = \frac{\rho_g R_g T_g}{1-\rho_g B_v} \tag{D.6}$$

is differentiated on both sides with respect to T_g holding P_g constant yielding

$$0 = \frac{(v-B_v)R - RT_g\left(\frac{\partial v}{\partial T_g} - \frac{\partial B_v}{\partial v}\frac{\partial v}{\partial T_g}\right)}{(v - B_v)^2} \tag{D.7}$$

Solving this equation for $\left(\frac{\partial v}{\partial T_g}\right)_{P_g}$ and dividing both sides by v will result in the necessary form for β

$$\beta = \frac{1}{v}\left(\frac{\partial v}{\partial T_g}\right)_{P_g} = \frac{1}{v}\left[\frac{v - B_v}{T_g\left(1 - \frac{\partial B_v}{\partial v}\right)}\right] \tag{D.8}$$

To solve for κ, both sides of Eq. (D.6) are first differentiated with respect to P_g while holding T_g constant, resulting in

$$1 = \frac{- RT_g\left(\frac{\partial v}{\partial P_g} - \frac{\partial B_v}{\partial v}\frac{\partial v}{\partial P_g}\right)}{(v - B_v)^2} \tag{D.9}$$

Solving this equation for $\left(\frac{\partial v}{\partial P_g}\right)_{T_g}$ and dividing both sides by -v yields

$$\kappa = -\left(\frac{1}{v}\right)\left(\frac{\partial v}{\partial P_g}\right)_{T_g} = \left(\frac{1}{v}\right)\left[\frac{(v - B_v)^2}{RT_g\left(1 - \frac{\partial B_v}{\partial v}\right)}\right] \tag{D.10}$$

Now, substituting the results from Eqs. (D.8) and (D.10) into Eq. (D.3) yields

$$\left(\frac{\partial e}{\partial v}\right)_{T_g} = \frac{\beta T_g}{\kappa} - P_g$$

$$= \frac{\left(\frac{1}{v}\right)\left[\frac{v - B_v}{T_g\left(1 - \frac{\partial B_v}{\partial v}\right)}\right](T_g)}{\left(\frac{1}{v}\right)\left[\frac{(v - B_v)^2}{RT_g\left(1 - \frac{\partial B_v}{\partial v}\right)}\right]} - P_g = \frac{RT}{v - B_v} - P_g \qquad (D.11)$$

Thus, regardless of the exact form of B_v, Eq. (D.3) will always be zero and

$$de = c_v dT \qquad (D.12)$$

only.

However, the ratio of specific heats, $\gamma = \frac{c_p}{c_v}$, will not be a constant for the gas that obeys Eq. (D.6). Again, utilizing Lee and Sears [19] one obtains

$$c_p - c_v = \frac{\beta^2 vT}{\kappa} \qquad (D.13a)$$

$$= \frac{\left(\frac{1}{v}\right)^2\left[\frac{v - B_v}{T_g\left(1 - \frac{\partial B_v}{\partial v}\right)}\right]^2 vT_g}{\left(\frac{1}{v}\right)\left[\frac{(v - B_v)^2}{RT_g\left(1 - \frac{\partial B_v}{\partial v}\right)}\right]} = \frac{R}{1 - \frac{\partial B_v}{\partial v}} \qquad (D.13b)$$

UNIVERSITY OF ILLINOIS

RECENT AERONAUTICAL AND ASTRONAUTICAL
ENGINEERING DEPARTMENT TECHNICAL REPORTS

Technical Report Number	Title	Author	Journal Publication
AAE 62-1	An Introduction to Viscoelastic Analysis	H. H. Hilton	Engineering Design for Plastics, Reinhold Publ. Corp., N.Y., 199-276 (1964).
AAE 62-2	A Method of Characteristics Analysis of Detonation Stability	R. A. Strehlow	
AAE 63-1	On Non-Stationary White Noise	Y. K. Lin	J. Acoust. Soc. Amer. 36:82-84 (1964).
AAE 63-2	Formulation and Evaluation of Approximate Analogies for Transient Temperature Dependent Linear Viscoelastic Media	H. H. Hilton and J. R. Clements	Proc. Conf. on Thermal Loading and Creep, Inst. Mech. Eng., London, 6.17-6.24(1964).
AAE 63-3	Free Vibrations of Continuous Skin-Stringer Panels with Non-Uniform Stringer Spacing and Panel Thickness	Y. K. Lin, T. J. McDaniel, B. K. Donaldson, C. F. Vail and W. J. Dwyer	AFML-TR-64-347, Wright-Patterson AFB (1965).
AAE 64-1	Random Vibrations of a Myklestad Beam	Y. K. Lin	AIAA J., 2:1448-1451 (1964).
AAE 64-2	On Detonation Initiation	R. A. Strehlow	AIAA J., 2:783-784 (1964).
AAE 64-3	A Theoretical Investigation of a Restrictive Model for Detonation Initiation	R. B. Gilbert	AIAA J., 4:1777-1783 (1966).

RECENT AERONAUTICAL AND ASTRONAUTICAL ENGINEERING DEPARTMENT TECHNICAL REPORTS (continued)

Technical Report Number	Title	Author	Journal Publication
AAE 64-4	Transfer Matrix Representation of Flexible Airplanes in Gust Response Study	Y. K. Lin	J. of Aircraft, 2:116-121 (1965).
AAE 64-5	Dynamic Characteristics of Continuous Skin-Stringer Panels	Y. K. Lin	Acoustical Fatigue in Aerospace Structures, Syracuse Univ. Press, 163-184 (1965).
AAE 64-6	Experimental Study of the Growth of Transverse Waves in Detonations	R. Liaugminas	See AAE 66-3
AAE 64-7	Nonstationary Excitation and Response in Linear Systems Treated as Sequences of Random Pulses	Y. K. Lin	Journal of the Acoustical Society of America, 38: 453-460 (1965).
AAE 65-1	Transverse Waves in Detonations	R. A. Strehlow and F. Dan Fernandes	Combustion and Flame, 9:109-119 (1965).
AAE 65-2	A Summary of Linear Viscoelastic Stress Analysis	H. H. Hilton	Solid Rocket Structural Integrity Abstracts, 2: 1-56 (1965).
AAE 65-3	Approximate Correlation Function and Spectral Density of the Random Vibration of an Oscillator with Non-Linear Damping	Y. K. Lin	AFMK-TR-66-62, Wright Patterson AFB (1966).
AAE 65-4	Investigation of the Flow Properties Downstream of a Shock Wave Propagating into a Convergent Duct	R. E. Cusey	See AAE 65-6

RECENT AERONAUTICAL AND ASTRONAUTICAL ENGINEERING DEPARTMENT TECHNICAL REPORTS (continued)

Technical Report Number	Title	Author	Journal Publication
AAE 65-5	A Method for the Determination of the Matrix of Impulse Response Functions with Special Reference to Applications in Random Vibration Problems	Y. K. Lin	AFFDL-TR-66-80, Wright Patterson AFB, 743-751 (1966).
AAE 65-6	Convergent Channel Shock Tube for Detonation Initiation Studies	A. J. Crooker	"Detonation and Initiation Behind an Accelerating Shock Wave" by R. A. Strehlow, A. J. Crooker, R. E. Cusey, Comb and Flame, 11:339-351 (1967).
AAE 66-1	A Comparison of Experimental and Theoretical Transverse Wave Spacings in Detonation	R. H. Watson	See AAE 66-3
AAE 66-2	A Simple Model for the Mechanism of Detonation	J. R. Eyman	See AAE 66-3
AAE 66-3	Transverse Wave Structure in Detonations	R. A. Strehlow, R. Liaugminas, R. H. Watson and J. R. Eyman	11th Symposium (International) on Combustion, Mono Book Corp. Baltimore, Md., (1967).
AAE 66-4	A Real Gas Analysis Using an Acoustic Model for the Transverse Wave Spacing in Detonations	R. E. Maurer	AIAA Journal, 7: 323-328, (1969).
AAE 67-1	Shock Tube Studies in Exothermic Systems	R. A. Strehlow	Phys. Fluids, 12: 96-100, (1969).

RECENT AERONAUTICAL AND ASTRONAUTICAL ENGINEERING DEPARTMENT TECHNICAL REPORTS (continued)

Technical Report Number	Title	Author	Journal Publication
AAE 67-2	Shock Tube Chemistry	R. A. Strehlow	Progress in High Temperature Physics and Chemistry, Pergamon Press, N.Y., 2: 127-176 (1968).
AAE 67-3	Structural Failure Criteria for Solid Propellants Under Multiaxial Stresses	A. R. Zak	J. Spacecraft, 5: 265-269 (1968)
AAE 67-4	Structural Analysis of Realistic Solid Propellant Materials	A. R. Zak	J. Spacecraft, 5: 270-275 (1968).
AAE 67-5	Characteristics of Transverse Waves in Detonations of H_2, C_2H_2, C_2H_4 and CH_4 - Oxygen Mixtures	C. D. Engel	AIAA Journal, 7: 492-496 (1969).
AAE 68-1	A Review of Shock Tube Chemistry	R. A. Strehlow	Progress in High Temperature Physics and Chemistry, Pergamon Press, N.Y., 2: 1-146 (1969).
AAE 68-2	On the Interpretation of Molecular Beam Data	A. Klavins	A. Klavins and L. H. Sentman Rev. Sci. Instr., 41: 1560-1567 (197(
AAE 68-3	Detonative Mach Stems	R. A. Strehlow H. O. Barthel	
AAE 68-4	On the Strength of Transverse Waves and Geometrical Detonation Cell Model for Gas Phase Detonations	J. R. Biller	R. A. Strehlow and J. R. Biller Comb. and Flame, 13: 577-582, (1970).
AAE 68-5	The MISTRESS User Manual	H. H. Hilton	
AAE 69-1	The Chemical Shock Tube - Implications of Flow Non-Idealities	R. A. Strehlow R. L. Belford	

RECENT AERONAUTICAL AND ASTRONAUTICAL ENGINEERING DEPARTMENT TECHNICAL REPORTS (continued)

Technical Report Number	Title	Author	Journal Publication
AAE 69-2	Phenomenological Investigation of Low Mode Marginal Planar Detonations	A. J. Crooker	Acta Astronautica, 1:303-315(1974).
AAE 69-3	Multi-Dimensional Detonation Wave Structure	R. A. Strehlow	Astronautica Acta, 15:345-358(1970).
AAE 69-4	An Experimental and Analytical Investigation of a Two-Dimensionally Stiffened Panel	A. R. Zak C. E. French	AFML-TR-68-390, Wright-Patterson AFB,(1969).
AAE 69-5	On the Kinetic Equations for a Dilute, Short Range Gas	T. J. Forster L. H. Sentman	with A.D. Grimm, Proc. Ninth International Symposium on Rarefied Gas Dynamics, A3.1-3.8 (1974).
AAE 69-6	The Sawtooth Column of the Supersonic Electric Arc in Sulfur Hexafluoride	C. E. Bond	AIAA J., 9: 510-512 (1971).
AAE 69-7	Theoretical and Experimental Analysis of Stiffened Panels Under Dynamic Conditions	A. R. Zak R. N. Yurkovich J. H. Schmidt	J. of Aircraft, 3: 149-155 (1971).
AAE 70-1	On the Interaction Between Chemical Kinetics and Gas-Dynamics in the Flow Behind a Cylindrical Detonation Front	S. Rajan	
AAE 70-2	Preliminary Studies on the Engineering Applications of Finite Difference Solutions of the Navier-Stokes Equations	W. F. Van Tassell	
AAE 70-3	Some Aspects of the Surface Boundary Condition in Kinetic Theory	A. Klavins	Proc. of International Symposium on Rarefied Gas Dynamics, Pisa, Italy (1970).

RECENT AERONAUTICAL AND ASTRONAUTICAL ENGINEERING DEPARTMENT TECHNICAL REPORTS (continued)

Technical Report Number	Title	Author	Journal Publication
AAE 70-4	A Study of the Transient Behavior of Fuel Droplets during Combustion: Theoretical Considerations for Aerodynamic Stripping	H. Krier	
AAE 70-5	On the Solid Body Model for an Accelerating Electric Arc	F. Klett	
AAE 71-1 UILU-ENG 71 0501	Detonative Mach Stems	R. A. Strehlow H. O. Barthel	
AAE 71-2 UILU-ENG 71 0502	An Investigation of Transient Phenomena in Detonations	R. J. Stiles	with R. A. Strehlow, A. A. Adamczyk, Astronautica Acta, 17: 509-527 (1972)
AAE 71-3 UILU-ENG 71 0503	On the Role of Tangential Velocity Changes in the Scattering of a Molecular Beam from A Solid Surface	C. C. Chrisman L. H. Sentman	Chemical Physics Letters, 26:407-413(1974).
AAE 72-1 UILU-ENG 72 0501	Unconfined Vapor Cloud Explosions - An Overview	R. A. Strehlow	Fourteenth Symposium on Combustion, 1189-1200 (1973).
AAE 72-2 UILU-ENG 72 0502	Application of Illiac IV Computer to Numerical Solutions of Structural Problems	H. H. Hilton A. R. Zak J. J. Kessler P. C. Rockenbach	
AAE 72-3 UILU-ENG 72 0503	On the Measurement of Energy Release Rates In Vapor Cloud Explosions	R. A. Strehlow L. D. Savage G. M. Vance	Combustion Science and Technology, 6: 307-312 (1972).

RECENT AERONAUTICAL AND ASTRONAUTICAL ENGINEERING DEPARTMENT TECHNICAL REPORTS (continued)

Technical Report Number	Title	Author	Journal Publication
AAE 72-4 UILU-ENG 72 0504	A Performance Comparison of Several Numerical Minimization Algorithms	J. E. Prussing	
AAE 73-1 UILU-ENG 73 0501	Stresses and Damping in the Matrix of a Composite Material	A. R. Zak	
AAE 73-2 UILU-ENG 73 0502	Early Burning Anomalies in the XM 645 Flechette Cartridge	H. Krier D. R. Hall	BRL Rept. No. 104 (1973).
AAE 73-3 UILU-ENG 73 0503	Equivalent Explosive Yield of the Explosion in the Alton Southern Gateway Yard, East St. Louis, Ill., January 22, 1972	R. A. Strehlow	
AAE 73-4 UILU-ENG 73 0504	Failure Studies of Gaseous Detonations	R. J. Salm	Acta Astronautica (in press).
AAE 73-5 UILU-ENG 73 0505	An Investigation of Hydrogen-Oxygen-Argon Detonations	J. R. Biller	
AAE 73-6 UILU-ENG 73 0506	Interior Ballistic Predictions Using Data From Closed and Variable-Volume Simulators	H. Krier S. A. Shimpi M. J. Adams	Proc. 11th JANNAF Combustion Meeting, CPIA Publ. 261:17-30(1974).
AAE 73-7 UILU-ENG 73 0507	Theory of Rotationally Symmetric Laminar Premixed Flames	G. M. Vance H. Krier	Comb. and Flame J., 22: 365-375 (1974).
AAE 73-8 UILU-ENG 73 0508	Burning of Fuel Droplets at Elevated Pressures	J. H. Rush H. Krier	Comb. and Flame J., 22: 377-382 (1974).
AAE 73-9 UILU-ENG 73 0509	An Impact Ignition Model for Solid Propellants	H. Krier H. H. Hilton O. Olorunsola D. L. Reuss	BRL Rept. No. 1707 (1974).

RECENT AERONAUTICAL AND ASTRONAUTICAL ENGINEERING DEPARTMENT TECHNICAL REPORTS (continued)

Technical Report Number	Title	Author	Journal Publication
AAE 73-10 UILU-ENG 73 0510	Optimal Multiple-Impulse Direct Ascent Fixed-Time Rendezvous	J. E. Prussing L. R. Gross	AIAA J., 12, 885-889 (1974).
AAE 73-11 UILU-ENG 73 0511	The Structure and Stability of Detonation Waves	R. A. Strehlow	
AAE 74-1 UILU-ENG 74 0501	Model of Flame Spreading and Combustion Through Packed Beds of Propellant Grains	H. Krier W. F. Van Tassell S. Rajan J. T. Ver Shaw	BRL Report No. 147 (1974). Int. J. Heat-Mass Transfer, 1377-86 (1975).
AAE 74-2 UILU-ENG 74 0502	On the Nature of Non-Ideal Blast Waves	R. A. Strehlow A. A. Adamczyk	WSS/CI Paper No. 74-12, Pullman, Wash. (1974).
AAE 74-3 UILU-ENG 74 0503	Viscous Incompressible Flow in Spiral Channels	W. F. VanTassell	
AAE 74-4 UILU-ENG 74 0504	Frequency Response Functions of a Disordered Periodic Beam	J. N. Yang Y. K. Lin	J. Sound and Vibration 38: 317-340 (1975).
AAE 74-5 UILU-ENG 74 0505	Predicting Uniform Gun Interior Ballistics: Part I. An Analysis of Closed Bomb Testing	H. Krier S. A. Shimpi	Comb. and Flame J. 25: 229-240 (1975).
AAE 74-6 UILU-ENG 74 0506	Predicting Uniform Gun Interior Ballistics: Part II. The Interior Ballistic Code	H. Krier M. J. Adams	Proc. 11th JANNAF Comb. Meeting, CPIA Publ. 261: 17-30 (1974).
AAE 74-7 UILU-ENG 74 0507	Predicting Uniform Gun Interior Ballistics: Part III. The Concept and Design of the Dynagun Ballistic Simulator	H. Krier J. W. Black	Proc. 11th JANNAF Comb. Meeting, CPIA Publ. 261: 31-43(1974).
AAE 74-8 UILU-ENG 74 0508	Process of Fluidization During Porous Solid Propellant Combustion	H. Krier J. T. Ver Shaw	AIAA Paper 75-242 (1975).
AAE 74-9 UILU-ENG 74 0509	An Analysis of Flame Propagation Through Coal Dust-Air Mixtures	J. L. Krazinski H. Krier	AIAA Paper 74-1111 (1974).

RECENT AERONAUTICAL AND ASTRONAUTICAL ENGINEERING DEPARTMENT TECHNICAL REPORTS (continued)

Technical Report Number	Title	Author	Journal Publication
AAE 74-10 UILU-ENG 74 0510	An Interior Ballistics Prediction of the M549 Rocket Assisted Projectile	H. Krier S. Shimpi E. Meister	
AAE 75-1 UILU-ENG 75 0501	Dynamically Induced Thermal Stresses in Composite Material, Structural Panels	A. Zak W. Drysdale	
AAE 75-2 UILU-ENG 75 0502	Numerical Analysis of Laminated, Orthotropic Composite Structures	A. R. Zak	
AAE 75-3 UILU-ENG 75 0503	The Characterization and Evaluation of Accidental Explosions	R. A. Strehlow W. E. Baker	NASA CR 134779 (June 1975). Also Progr. Energy & Comb. Sc. (in press).
AAE 75-4 UILU-ENG 75 0504	Program Manual for the Eppler Airfoil Inversion Program	W. G. Thomson	
AAE 75-5 UILU-ENG 75 0505	Design of High Lift Airfoils with a Stratford Distribution by the Eppler Method	W. G. Thomson	
AAE 75-6 UILU-ENG 75 0506	Prediction of Flame Spreading and Pressure Wave Propagation in Propellant Beds	H. Krier	AIAA J. 14: 301-309 (1976)
AAE 75-7 UILU-ENG 75 0507	Vigorous Ignition of Granulated Beds by Blast Impact	H. Krier S. Gokhale	Int. J. Heat-Mass Transfer 19: 915-923 (1976)
AAE 75-8 UILU-ENG 75 0508	Solid Propellant Burning Evaluation with the Dynagun Ballistic Simulator	H. Krier T. G. Nietzke M. J. Adams J. W. Black E. E. Meister	J. Ballistics 1: 103-149 (1976)
AAE 75-9 UILU-ENG 75 0509	Structural Reliability & Minimum Weight Analysis for Combined Random Loads & Strengths	H. H. Hilton	AIAA J. (in press)

RECENT AERONAUTICAL AND ASTRONAUTICAL ENGINEERING DEPARTMENT TECHNICAL REPORTS (Continued)

Technical Report Number	Title	Author	Journal Publication
AAE 75-10 UILU-ENG 75 0510	Linear Viscoelastic Analysis with Random Material Properties	H. H. Hilton J. Hsu J. S. Kirby	
AAE 76-1 UILU-ENG 76 0501	Two Degree of Freedom Flutter of Linear Viscoelastic Wings in Two Dimensional Flow	C. F. Vail H. H. Hilton	In press AIAA J.
AAE 76-2 UILU-ENG 76 0502	An Error Analysis of Computerized Aircraft Synthesis	V. V. Volodin H. H. Hilton	In press J. of Aircraft
AAE 76-3 UILU-ENG 76 0503	Reactive Two-Phase Flow Models Applied to the Prediction of Detonation Transition in Granulated Propellant	H. Krier M. Dimitstein S. S. Gokhale	AIAA J. 16: 177-183 (1978)
AAE 76-4 UILU-ENG 76 0504	Transient Temperature Response of Charring Composite Slabs	J. E. Prussing H. Krier	Int'l J. Heat Mass Transfer. 21: 519-522 (1978)
AAE 76-5 UILU-ENG 76 0505	Nonlinear Response of Laminated Composite Material Cylindrical Shells	A. R. Zak J. N. Craddock	
AAE 76-6 UILU-ENG 76 0506	An Investigation of Blast Waves Generated from Non-Ideal Energy Sources	A. A. Adamczyk	
AAE 77-1 UILU-ENG 77 0501	Nonlinear Dynamic Analysis of Flat Laminated Plates by the Finite Element Method	A. R. Zak	
AAE 77-2 UILU-ENG 77 0502	An Investigation of Blast Waves Generated by Constant Velocity Flames	R. T. Luckritz	
AAE 77-3 UILU-ENG 77 0503	On the Blast Waves Produced by Constant Velocity Combustion Waves	R. A. Strehlow R. D. Luckritz	
AAE 77-4 UILU-ENG 77 0504	Direct Initiation of Detonation by Non-Ideal Blast Waves	R. J. Cesarone	
AAE 77-5 UILU-ENG 77 0505	The Blast Wave Generated by Constant Velocity Flames	S. A. Shimpi R. A. Strehlow	

RECENT AERONAUTICAL AND ASTRONAUTICAL ENGINEERING DEPARTMENT TECHNICAL REPORTS (Continued)

Technical Report Number	Title	Author	Journal Publication
AAE 77-6 UILU-ENG 77 0506	Exploratory Studies of Flame and Explosion Quenching	R. A. Strehlow L. C. Sorenson L. D. Savage H. Krier	
AAE 77-7 UILU-ENG 77 0507	The Trajectory of a Liquid Droplet Injected Into the Wake of an Aircraft in Ground Effect	M. B. Bragg	
AAE 77-8 UILU-ENG 77 0508	Comparison of Viscoelastic and Structural Damping in Flutter	H. H. Hilton	
AAE 77-9 UILU-ENG 77 0509	The Blast Wave Generated by Constant Velocity Flames	R. A. Strehlow R. T. Luckritz A. A. Adamczyk S. Shimpi	
AAE 77-10 UILU-ENG 77 0510	Wind Energy: History, Economics, and the Vertical Wind Turbine	T. R. Richards	
AAE 77-11 UILU-ENG 77 0511	Final Report: Low Speed Airfoil Study	A. I. Ormsbee	
AAE 77-12 UILU-ENG 77 0512	Final Report: Propeller Study, Part I, Introduction and Overview	A. I. Ormsbee	
AAE 77-13 UILU-ENG 77 0513	Final Report: Propeller Study, Part II, The Design of Propellers for Minimum Noise	C. J. Woan	
AAE 77-14 UILU-ENG 77 0514	Final Report: Propeller Study, Part III, Experimental Determination of Thrust & Torque on the YO-3A Aircraft	S. A. Siddiqi K. R. Sivier A. I. Ormsbee	
AAE 77-15 UILU-ENG 77 0515	Direct Initiation of Detonation	R. A. Strehlow H. O. Barthel	

RECENT AERONAUTICAL AND ASTRONAUTICAL ENGINEERING DEPARTMENT TECHNICAL REPORTS (Continued)

Technical Report Number	Title	Author	Journal Publication
AAE 77-16 UILU-ENG 77 0516	The Effects of Energy Distribution Rates and Density Distribution on Blast Wave Structure	R. A. Strehlow L. H. Sentman	
AAE 77-17 UILU ENG 77 0517	Modeling of Convective Mode Combustion Through Granulated Propellant to Predict Transition to Detonation	H. Krier J. A. Kezerle	17th Combustion Symposium: In Press
AAE 78-1 UILU ENG 78 0501	Unsteady Internal Boundary Layer Flows with Application to Gun Barrel Heat Transfer and Erosion	M. J. Adams H. Krier	
AAE 78-2 UILU ENG 78 0502	Extracting Burning Rates for Multiperforated Propellant from Closed Bomb Testing	H. Krier	
AAE 78-3 UILU ENG 78 0503	Lean Limit Flammability Study of Methane-Air Mixtures in a Square Flammability Tube	J. Jarosinski R. A. Strehlow	
AAE 73-4 UILU ENG 78 0504	Interim Technical Report AFOSR 77-3336: "An Investigation of the Ignition Delay Times For Propylene Oxide-Oxygen-Nitrogen Mixtures"	E. E. Meister	
AAE 78-5 UILU ENG 78 0505	Final Report: A Distribution Model for the Aerial Application of Granular Agricultural Particles	S. T. Fernandes A. I. Ormsbee	
AAE 78-6 UILU ENG 78 0506	The Thermal Structure of a Methane-Air Flame Propagating in a Square Flammability Tube	J. Jarosinski R. A. Strehlow	
AAE 78-7 UILU ENG 78 0507	The Effects of Energy Distribution Rates and Density Distribution on Blast Wave Structure	R. A. Strehlow L. H. Sentman	
AAE 78-8 UILU ENG 78 0508	The Effect of a Zero G Environment on Flammability Limits as Determined Using a Standard Flammability Tube Apparatus	R. A. Strehlow D. L. Reuss	

RECENT AERONAUTICAL AND ASTRONAUTICAL ENGINEERING DEPARTMENT TECHNICAL REPORTS (Continued)

Technical Report Number	Title	Author	Journal Publication
AAE 79-1 UILU-ENG 79 0501	An Approximate Finite Element Method of Stress Analysis of Non-Axisymmetric Bodies with Elastic-Plastic Material	J. N. Craddock A. R. Zak	
AAE 79-2 UILU-ENG 79 0502	Stability of Bridge Motion in Turbulent Winds	Y. K. Lin S. T. Ariaratnam	
AAE 79-3 UILU ENG 79 0503	Rotor Blade Dynamics in Hovering Flights	C.Y.R. Hong	
AAE 79-4 UILU ENG 79 0504	Finite Element Analysis of A Dynamically Loaded Flat Laminated Plate	D. W. Pillasch A. R. Zak	
AAE 79-5 UILU ENG 79 0505	An Efficient Rotational Nonequilibrium Model of a CW Chemical Laser	L. H. Sentman	
AAE 79-6 UILU ENG 79 0506	Column Response to Vertical-Horizontal Earthquakes	Y. K. Lin T. Y. Shih	
AAE 79-7 UILU ENG 79 0507	Users Guide for Programs MNORO & AFOPTMNORO	L. H. Sentman	
AAE 79-8 UILU ENG 79 0508	The Blast Wave from Deflagrative Explosions, an Acoustic Approach	R. A. Strehlow	
AAE 80-1 UILU ENG 80 0501	Gas Flow Resistance Measurements Through Packed Beds at High Reynolds Numbers	S. F. Wilcox H. Krier	
AAE 80-2 UILU ENG 80 0502	Fluid Mechanical Processes of Deflagration to Detonation Transition in Beds of Porous Reactive Solids	S. Hoffman H. Krier	
AAE 80-3 UILU ENG 80 0503	Dynamic Analysis of Orthotropic, Layered Plates Subject to Explosive Loading	D. W. Pillasch A. R. Zak	

UNCLASSIFIED
SECURITY CLASSIFICATION OF THIS PAGE (When Data Entered)

REPORT DOCUMENTATION PAGE		READ INSTRUCTIONS BEFORE COMPLETING FORM
1. REPORT NUMBER AFOSR-TR-80-1064	2. GOVT ACCESSION NO. AD-A090558	3. RECIPIENT'S CATALOG NUMBER
4. TITLE (and Subtitle) FLUID MECHANICAL PROCESSES OF DEFLAGRATION TO DETONATION TRANSITION IN BEDS OF POROUS REACTIVE SOLIDS		5. TYPE OF REPORT & PERIOD COVERED INTERIM TECH REPORT #2 July 1978 - May 1980 6. PERFORMING ORG. REPORT NUMBER Tech Report AAE 80-2
7. AUTHOR(s) Stephen J. Hoffman Herman Krier		8. CONTRACT OR GRANT NUMBER(s) AFOSR 77-3336
9. PERFORMING ORGANIZATION NAME AND ADDRESS University of Illinois at Champaign-Urbana Urbana, Illinois 61801		10. PROGRAM ELEMENT, PROJECT, TASK AREA & WORK UNIT NUMBERS 2308/A2 61102F
11. CONTROLLING OFFICE NAME AND ADDRESS Air Force Office of Scientific Research/NA Building 410 Bolling Air Force Base, DC 20332		12. REPORT DATE March 1980 13. NUMBER OF PAGES 95
14. MONITORING AGENCY NAME & ADDRESS(if different from Controlling Office)		15. SECURITY CLASS. (of this report) UNCLASSIFIED 15a. DECLASSIFICATION/DOWNGRADING SCHEDULE

16. DISTRIBUTION STATEMENT (of this Report)

Approved for public release; distribution unlimited

17. DISTRIBUTION STATEMENT (of the abstract entered in Block 20, if different from Report)

18. SUPPLEMENTARY NOTES

19. KEY WORDS (Continue on reverse side if necessary and identify by block number)

Deflagration to detonation transition
Two-phase reactive fluid mechanics
Solid propellant combustion hazards

20. ABSTRACT (Continue on reverse side if necessary and identify by block number)

Fluid mechanical processes which characterize the transition from deflagration to detonation in porous solid propellant are modelled. The report summarizes the predictions of the unsteady two-phase flow as a function of four basic elements, namely, (i) the compressibility of the solid, (ii) the permeability of the hot product gases into the unignited porous solid, (iii) the enhancement of surface burning area (due to additional material fracture) and (iv) the propellant burning rate, functionally increasing at the high

DD FORM 1 JAN 73 1473 EDITION OF 1 NOV 65 IS OBSOLETE

UNCLASSIFIED
SECURITY CLASSIFICATION OF THIS PAGE (When Data Entered)

pressures developed during the transient. It is concluded that any of the above four mechanisms or combinations of mechanisms are necessary as precursors to the transition to detonation.

The work reported clearly defines the limited data-base now available which is necessary to verify the concepts presented in the fluid mechanics model that is being developed to predict DDT. It is concluded that eventual understanding for the prevention of DDT in high-energy solid propellants will require both the type of unsteady flow analysis modeled herein in addition to flow experiments with porous or granular beds of compressible particles.


DA
FIL